ETH
Eidgenössische Technische Hochschule Zürich
Swiss Federal Institute of Technology Zurich

Seminar for Applied Mathematics SAM

Large deformation shape uncertainty quantification in acoustic scattering

R. Hiptmair and L. Scarabosio and C. Schillings and Ch. Schwab

Research Report No. 2015-31
November 2015

Seminar für Angewandte Mathematik
Eidgenössische Technische Hochschule
CH-8092 Zürich
Switzerland

Large deformation shape uncertainty quantification in acoustic scattering*

R. Hiptmair, L. Scarabosio, C. Schillings, Ch. Schwab

November 3, 2015

Abstract

We address shape uncertainty quantification for the two-dimensional Helmholtz transmission problem, where the shape of the scatterer is the only source of uncertainty. In the framework of the so-called deterministic approach, we provide a high-dimensional parametrization for the interface. Each domain configuration is mapped to a nominal configuration, obtaining a problem on a fixed domain with stochastic coefficients. To compute surrogate models and statistics of quantities of interest, we apply an adaptive, anisotropic Smolyak algorithm, which allows to attain high convergence rates that are independent of the number of dimensions activated in the parameter space. We also develop a regularity theory with respect to the spatial variable, with norm bounds that are independent of the parametric dimension. The techniques and theory presented in this paper can be easily generalized to any elliptic problem on a stochastic domain.

1 Introduction

In nano-optics applications, imperfections in the manufacturing process may lead to a considerable uncertainty in the shape of nano-devices. The aim of the present work is to quantify how such shape variations affect the optical response of a nano-sized scatterer to some electromagnetic excitation. Our focus is on the estimation of surrogate models (interpolation) and statistics (quadrature) of quantities of interest.

Since the shape fluctuations cannot be considered to be small compared to the scatterer size, a perturbative approach [22, 24] is not suitable for our framework. On the other hand, the slow convergence rate of Monte Carlo sampling renders it computationally inefficient for such kind of applications, since each sample would require the numerical solution of a full electromagnetic field problem. Adopting the multilevel version of the Monte Carlo algorithm (MLMC) would still require a massive computational effort in order to reach a certain accuracy. Furthermore, Monte Carlo algorithms, while being very simple as quadrature rules, are not well suited for interpolation.

Instead, in the present work we model the uncertain shape through a *high-dimensional parametrization approach*, and then apply an algorithm for interpolation and quadrature that, exploting some regularity properties of the quantity of interest, allows to achieve convergence rates which are much higher than the ones attainable with Monte Carlo algorithms and do not suffer from the so-called 'curse of dimensionality'.

We illustrate the method on a two-dimensional *Helmholtz transmission problem* with an incoming plane wave, where the material parameters are assumed to be known exactly; the shape of the scatterer is thus the only source of uncertainty. We are going to focus on the case of a particle in free space, of which the geometry is depicted in Figure 1.1.

*Research supported by ERC under Grant AdG247277 and by ETH under CHIRP Grant CH1-01 11-1.

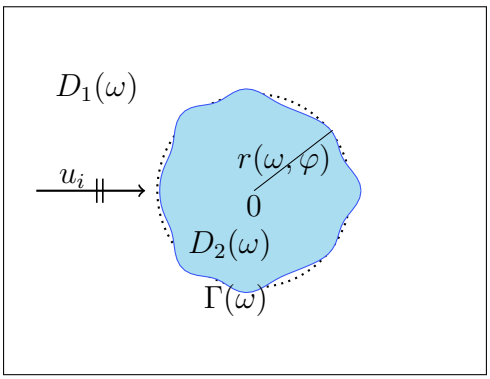

Figure 1.1: Particle in free space

1.1 Model problem

Let $(\Omega, \mathcal{A}, \mathbb{P})$ be a probability space, with $\mathcal{A}$ a σ-algebra on the power set $\mathscr{P}(\Omega)$ and $\mathbb{P}$ a probability measure on $(\Omega, \mathcal{A})$. For every $\omega \in \Omega$, we formally define $\Gamma(\omega)$ to be the boundary of the scatterer, $D_1(\omega)$ the exterior unbounded domain, and $D_2(\omega)$ the domain occupied by the scatterer. We assume that $D_1(\omega) \cup \Gamma(\omega) \cup D_2(\omega) = \mathbb{R}^2$ for every $\omega \in \Omega$.

The transmission problem for the Helmholtz equation can be written as

$$\begin{cases} -\nabla \cdot (\alpha(\Gamma(\omega), \boldsymbol{x}) \nabla u) - k^2(\Gamma(\omega), \boldsymbol{x}) u = 0 \quad \text{in } \mathbb{R}^2 & \text{(1.1a)} \\ \lim\limits_{|\boldsymbol{x}| \to \infty} \sqrt{|\boldsymbol{x}|} \left(\dfrac{\partial}{\partial |\boldsymbol{x}|} - ik_1 \right) (u(\omega) - u_i)(\boldsymbol{x}) = 0, & \text{(1.1b)} \\ \text{for } \mathbb{P}\text{–}a.e.\ \omega \in \Omega, \end{cases}$$

with uniformly positive, real-valued, piecewise-constant coefficients in each subdomain:

$$\alpha(\Gamma(\omega), \boldsymbol{x}) = \begin{cases} 1 & \text{if } \boldsymbol{x} \in D_1(\omega) \\ \mu & \text{if } \boldsymbol{x} \in D_2(\omega) \end{cases} \qquad k^2(\Gamma(\omega), \boldsymbol{x}) = \begin{cases} k_1^2 & \text{if } \boldsymbol{x} \in D_1(\omega) \\ \mu\, k_2^2 & \text{if } \boldsymbol{x} \in D_2(\omega). \end{cases} \tag{1.2}$$

The unknown $u = u(\omega, \boldsymbol{x})$ represents the total field, whereas k_1 and k_2 denote the wavenumbers in free space and in the scatterer, respectively; μ is a positive real coefficient. Equation (1.1b) is the so-called Sommerfeld radiation condition, where $u_i(\boldsymbol{x}) = e^{i\boldsymbol{k}_1 \cdot \boldsymbol{x}}$ is the incoming plane wave. It corresponds to the radiation condition in free space.

We work in the *large wavelength regime*, which excludes the presence of resonant geometric structures; thus, the results of this work are not restricted to the Helmholtz equation, but also hold for any elliptic equation.

The two-dimensional Helmholtz equation describes the scattering of an electromagnetic wave from a cylinder of infinite length, and the unknown u corresponds to the out-of-plane component of the electric field (TE mode) or of the magnetic field (TM mode), depending on the meaning conferred to the coefficients in the equation (see e.g. [34]). The same results and methodology presented in this paper, however, still hold for the three-dimensional Helmholtz equation, when the Fourier harmonics used to model the shape variations (see Section 2) are replaced by spherical harmonics.

1.2 Outline and related work

The parametric approach to represent the uncertainty was developed by Ghanem and Spanos (e.g. [19]) from the pioneering ideas of Wiener [39]. In this framework, in Section 2 we give

a probabilistic description of the interface $\Gamma = \Gamma(\omega)$, so that it will then depend on $\omega \in \Omega$ indirectly through a deterministic high-dimensional parameter representing the stochasticity. In particular, we express the variations of the scatterer boundary through an affine combination of a finite number of independent, uniformly distributed random variables, as it is commonly done to model the stochastic diffusion coefficient in the scalar diffusion model (see [12, 13, 37], just to mention some). Such an expansion can be regarded as an approximation to the exact probability distribution of the interface [41].

In Section 3, we use the domain mapping approach introduced by Xiu and Tartakovsky in [38, 41] to map each domain realization to a nominal configuration, fixed for all realizations, using a parameter-dependent map. A similar technique has been adopted in [8] and [23] too. An alternative method is the fictitious domain approach introduced by Canuto and Kozubek in [7].

The domain mapping allows us, in Section 4, to write a variational formulation for (1.1) on the *nominal* configuration with parameter-dependent coefficients, bringing the problem to a framework for which theory and discretization algorithms are well established.

In Section 5, we address the discretization of the latter variational formulation with respect to the parameter representing the stochasticity. Two main methods can be used: the stochastic Galerkin and the stochastic collocation method.

The stochastic Galerkin approach (see [37] for a comprehensive review) is not well suited for our application, the reason being that the coefficients in the PDE on the nominal configuration do not depend in an affine way on the high-dimensional parameter. In this case, the manipulation of the equations required by the stochastic Galerkin method, apart from leading to a fully coupled system of equations, would not be straightforward at all. We use instead a sparse collocation method. Stochastic collocation was introduced independently by Babuška, Nobile and Tempone in [1] and by Xiu and Hesthaven in [40]; we refer to [2] for a comparison of stochastic collocation with stochastic Galerkin in terms of accuracy versus computational work. To overcome the so-called *curse of dimensionality* due to the high dimension of the parameter space, the algorithms developed for both stochastic Galerkin and stochastic collocation employ sparse tensor approximation, and the convergence rates are shown to be independent or very weakly dependent on the number of dimensions considered. Here, we use the sparse adaptive Smolyak algorithm for stochastic quadrature and interpolation described in [35], and pioneered in the earlier work [18] of Gerstner and Griebel.

In the same section we also discuss the fulfillment, in our framework, of the key assumption of all convergence theorems, that is the holomorphy of the quantity of interest (e.g. the solution to (1.1) or linear functionals of it) with respect to an extension of the high-dimensional parameter to the complex plane. An important point is that, although due to the domain transformation introduced in Section 4 we need a stronger regularity constraint for the scatterer boundary than the one that is usually needed for the diffusion coefficient in elliptic problems on deterministic domains (namely, Fourier coefficients in $\ell^p(\mathbb{N})$ with $0 < p < \frac{1}{2}$ instead of $0 < p < 1$), such a stronger condition does not affect the convergence rates for sparse interpolation and quadrature.

In Section 6, we address the space discretization on the nominal configuration and couple it to the results of the previous section. For the spatial problem, we use a finite element discretization. We point out that a boundary element formulation (as used, for example, in [24]) is not applicable in the context of the mapping approach, due to variable coefficients in the resulting variational formulation. After discussing space regularity results for the solution at each collocation point, we couple finite element convergence estimates to convergence estimates for sparse stochastic collocation, obtaining convergence results for the fully discretized problem and linear output functionals. We first consider the simpler case of uniform finite element discretization for all the parameter realizations, and then the case when different space discretizations are used for different collocation points. For the former approach, the procedure that we present is

quite similar to the one presented in [8]. There, however, the convergence rates presented for the sparse grid error are not independent of the number of dimensions involved, and the effect of the amplitude of the stochastic perturbations on the smoothness of the solution and thus on the convergence rate of the finite element discretization is not taken into account. The results that we obtain for the case that the space discretization is different for each collocation point can be thought as a starting point for a parameter-adaptive space discretization to reduce the global computational effort, with a similar strategy as the ones proposed in [4] and [16] in the stochastic Galerkin framework.

In Section 7, we show that in numerical experiments we achieve the predicted theoretical convergence rates for both sparse interpolation and sparse quadrature on the nominal configuration.

In Section 8, we address the difficulties that arise for computing moments of the solution in physical space, where the interface is different for each realization. These are due to the discontinuity of the material properties across the interface (see (1.2)). Similar problems were encountered in [32] in the framework of the second order wave equation with discontinous random velocity.

2 Parametrization of the interface

In the first part of this section, we give a probabilistic model for the interface Γ. Using the probabilistic characterization, in the second part of the section we convert the stochastic problem to a deterministic problem on a high-dimensional parameter domain; this approach is particularly relevant in the perspective of a discretization, since we will see that, differently from the probability space Ω, the space where the deterministic parameter lives is suitable for discretization.

2.1 Probabilistic modeling of the interface

In order to have a simple representation of the interface , we require:

Assumption 2.1. *For $\mathbb{P}$–a.e. $\omega \in \Omega$, the domain $D_2(\omega)$ is star-shaped with respect to the origin and the interface $\Gamma(\omega)$ is of class C^1.*

In this way, $D_2(\omega)$ can be fully described by a stochastic, angle-dependent radius $r = r(\omega, \varphi) \in C^k_{\text{per}}([0, 2\pi))$ for $\mathbb{P}$–*a.e.* $\omega \in \Omega$ and some $k \geq 1$, representing the interface $\Gamma = \Gamma(\omega)$. The techniques we are going to present can be extended to the case of an interface that is only piecewise of class C^k ($k \geq 1$), but for ease of treatment we will not consider this case.

As it is commonly done in the framework of partial differential equations with stochastic diffusion coefficient (see e.g. [12, 13, 37]), we expand the uncertain radius as:

$$r(\omega, \varphi) = r_0(\varphi) + \sum_{j=1}^{J} c_j Y_{2j-1}(\omega) \cos(j\varphi) + s_j Y_{2j}(\omega) \sin(j\varphi), \ \varphi \in [0, 2\pi), \ J \in \mathbb{N}, \omega \in \Omega. \quad (2.1)$$

In this formal expression, $r_0 = r_0(\varphi) \in C^k_{\text{per}}([0, 2\pi))$, $k \geq 1$, is referred to as the nominal shape, and it can be considered as an approximate parametrization of the mean shape. The truncation of the expansion in (2.1) is commonly referred to in the literature [1] as *finite noise assumption*. In the following, in particular in Section 6, we will ensure that all the estimates we will obtain hold *uniformly* in the truncation parameter $J \in \mathbb{N}$.

The random variables $\{Y_j\}_{j\geq 1}^{2J}$ are assumed to satisfy:

Assumption 2.2. *$\{Y_j\}_{j\geq 1}^{2J}$ are i.i.d. with $Y_j \sim \mathcal{U}[-1, 1]$ for every $1 \leq j \leq 2J$ and every $J \in \mathbb{N}$.*

In particular $\{Y_j\}_{j\geq 1}^{2J}$ have compact image, namely $|Y_j| \leq 1$ for every j. Thus, the only way to have a J-independent bound on the radius expansion (2.1) and a decay of its Fourier coefficients is to impose some constraints on the real coefficient sequences.

To ensure $\mathbb{P}$-a.s. boundedness and positivity at each angle φ for the stochastic radius r, we require that $r = r(\omega, \varphi)$ varies inside the range $[\frac{r_0(\varphi)}{2}, \frac{3r_0(\varphi)}{2}]$:

Assumption 2.3. *The coefficient sequences $\mathcal{C}$ and $\mathcal{S}$ in* (2.1) *satisfy*

$$\sum_{j\geq 1}(|c_j| + |s_j|) \leq \frac{r_0^-}{2},$$

with $r_0^- = inf_{\varphi\in[0,2\pi)} r_0(\varphi) > 0$.

For the Fourier coefficients, we require them to have a 'sufficiently fast' polynomial decay, in the sense made precise below. This can be ensured by either of the two following assumptions:

Assumption 2.4.A. *The sequences $\mathcal{C} := (c_j)_{j\geq 1}$ and $\mathcal{S} := (s_j)_{j\geq 1}$ have a monotonically decreasing majorant which belongs to $\ell^p(\mathbb{N})$ with $0 < p < \frac{1}{2}$.*

Assumption 2.4.B. *For every $\omega \in \Omega$, the radius $r(\omega, \varphi)$ as given in* (2.1) *belongs to $C^k_{per}([0, 2\pi))$, for an integer $k \geq 3$, with an ω-independent bound on $\left\| \frac{d^k r}{d\varphi^k}(\omega) \right\|_{L^1_{per}([0,2\pi))}$.*

We will see in Section 6, more precisely in Lemma 6.1, that Assumption 2.4.A implies Assumption 2.4.B, with a smoothness parameter $k = k(p)$, but only if p is small enough. Conversely, we have:

Proposition 2.5. *If Assumption 2.4.B is fulfilled, then the coefficients in* (2.1) *satisfy*

$$|c_j| \leq C(k)\frac{1}{1+j^k}, \quad |s_j| \leq C(k)\frac{1}{1+j^k} \quad j \geq 1, \tag{2.2}$$

with the same k as in Assumption 2.4.B and for a positive constant $C(k)$ dependent on k but independent of $j \geq 1$.

In particular, the sequences $\mathcal{C}$ and $\mathcal{S}$ have a monotonically decreasing majorant belonging to $\ell^p(\mathbb{N})$ for every $p > \frac{1}{k}$; since $k \geq 3$, we can choose p to be $0 < p < \frac{1}{2}$. In other words, if Assumption 2.4.B holds, then also Assumption 2.4.A does.

Proof. This is a consequence of the relationship between smoothness of a function and decay of its Fourier coefficient. We refer to the subsection A.2 in the appendix for the detailed proof. □

Remark 2.6. *Equation* (2.1) *can be rewritten as*

$$r(\omega, \varphi) = r_0(\varphi) + \sum_{l=1}^{L} \beta_l Y_l(\omega)\psi_l(\varphi), \quad \varphi \in [0, 2\pi), \quad L \in \mathbb{N}, \tag{2.3}$$

with $\psi_l = \cos(\frac{l+1}{2}\varphi)$ and $\beta_l = c_{\frac{l+1}{2}}$ if l is odd, $\psi_l = \sin(\frac{l}{2}\varphi)$ and $\beta_l = s_{\frac{l}{2}}$ if l is even. The truncation L is given by $L = 2J$, with J as in (2.1).

In general, any basis $(\psi_l)_{l\geq 1}$ of $L^2_{per}([0, 2\pi))$ could be considered, provided that $\psi_l \in C^1_{per}([0, 2\pi))$ for each $l \geq 1$. Nevertheless, the choice of the Fourier basis is particularly relevant in view of possible applications, when, for instance, (2.3) *is obtained from the Karhunen-Loève expansion of a rotationally invariant covariance kernel.*

2.2 Parametric formulation

In this subsection we recall via application to our case the standard parametrization procedure followed in stochastic Galerkin and stochastic collocation frameworks; we refer to [37] for an exhaustive survey of the topic.

From Assumption 2.2, we know that for each random variable $Y_j : \Omega \to \mathcal{P}_j$, $1 \leq j \leq 2J$, with $\mathcal{P}_j = [-1, 1]$ endowed with the Borel σ-algebra Σ_j, the distribution μ_j of Y_j is the uniform distribution. Then the sequence $(Y_j)_{j\geq 1}^{2J}$ defines a map

$$\boldsymbol{Y} : \Omega \to \mathcal{P}_J := \bigotimes_{j=1}^{2J} \mathcal{P}_j = [-1, 1]^{2J}, \quad \omega \mapsto (Y_j(\omega))_{j=1}^{2J}, \tag{2.4}$$

measurable with respect to the product σ-algebra $\Sigma := \bigotimes_{j=1}^{2J} \Sigma_j$ on $\mathcal{P}_J$. $\mathcal{P}_J$ is commonly referred to as the *parameter space*.

The random variables Y_j being independent, the distribution of $\boldsymbol{Y}$ is the product probability measure $\mu := \bigotimes_{j=1}^{2J} \mu_j$.

Now, we denote by $\boldsymbol{y} = (y_j)_{j=1}^{2J} \in \mathcal{P}_J$ one realization of the random variable $\boldsymbol{Y}$, so that we can rewrite (2.1) as

$$r(\boldsymbol{y}, \varphi) = r_0(\varphi) + \sum_{j=1}^{J} c_j y_{2j-1} \cos(j\varphi) + s_j y_{2j} \sin(j\varphi), \quad \boldsymbol{y} = (y_j)_{j=1}^{2J} \in \mathcal{P}_J,\ \varphi \in [0, 2\pi). \tag{2.5}$$

Remark 2.7. *In Assumption 2.2, the uniform distribution hypothesis for the random variables serves as a model and can be easily relaxed (see subsection A.3 in the appendix). The requirement that the random variables are mutually independent is instead harder to loosen. This is due to the fact that, if such condition is not fulfilled, then the joint probability distribution μ cannot be expressed as product of the univariate distributions anymore and one would need to adapt the theoretical convergence analysis under some assumptions on μ.*

3 Mapping to nominal geometry

In the first subsection we give a general description of the approach, while in the second subsection we apply it to our specific case of a particle in free space.

3.1 General description

To overcome the unboundedness of the domain, consider, in the domain with interface $\Gamma(\boldsymbol{y})$, a circle ∂K_R of arbitrary radius R containing the scatterer $D_2(\boldsymbol{y})$ in its interior. We consider ∂K_R to be *fixed for all realizations* $\boldsymbol{y} \in \mathcal{P}_J$, $J \in \mathbb{N}$, and we denote by K_R the region enclosed inside ∂K_R, no matter which realization $\Gamma(\boldsymbol{y})$ of the interface is considered.

Following the approach introduced, for instance, in [11], [23] and [41], we consider a *nominal configuration* of the domain K_R, where the interface $\hat{\Gamma}$ is *fixed*, i.e. independent of the realization $\boldsymbol{y}$, and a bijective parameter-dependent mapping

$$\begin{array}{rccc} \Phi(\boldsymbol{y}) : & K_R & \longrightarrow & K_R \\ & (\hat{x}_1, \hat{x}_2) & \mapsto & (x_1, x_2) \end{array} \tag{3.1}$$

from the nominal configuration to the domain K_R with interface $\Gamma(\boldsymbol{y})$.

A possible choice for $\hat{\Gamma}$ is the interface associated to the nominal radius r_0, or, in other words, to the case when $\boldsymbol{y} = \boldsymbol{0}$. In the following, we denote by $\hat{D}_2$ the scatterer region when

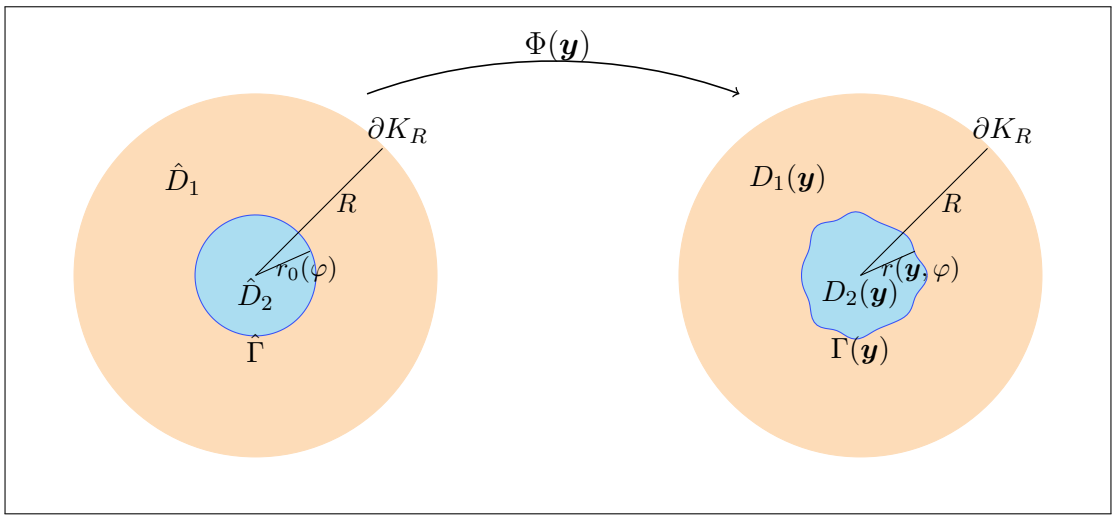

Figure 3.1: Mapping for the case of particle in free space.

the interface is $\hat{\Gamma}$, and $\hat{D}_1 := \mathbb{R}^2 \setminus \hat{D}_2$. In order to preserve the well-posedness of the problem as it will be discussed in Section 4, we formulate the following assumptions on Φ:

Assumption 3.1. *For every $\boldsymbol{y} \in \mathcal{P}_J$ and an integer $k \geq 1$, the mapping $\Phi(\boldsymbol{y}) : K_R \to K_R$ fulfills the following properties:*

(i) *$\Phi(\boldsymbol{y})$ is a C^k-orientation preserving diffeomorphism in each of the two subdomains $\hat{D}_1 \cap K_R$ and $\hat{D}_2$, with uniformly bounded norms, i.e.:*

$$\|\Phi(\boldsymbol{y})\|_{C^k_{\hat{pw}}(\overline{K_R})} \leq C_1, \quad \|\Phi^{-1}(\boldsymbol{y})\|_{C^k_{pw_{\boldsymbol{y}}}(\overline{K_R})} \leq C_2,$$

where C_1 and C_2 are independent of the truncation dimension $J \in \mathbb{N}$, and $\|\cdot\|_{C^k_{\hat{pw}}(\overline{K_R})} := \|\cdot\|_{C^k(\overline{\hat{D}_1 \cap K_R}) \cap C^k(\overline{\hat{D}_2})}$ (similarly in $\|\cdot\|_{C^k_{pw_{\boldsymbol{y}}}(\overline{K_R})}$ the discontinuities are allowed across $\Gamma(\boldsymbol{y})$).

(ii) *$\Phi(\boldsymbol{y})$ is the identity on ∂K_R:*

$$\Phi(\boldsymbol{y}, \hat{\boldsymbol{x}}) = \boldsymbol{x} \text{ for all } \hat{\boldsymbol{x}} \in \partial K_R.$$

(iii) *Let $\sigma_1 = \sigma_1(\boldsymbol{y}, \boldsymbol{x})$, $\sigma_2 = \sigma_2(\boldsymbol{y}, \boldsymbol{x})$ be the singular values of $D\Phi^{-1}(\boldsymbol{y})$; we require that there exist constants $\sigma_{min}, \sigma_{max} > 0$ independent of the truncation dimension $J \in \mathbb{N}$ such that*

$$\sigma_{min} \leq \|\sigma_1(\boldsymbol{y}, \cdot)\|_{C^0_{pw_{\boldsymbol{y}}}(\overline{K_R})}, \|\sigma_2(\boldsymbol{y}, \cdot)\|_{C^0_{pw_{\boldsymbol{y}}}(\overline{K_R})} \leq \sigma_{max} \quad \text{for all } \boldsymbol{y} \in \mathcal{P}_J,$$

(or, equivalently, analogous bounds hold for the singular values of $D\Phi(\boldsymbol{y})$).

3.2 The domain mapping for a particle in free space

In this case, we choose $r_0(\varphi)$ as the boundary of the scatterer in the nominal configuration, and map it to the boundary of the actual scatterer. The movement of the interface is propagated in the regions inside and outside the scatterer using a mollifier. In formulae, we have:

$$\boldsymbol{x}(\boldsymbol{y}) = \Phi(\boldsymbol{y}, \hat{\boldsymbol{x}}) = \hat{\boldsymbol{x}} + \chi(\hat{\boldsymbol{x}}) \left(r(\boldsymbol{y}, \hat{\varphi}) - r_0(\hat{\varphi}) \right), \tag{3.2}$$

with $\hat{\varphi} = \arg(\hat{\boldsymbol{x}}) = \arg(\boldsymbol{x}) = \varphi$. The map $\chi : K_R \mapsto K_R$ is a mollifier, satisfying the following conditions:

- $\chi(\hat{\boldsymbol{x}}) = \chi(\|\hat{\boldsymbol{x}}\|, r_0)$, that is, χ acts on the radial component of $\hat{\boldsymbol{x}} \in K_R$, and its dependence on the angle $\hat{\varphi}$ is only due to the fact that it depends on $r_0 = r_0(\varphi)$, $\varphi \in [0, 2\pi)$;

- $0 \leq \chi(\hat{\boldsymbol{x}}) \leq 1$, $\hat{\boldsymbol{x}} \in K_R$, with $\chi(\hat{\boldsymbol{x}}) = 0$ for $\|\hat{\boldsymbol{x}}\| \leq \frac{r_0^-}{4}$ (r_0^- being the quantity defined in Assumption 2.3) and for $\|\hat{\boldsymbol{x}}\| \geq \tilde{R}$ ($\tilde{R} \in \mathbb{R}$, $\sup_{[0,2\pi)} r_0(\varphi) + \frac{r_0^-}{2} < \tilde{R} \leq R$), and with $\chi(\hat{\boldsymbol{x}}) = 1$ for $\|\hat{\boldsymbol{x}}\| = r_0$;

- χ is monotone increasing for $\frac{r_0^-}{4} \leq \|\hat{\boldsymbol{x}}\| \leq r_0(\varphi)$ and monotone decreasing for $r_0(\varphi) \leq \|\hat{\boldsymbol{x}}\| \leq \tilde{R}$.

The map is illustrated in Figure 3.1. It fulfills Assumption 3.1 if the cut-off function satisfies the following:

Assumption 3.2. *The mollifier χ in (3.2) has in $\hat{D}_2$ and in $\hat{D}_1 \cap K_R$ at least the same smoothness as the nominal radius r_0 has in $[0, 2\pi)$. Furthermore,* $\max\left\{\|\chi\|_{C^1(\hat{D}_2)}, \|\chi\|_{C^1(\hat{D}_1 \cap K_R)}\right\} \leq C_\chi$, *for $C_\chi \in \mathbb{R}, 0 < C_\chi < \frac{\sqrt{2}}{r_0^-}$.*

We postpone the proof to Section 6 (Lemma 6.2).

In the region $\hat{D}_1 \cap K_R$, the multiplication by a mollifier is not, of course, the only way of propagating the movement of the interface. Among the valid alternatives we mention, for instance, the use of a harmonic extension [29].

4 Variational formulation and well-posedness of the model problem

In the first subsection we derive the variational formulation for the model problem (1.1), while in the second part of this section we address its well-posedness (in Hadamard's sense).

4.1 Variational formulation

As in the previous section, we consider the space K_R enclosed inside a circle of radius $R > 0$, the latter *fixed for all realizations* $\boldsymbol{y} \in \mathcal{P}_J$, and containing the scatterer in its interior (see Figure 4.1). Then, using the Dirichlet-to-Neumann map (DtN, see [33, Section 2.6.3]), we can state the variational formulation for (1.1) on the *bounded* domain K_R. Applying the parametric description of the uncertain interface developed in Section 2, we obtain:

Find $u(\boldsymbol{y}) \in V$:

$$\begin{aligned} a_y(u(\boldsymbol{y}), v) &:= \int_{K_R} \alpha(\boldsymbol{y}, \boldsymbol{x})\, \nabla u(\boldsymbol{y}) \cdot \nabla v - k^2(\boldsymbol{y}, \boldsymbol{x})\, u(\boldsymbol{y}) \cdot v \, d\boldsymbol{x} \\ &\quad - \int_{\partial K_R} DtN(u(\boldsymbol{y}))v \, dS \\ &= \int_{\partial K_R} \left(-DtN(u_i) + \frac{\partial u_i}{\partial \boldsymbol{n}_R}\right) v \, dS \quad \text{for all } v \in V \text{ and all } \boldsymbol{y} \in \mathcal{P}_J, \end{aligned} \tag{4.1}$$

where $V := H^1(K_R)$ and $\boldsymbol{n}_R$ is the outer normal to K_R.

Now, we use the inverse of the map $\Phi(\boldsymbol{y})$, $\boldsymbol{y} \in \mathcal{P}_J$, introduced in Section 3, to map the physical configuration with interface $\Gamma(\boldsymbol{y})$ to the nominal configuration (with interface $\hat{\Gamma}$).

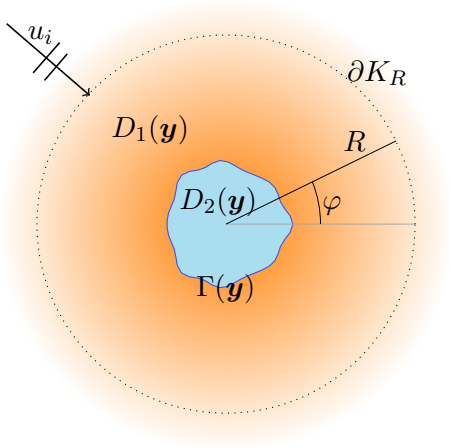

Figure 4.1: Domain considered in (4.1)

Reordering the terms, we obtain the following parametric, variational formulation on the *fixed*, deterministic configuration with interface $\hat{\Gamma}$:

$$\begin{aligned}
&\text{Find } \hat{u}(\boldsymbol{y}) \in \hat{V} : \\
&\quad \hat{a}_y(\hat{u}(\boldsymbol{y}), \hat{v}) = \int_{K_R} \hat{\alpha}(\boldsymbol{y}, \hat{\boldsymbol{x}})\, \hat{\nabla}\hat{u}(\boldsymbol{y}) \cdot \hat{\nabla}\hat{v}\, d\hat{\boldsymbol{x}} - \hat{k}^2(\boldsymbol{y}, \hat{\boldsymbol{x}})\, \hat{u}(\boldsymbol{y}) \cdot \hat{v}\, d\hat{\boldsymbol{x}} \\
&\qquad\qquad - \int_{\partial K_R} DtN(\hat{u}(\boldsymbol{y}))\hat{v}\, dS \\
&\qquad\qquad = \int_{\partial K_R} \left(-DtN(u_i) + \frac{\partial u_i}{\partial \boldsymbol{n}_R} \right) \hat{v}\, dS \quad \text{for all } \hat{v} \in \hat{V} \text{ and all } \boldsymbol{y} \in \mathcal{P}_J, \qquad (4.2)
\end{aligned}$$

where $\hat{V} = H^1(K_R) = V$ and

$$\begin{aligned}
\hat{\alpha}(\boldsymbol{y}, \hat{\boldsymbol{x}}) &= D\Phi(\boldsymbol{y})^{-1} D\Phi(\boldsymbol{y})^{-\top} \det D\Phi(\boldsymbol{y}) \alpha(\boldsymbol{y}, \Phi^{-1}(\boldsymbol{y})(\boldsymbol{x})) \\
\hat{k}^2(\boldsymbol{y}, \hat{\boldsymbol{x}}) &= \det D\Phi(\boldsymbol{y}) k^2(\boldsymbol{y}, \Phi^{-1}(\boldsymbol{y})(\boldsymbol{x})), \qquad (4.3)
\end{aligned}$$

with $D\Phi(\boldsymbol{y})$ the Jacobian matrix of $\Phi(\boldsymbol{y})$. In (4.2), $\hat{\nabla}$ denotes the gradient with respect to $\hat{\boldsymbol{x}} \in K_R$, the coordinates in the nominal configuration.

Remark 4.1. *Formulas* (4.3) *explain why we have to require* $k \geq 1$ *in Assumption 3.1 and* $p < \frac{1}{2}$ *in Assumption 2.4.A (since in general* $D\Phi$ *and its inverse will depend on* $\dfrac{\partial r}{\partial \varphi}$*).*

We are now in a position to give a rigorous definition for the solution to (4.1):

Definition 4.2. *The function* $u(\boldsymbol{y})$, $\boldsymbol{y} \in \mathcal{P}_J$, *is a solution to* (4.1) *if and only if its pullback* $(\Phi^*(\boldsymbol{y})u(\boldsymbol{y}))(\hat{\boldsymbol{x}}) := u(\Phi(\boldsymbol{y}, \hat{\boldsymbol{x}})) \in H^1(K_R)$ *is a solution to* (4.2).

4.2 Well-posedness of the model problem

As regards existence and uniqueness of the solution, they are ensured by the following theorem:

Theorem 4.3. *The solution to the variational formulation* (4.1) *exists and is unique, for every* $J \in \mathbb{N}$ *and every* $\boldsymbol{y} \in \mathcal{P}_J$. *Equivalently, if Assumption 3.1 is fulfilled, then* (4.2) *admits a unique solution for every* $J \in \mathbb{N}$ *and every* $\boldsymbol{y} \in \mathcal{P}_J$.

Proof. The boundedness of K_R allows us to apply the Fredholm Alternative [30, Theorem 2.27] to get existence of the solution to (4.2), while uniqueness is ensured by the sign properties of the DtN map. We refer to subsection A.4 in the appendix for the detailed proof. □

To have well-posedness of the problem, we still have to prove that the solution to (4.2) depends continuously on the data, which in our case consist of the incoming wave u_i. Thus, we would desire to have a bound on the $H^1(K_R)$-norm of $\hat{u}$ by some norm of u_i. This stability property will be needed later for convergence purposes (Section 5).

Unfortunately, a $\boldsymbol{y}$-uniform stability result cannot be achieved in general for the Helmholtz equation. The reason being that, without any limitation on the wavenumber modulus, it can happen that a small wavenumber excites resonances at the boundary of the scatterer, with an uncontrollable increase of the amplitude of the field u in that region.

Therefore, we formulate the following hypothesis:

Assumption 4.4 (Large wavelength assumption)**.** *The wavenumbers in* (1.2) *satisfy the condition:*

$$k_1^2, k_2^2 \leq \tau\, C(R), \quad \text{for some } 0 < \tau < \min\{1, \mu\}, \tag{4.4}$$

with

$$C(R) = \inf_{w \in H^1(K_R)} \frac{|w|^2_{H^1(K_R)} + \|w\|^2_{L^2(\partial K_R)}}{\|w\|^2_{L^2(K_R)}}. \tag{4.5}$$

For reasons that will become clearer in Section 5, we need a bound for the solution on the nominal configuration which is uniform over all the realizations, i.e. independent of the truncation dimension $J \in \mathbb{N}$ and of $\boldsymbol{y} \in \mathcal{P}_J$ in (2.5). To this aim, a necessary condition is to prove coercivity of the bilinear form $\hat{a}_y(\cdot,\cdot)$ with a positive coercivity constant uniform in $J \in \mathbb{N}$. The following lemma shows that, if the domain mapping satisfies Assumption 3.1, then Assumption 4.4 ensures uniform stability for (4.2) under some constraints on the constant τ:

Lemma 4.5. *Let Assumption 3.1 be satisfied. There exists a constant $0 < T < 1$ independent of $J \in \mathbb{N}$ such that, if Assumption 4.4 holds with $\tau < T$, then:*

(a) the bilinear form $\hat{a}_y(\cdot,\cdot)$ in (4.2) *is coercive, with coercivity constant independent of $J \in \mathbb{N}$ and $\boldsymbol{y} \in \mathcal{P}_J$;*

(b) there exist positive constants B_1, B_2 independent of $J \in \mathbb{N}$ and of $\boldsymbol{y} \in \mathcal{P}_J$ (but which do depend on $\mu, \sigma_{min}, \sigma_{max}, k_1, k_2$ and R) such that, for every $\boldsymbol{y} \in \mathcal{P}_J$:

$$\|\hat{u}(\boldsymbol{y})\|_{H^1(K_R)} \leq B_1 \|u_i\|_{H^{\frac{1}{2}}(\partial K_R)} + B_2 \left\| \frac{\partial u_i}{\partial \boldsymbol{n}_R} \right\|_{H^{-\frac{1}{2}}(\partial K_R)}. \tag{4.6}$$

The bound is uniform over the realizations once we use the analytic expression for $\dfrac{\partial u_i}{\partial \boldsymbol{n}_i}$, i.e. $\dfrac{\partial u_i}{\partial \boldsymbol{n}_R} = \boldsymbol{k}_1 \cdot \boldsymbol{n}_R e^{i\boldsymbol{k}_1 \cdot \boldsymbol{x}}$ for the incoming wave.

Proof. Here we just give a sketch of the proof, the details can be found in subsection A.5 of the appendix.

Using the upper and lower bounds for singular values of the mapping Φ given by Assumption 3.1 (*iii*) and the inequality (4.4) in Assumption 4.4, one obtains that $\hat{a}_y(\cdot,\cdot)$ is coercive with coercivity constant independent of $J \in \mathbb{N}$ and $\boldsymbol{y} \in \mathcal{P}_J$ if we choose $T := \sigma^2_{\min} \min\left\{ \frac{\sigma^2_{\min}}{\sigma^2_{\max}} \min\{1, \mu\}, 1 \right\}$. This proves part (*a*). Then part (*b*) follows immediately applying the stability bound given by the Lax Milgram lemma. □

The variational form (4.2) is now ready to be discretized. Notice that in this case *two* discretizations are needed: the discretization in the parameter space and the discretization in the physical space. The former will be considered in Section 5, while for the latter we will rely on a standard finite element discretization, of which we will give more details in Section 6.

5 Stochastic collocation and Smolyak algorithm

In this section we address the parameter space discretization of (4.2) through stochastic collocation. In the first subsection we recall the main features of sparse interpolation and quadrature. In the second subsection, we describe the sparse adaptive Smolyak algorithm used in our numerical experiments to select the collocation points. In the third and last subsection, we show that the hypothesis for the convergence theorems for the sparse interpolation and quadrature hold for the Helmholtz transmission problem.

In the first two subsections, we present the results in the general case that the parameter space is $\mathcal{P} := [-1,1]^d$ with d large and possibly infinite (in the latter case we write $[-1,1]^\infty = \bigotimes_{j=1}^{\infty}[-1,1]$ for the set of infinite sequences where every term is in $[-1,1]$). When we apply them to our model problem, we consider then $\mathcal{P}_J = [-1,1]^{2J}$ as parameter space (i.e. $d = 2J$).

5.1 High-dimensional sparse polynomial interpolation and quadrature

Here we only recall the main definitions and properties that will be used in the continuation of the paper. For an exhaustive survey on stochastic collocation, we refer to [1] and [40]. Details on sparse polynomial interpolation and sparse quadrature can be found in [9] and [35], respectively.

Univariate operators and tensorization

Let $\left(\zeta_j^k\right)_{j=0}^{n_k}$ be a sequence of distinct points in $\mathcal{P}_l = [-1,1]$ (for a generic $l \geq 1$), associated to the weights $\left(w_j^k\right)_{j=0}^{n_k}$. The the univariate polynomial interpolation operator I_k and the univariate quadrature operator Q_k associated to the points $\{\zeta_0, \ldots, \zeta_{n_k}\}$ are defined as

$$I_k g = \sum_{i=0}^{n_k} g(\zeta_i) l_i^{n_k}, \quad Q_k g = \sum_{i=0}^{n_k} w_i^{n_k} \cdot g(\zeta_i^k) = \int_{-1}^{1} I_k g(\zeta)\, d\zeta, \tag{5.1}$$

where g is a real- or complex-valued function defined on $[-1,1]$ and $l_i^{n_k}(y) = \prod_{\substack{j=0 \\ j\neq i}}^{n_k} \frac{y-\zeta_j}{\zeta_i-\zeta_j}$ is the Lagrange polynomial associated to the nodes $\{\zeta_0, \ldots, \zeta_k\}$.

Let $\mathcal{I}(\cdot)$ be the exact integration operator. For the quadrature operators, we require:

Assumption 5.1. *For each $k \in \mathbb{N}_0$, the univariate quadrature formula Q_k associated to the quadrature points $\left(\zeta_j^k\right)_{j=0}^{n_k}$ satisfies:*

(i) Q_k is of order k, i.e. $(\mathcal{I} - Q_k)(p_k) = 0$ for all $p_k \in \mathbb{P}_k$, with $\mathbb{P}_k$ the set of polynomials up to the k-th degree;

(ii) one of the two following condition holds:

(a) $w_j^k > 0$ for each $0 \leq j \leq n_k$;

(b) the Lebesgue constants λ_k of I_k, $k \geq 0$, grow at most polynomially with n_k.

The univariate interpolation and quadrature difference operators are defined as

$$\Delta_k^I = I_k - I_{k-1}, \quad \Delta_k^Q = Q_k - Q_{k-1}, \quad k \geq 0, \tag{5.2}$$

where we set $I_{-1} = 0$, so that $\Delta_0^I g = g(\zeta_0)$, and $Q_{-1} = 0$; moreover, we require $\zeta_0^0 = 0$, $w_0^0 = 1$, so that $Q_0 g = g(0)$. Therefore, (5.1) can be rewritten as

$$I_k = \sum_{j=0}^{k} \Delta_j^I, \quad Q_k = \sum_{j=0}^{k} \Delta_j^Q. \tag{5.3}$$

We remark that any univariate family of interpolation points can be used for the above construction, in particular the sequences need not to be nested.

To extend these concepts to the multi-dimensional case, we introduce the set

$$\mathcal{F} = \left\{ \nu \in \mathbb{N}_0^{\mathbb{N}} : \sharp \operatorname{supp} \nu < \infty \right\}, \tag{5.4}$$

with $\mathbb{N}_0 = \mathbb{N} \cup \{0\}$ and the support of a multi-index defined as $\operatorname{supp} \nu = \{j \in \mathbb{N} : \nu_j \neq 0\}$.

To any multi-index $\nu \in \mathcal{F}$, we associate the set of multivariate points $\boldsymbol{\zeta}_\nu = \bigotimes_{j \geq 1} \left(\zeta_i^{\nu_j}\right)_{i=0}^{n_{\nu_j}} \subset \mathcal{P}$ and the tensorized multivariate operators

$$I_\nu = \bigotimes_{j \geq 1} I_{\nu_j} \quad \text{and} \quad \Delta_\nu^I = \bigotimes_{j \geq 1} \Delta_{\nu_j}^I, \tag{5.5}$$

$$Q_\nu = \bigotimes_{j \geq 1} Q_{\nu_j} \quad \text{and} \quad \Delta_\nu^Q = \bigotimes_{j \geq 1} \Delta_{\nu_j}^Q. \tag{5.6}$$

We refer to [9, p.608] and [35, p.9] for a more rigorous definition, using induction, of the tensorized interpolation and quadrature operators respectively.

Sparse interpolation and quadrature operators

To define sparse interpolation and quadrature operators, we introduce the following notion:

Definition 5.2. *(Definition 3.1 in [35]) A subset $\Lambda \subset \mathcal{F}$ of finite cardinality N is called downward closed*[1] *if $\{0\} \subset \Lambda$ and if, for every $\nu \in \Lambda$, $\nu \neq 0$, it holds that $\nu - e_j \in \Lambda$ for all $j \in \operatorname{supp} \nu$, where $e_j \in \{0,1\}^{\mathbb{N}}$ denotes the index vector with 1 in position $j \in \mathbb{N}$ and 0 in all other positions $i \in \mathbb{N} \setminus \{j\}$.*

For any downward closed set $\Lambda \subset \mathcal{F}$, the sparse interpolation and quadrature operator are

$$I_\Lambda = \sum_{\nu \in \Lambda} \Delta_\nu^I, \quad Q_\Lambda = \sum_{\nu \in \Lambda} \Delta_\nu^Q, \tag{5.7}$$

with Δ_ν^I and Δ_ν^Q the multivariate difference operators defined in (5.5) and (5.6), respectively. Theorem 2.1 in [9] and Theorem 4.2 in [35] ensure that these operators are well defined.

We have introduced the definitions for the case that g is a real- or complex-valued function, but they can be extended in a straightforward way to functions taking values in separable Banach spaces, see [9] and [35] for details.

Best N-term convergence rates for sparse interpolation and quadrature

For $s > 1$, we define the Bernstein ellipse in the complex plane as $\mathcal{E}_s := \left\{ \frac{w+w^{-1}}{2} : 1 \leq |w| \leq s \right\}$. Given a sequence $\boldsymbol{\rho} := (\rho_l)_{l \geq 1}$, $\mathcal{E}_{\boldsymbol{\rho}} = \bigotimes_{l \geq 1} \mathcal{E}_{\rho_l}$ denotes the tensorized polyellipse [11].

[1] Also referred to in the literature as *lower index sets* or *monotone index sets*.

For the convergence results for the sparse interpolation and quadrature operators to hold, we need that the function that we want to interpolate or of which we want to compute the integral fulfills some regularity properties [11, 35, 36]:

$(\boldsymbol{b}, p, \varepsilon)$-holomorphy assumption
Let $g : \mathcal{P} \to V$ denote a bounded, continuous function of countably many variables $y_1, y_2, ...$, defined on $\mathcal{P} = [-1, 1]^\infty$ and taking values in a separable Hilbert space V. We require that:
(i) Given a positive sequence $\boldsymbol{b} = (b_l)_{l\geq 1} \in \ell^p(\mathbb{N})$ for some $0 < p < 1$, there exists a real number $0 < \varepsilon < 1$ such that, for every $(\boldsymbol{b}, \varepsilon)$-admissible sequence of poly-radii, i.e. for every sequence $\boldsymbol{\rho} = (\rho_l)_{l\geq 1}$ such that $\rho_l > 1$ and

$$\sum_{l\geq 1}(\rho_l - 1)b_l \leq \varepsilon, \tag{5.8}$$

the solution map $\boldsymbol{y} \mapsto g(\boldsymbol{y})$ admits a holomorphic extension to a set of the form $\mathcal{O}_{\boldsymbol{\rho}} := \bigotimes_{l\geq 1} \mathcal{O}_{\rho_l}$, with $\mathcal{O}_{\rho_l} \subset \mathbb{C}$ an open set containing $\mathcal{E}_{\rho_l}$, $l \geq 1$.
(ii) *g* satisfies an a priori estimate (uniform upper bound)

$$\sup_{\boldsymbol{z}\in\mathcal{E}_{\boldsymbol{\rho}}} \|g(\boldsymbol{z})\|_V \leq B(\varepsilon)$$

for a constant $B = B(\varepsilon)$ independent of $\boldsymbol{\rho}$ and the dimension of the parameter space.

Lemma 5.2 in [11] ensures that, for $s > 1$, the open set $\mathcal{O}_s := \{z \in \mathbb{C} : \text{dist}(z, [-1, 1]) < s - 1\}$ is an open neighborhood of $\mathcal{E}_s$. Then, it's sufficient to verify the $(\boldsymbol{b}, p, \varepsilon)$-holomorphy assumption on sets of the form

$$\mathcal{O}_{\boldsymbol{\rho}} = \bigotimes_{l\geq 1} \mathcal{O}_{\rho_l}, \quad \text{with } \mathcal{O}_{\rho_l} = \{z \in \mathbb{C} : \text{dist}(z, [-1, 1]) < \rho_l - 1\}\,,\ l \geq 1. \tag{5.9}$$

Under the $(\boldsymbol{b}, p, \varepsilon)$-holomorphy assumption, one can prove the following convergence results:

Theorem 5.3. *(Theorem 4.4 in [9]) Let the $(\boldsymbol{b}, p, \varepsilon)$-holomorphy assumption be satisfied. If the univariate sequence $\left(\zeta_j^k\right)_{j=0}^{n_k}$ is chosen so that its Lebesgue constant λ_k satisfies $\lambda_k \leq (k + 1)^\theta$ for some $\theta > 1$, then there exists a sequence $(\Lambda_N)_{N\geq 1}$ of downward closed sets $\Lambda_N \subset \mathcal{F}$ such that $\sharp\Lambda_N = N$ and*

$$\|g - I_\Lambda g\|_{L^\infty(\mathcal{P},V)} \leq CN^{-s}, \quad s = \frac{1}{p} - 1. \tag{5.10}$$

Theorem 5.4. *(Lemma 4.10 in [35]) Let the $(\boldsymbol{b}, p, \varepsilon)$-holomorphy assumption and Assumption 5.1 be satisfied. Then there exists a sequence $(\Lambda_N)_{N\geq 1}$ of downward closed sets $\Lambda_N \subset \mathcal{F}$ such that $\sharp\Lambda_N \leq N$ and*

$$\|\mathcal{I}(g) - Q_\Lambda g\|_V \leq CN^{-s}, \quad s = \frac{1}{p} - 1. \tag{5.11}$$

These two results show convergence rates which depend only on p, referred to as the "sparsity class of the unknown", while they do not depend on the number of dimensions activated. This means that we can break the curse of dimensionality by algorithms which adaptively construct downward closed index sets for the sparse interpolation and quadrature operators, as the algorithm that we present in the next subsection.

5.2 The sparse adaptive Smolyak algorithm

The idea is to identify the index set Λ_N of the N indices in $\mathcal{F}$ giving the highest contribution to the approximations (5.7). However, the index set Λ_N built in this way would be nested but not downward closed and, even worse, the cardinality of the set that should be considered grows

exponentially with the number of dimensions activated and it would be infinite in the case of countably many parameters. To overcome this, one considers a local subset, referred to as the *reduced set of neighbors* of a given finite set $\Lambda \subset \mathcal{F}$, specifically [18]:

$$\mathcal{N}(\Lambda) = \{\nu \notin \Lambda : \nu - e_j \in \Lambda, \text{ for all } j \in \operatorname{supp} \nu \text{ and } \nu_j = 0, \text{ all } j > j(\Lambda) + 1\} \tag{5.12}$$

for any downward closed index set Λ, where $j(\Lambda) = \max\{j : \nu_j > 0 \text{ for some } \nu \in \Lambda\}$. Using this set of neighbors, at each iteration at most one additional dimension can be activated.

The algorithm constructs then an anisotropic downward closed index set Λ comprising those indices in $\mathcal{N}(\Lambda)$ which are expected to contribute most to the approximation (see [35] for more details):

Algorithm 1 Sparse adaptive Smolyak algorithm.

1: **function** ASG
2: Set $\Lambda_1 = \{0_{\mathcal{F}}\}, k = 1$ and compute $\Delta_0^Q(g)$.
3: Determine the reduced set of neighbors $\mathcal{N}(\Lambda_1)$.
4: Compute $\Delta_\nu^Q(g)$, for all $\nu \in \mathcal{N}(\Lambda_1)$.
5: **while** $\sum_{\nu \in \mathcal{N}(\Lambda_k)} \|\Delta_\nu^Q(g)\|_V > tol$ **do**
6: Set $\Lambda_{k+1} = \Lambda_k \cup \left\{\mu \in \mathcal{N}(\Lambda_k) : \|\Delta_\mu^Q(g)\|_V \geq \vartheta \max_{\nu \in \mathcal{N}_\Lambda} \|\Delta_\nu^Q(g)\|_V\right\}$.
7: Determine the reduced set of neighbors $\mathcal{N}(\Lambda_{k+1})$.
8: Compute $\Delta_\nu^Q(g)$, for all $\nu \in \mathcal{N}(\Lambda_{k+1})$.
9: Set $k = k + 1$.
10: **end while**
11: **end function**

In line 6, $\vartheta \in [0, 1]$ is a parameter chosen at the beginning of the algorithm, and determining how many indices in the reduced set of neighbors are included in the set Λ at each iteration. For $\theta = 1$, we have $\Lambda_{k+1} = \Lambda_k \cup \{\bar{\nu}\}$ with $\bar{\nu} = \operatorname{argmax}_{\nu \in \mathcal{N}_\Lambda} \|\Delta_\nu^Q(g)\|_V$.

For the interpolation, the difference operators are the ones defined in (5.5). For each $\nu \in \mathcal{F}$, $\|\Delta_\nu^Q(g)\|_V$ is replaced by $\|\Delta_\nu^I(g)\|_{L^\infty(\mathcal{P},V)}$, and the stopping criterion $\sum_{\nu \in \mathcal{N}(\Lambda_k)} \|\Delta_\nu^Q(g)\|_V \leq tol$ at line 5 of Algorithm 1 is substituted by the condition $\max_{\nu \in \mathcal{N}(\Lambda_k)} \|\Delta_\nu^I(g)\|_V \leq tol$.

5.3 Analyticity and uniform boundedness of solutions to elliptic PDEs

Let us now return to our model problem as stated in (4.2). We need to show that this case satisfies the $(\boldsymbol{b}, p, \varepsilon)$-holomorphy assumption, so that the convergence results stated in Theorem 5.3 and Theorem 5.4 hold.

If we proceeded as in [11, Section 6.3] and chose for $\boldsymbol{b}$ the sequence $b_l = \|\beta_l \psi_l\|_{C^0_{\text{per}}([0,2\pi))} + \|\beta_l \psi_l'\|_{C^0_{\text{per}}([0,2\pi))}$, with β_l and ψ_l, as in Remark 2.6, $l \geq 1$, then we would get a suboptimal convergence rate. Namely, if $(\beta_l)_{l \geq 1} \in \ell^p(\mathbb{N})$, we would get that the sequence $\boldsymbol{b}$ belongs to $\ell^{\frac{p}{1-p}}(\mathbb{N})$, due to the presence of the derivative; this would decrease the theoretical convergence rate to $s = \frac{1-p}{p} - 1 = \frac{1}{p} - 2$, fact that is not observed in the numerical experiments reported in Section 7.

We show here that we can actually still achieve a theoretical convergence rate of $s = \frac{1}{p} - 1$, which agrees with the results of Section 7. This constitutes, to our opinion, one of the main contributions of this paper. We replace the definition of $(\boldsymbol{b}, \varepsilon)$-admissible sequence of polyradii by the following:

Definition 5.5. *A sequence $\boldsymbol{\rho} = (\rho_l)_{l\geq 1}$ of polyradii, with $\rho_l \geq 1$ for every $l \in \mathbb{N}$, is said to be $(\boldsymbol{b}, \varepsilon)^*$-admissible if it is $(\boldsymbol{b}, \varepsilon)$-admissible as defined in* (5.8) *and if additionally it satisfies*

$$\sum_{l\geq 1} l(\rho_l - 1)b_l \leq C(\varepsilon) \tag{5.13}$$

with $C = C(\varepsilon) > 0$ a function such that $C \to 0$ as $\varepsilon \to 0$.

We use the term $(\boldsymbol{b}, p, \varepsilon)^*$-holomorphy assumption to denote the $(\boldsymbol{b}, p, \varepsilon)$-holomorphy assumption when $(\boldsymbol{b}, \varepsilon)$-admissible sequences are replaced by $(\boldsymbol{b}, \varepsilon)^*$-admissible sequences.

Our plan is to show that the $(\boldsymbol{b}, p, \varepsilon)^*$-holomorphy assumption is fulfilled; then, at the end of this subsection, we prove that Theorems 5.3 and 5.4 still hold if the $(\boldsymbol{b}, p, \varepsilon)$-holomorphy assumption is replaced by the $(\boldsymbol{b}, p, \varepsilon)^*$-holomorphy assumption.

We now choose the sequence $\boldsymbol{b}$ as

$$b_l = \|\beta_l \psi_l\|_{C^0_{\mathrm{per}}([0,2\pi))} = |\beta_l|, \quad l \geq 1. \tag{5.14}$$

Notice that, thanks to Assumption 2.4.A on the sequence $(\beta_l)_{l\geq 1}$ (i.e. existence of a monotone majorant belonging to $\ell^p(\mathbb{N})$ with $p < \frac{1}{2}$), there exist sequences of polyradii that are $(\boldsymbol{b}, \varepsilon)^*$-admissible.

Remark 5.6. *The condition expressed by the inequality in* (5.13)*, differently from the condition $\boldsymbol{b} \in \ell^p(\mathbb{N})$, entails an implicit ordering of the dimensions of the parameter space with respect to decreasing significance. However, thanks to Assumption 2.4.A, the bound $C(\varepsilon)$ in* (5.13) *does not depend on the sequence $\boldsymbol{b}$ itself but on its (monotonically decreasing) majorant.*

We first address the uniform bound required by part (ii) of the $(\boldsymbol{b}, p, \varepsilon)$-holomorphy assumption.

In order to ensure well-posedness of the problem with a parameter-independent upper bound on the solution for $\boldsymbol{z} \in \mathcal{O}_{\boldsymbol{\rho}}$, with $\boldsymbol{\rho}$ a $(\boldsymbol{b}, \varepsilon)^*$-admissible sequence, we have to impose a slightly stronger requirement than Assumption 3.1:

Assumption 5.7. *(i) The domain mapping $\Phi = \Phi(\boldsymbol{y})$, its Jacobian matrix $D\Phi(\boldsymbol{y})$ and its inverse $D\Phi^{-1}(\boldsymbol{y})$, $\boldsymbol{y} \in \mathcal{P}_J$, $J \in \mathbb{N}$, admit a holomorphic extension to the subsets $\mathcal{O}_{\boldsymbol{\rho}} \subset \mathbb{C}^{\mathbb{N}}$ as defined in* (5.9)*, for any $(\boldsymbol{b}, \varepsilon)^*$-admissible sequence of polyradii $\boldsymbol{\rho}$.*
(ii) For every $\boldsymbol{z} \in \mathcal{O}_{\boldsymbol{\rho}}$, $\Phi = \Phi(\boldsymbol{z})$ fulfills Assumption 3.1, with bounds possibly depending on ε. For Assumption 3.1(i), the requirement on the diffeomorphism to be orientation-preserving is replaced by: there exists a real constant $\sigma_- = \sigma(\varepsilon) > 0$ independent of $\boldsymbol{z} \in \mathcal{O}_{\boldsymbol{\rho}}$ such that

$$\operatorname{Re}\det D\Phi(\boldsymbol{z}) > \sigma(\varepsilon) \quad \text{for every } \boldsymbol{z} \in \mathcal{O}_{\boldsymbol{\rho}}. \tag{5.15}$$

Since in general the domain mapping Φ will depend on $r = r(\boldsymbol{z})$, $\boldsymbol{z} \in \mathcal{O}_{\boldsymbol{\rho}}$, to have Assumption 5.7 fulfilled we can expect that we need to ensure $\boldsymbol{z}$-uniform bounds and holomorphy of the radius and its derivative with respect to $\varphi \in [0, 2\pi)$. We show that $\boldsymbol{z}$-uniform bounds hold for $\operatorname{Re} r(\boldsymbol{z})$, $|r(\boldsymbol{z})|$ and $\left|\dfrac{\partial r}{\partial \varphi}(\boldsymbol{z})\right|$, and that such bounds are sufficient for the mapping 3.2 to satisfy Assumption 5.7. The analyticity proof is postponed to a later part of this subsection.

Assumption 2.3 ensures that there exist $0 < r^-, r^+ < \infty$ such that

$$r^- \leq r(\boldsymbol{y}, \varphi) \leq r^+ \quad \text{for a.e. } \varphi \in [0, 2\pi), \text{ all } J \in \mathbb{N}, \text{ and all } \boldsymbol{y} \in \mathcal{P}_J \tag{5.16}$$

(more precisely in our case $r^- = \frac{r_0^-}{2}$, $r^+ = r_0^+ + \frac{r_0^-}{2}$, with $r_0^+ = \sup_{\varphi\in[0,2\pi)} r_0(\varphi)$ and r_0^- as in 2.3). Moreover, Assumption 2.4.A guarantees (see e.g. subsection A.7 in the appendix) that there exists a J- and $\boldsymbol{y}$- independent constant $0 < C_r < \infty$ such that

$$\left\|\frac{\partial r}{\partial\varphi}(\boldsymbol{y})\right\|_{C^0_{\mathrm{per}}([0,2\pi))} \leq \left\|\frac{\partial r_0}{\partial\varphi}\right\|_{C^0_{\mathrm{per}}([0,2\pi))} + C_r \quad \text{for all } J\in\mathbb{N} \text{ and all } \boldsymbol{y}\in\mathcal{P}_J. \tag{5.17}$$

Using these facts, we can prove the following:

Lemma 5.8. *Let $\boldsymbol{b}$ be as in (5.14) and $0 < \varepsilon < \frac{r^-}{2}$, with r^- as in (5.16). Then, for every $(\boldsymbol{b},\varepsilon)^*$-admissible sequence $\boldsymbol{\rho}$ and every $\boldsymbol{z}\in\mathcal{O}_{\boldsymbol{\rho}}$, with $\mathcal{O}_{\boldsymbol{\rho}}$ as in (5.9), we have the $\boldsymbol{z}$-independent bounds*

$$\frac{r^-}{2} \leq \operatorname{Re} r(\boldsymbol{z},\varphi), \qquad \varphi\in[0,2\pi), \tag{5.18}$$

$$\frac{r^-}{2} \leq |r(\boldsymbol{z},\varphi)| \leq r^+ + \varepsilon, \qquad \varphi\in[0,2\pi), \tag{5.19}$$

$$\left|\frac{\partial r}{\partial\varphi}(\boldsymbol{z},\varphi)\right| \leq \left\|\frac{\partial r_0}{\partial\varphi}\right\|_{C^0_{per}([0,2\pi))} + C(\varepsilon), \qquad \varphi\in[0,2\pi), \tag{5.20}$$

with r^+ as in (5.16) and $C(\varepsilon)$ as in (5.13).

In particular, the mapping Φ defined in (3.2) fulfills Assumption 5.7 (ii).

Proof. The results follow immediately from the bounds (5.16) and (5.17). We refer to subsection A.6 in the appendix for the complete proof. □

The same argument used in the proof of Lemma 4.5 leads to:

Proposition 5.9. *Let the sequence $\boldsymbol{b}$ be as in (5.14) and $0 < \varepsilon < \frac{r^-}{2}$, with r^- as in (5.16).*

If the mapping Φ satisfies Assumption 5.7, then part (ii) of the $(\boldsymbol{b},p,\varepsilon)^*$-holomorphy assumption is fulfilled, i.e. there exist constants $B_1 = B_1(\varepsilon)$ and $B_2 = B_2(\varepsilon)$ such that

$$\sup_{\boldsymbol{z}\in\mathcal{O}_{\boldsymbol{\rho}}} \|\hat{u}(\boldsymbol{z})\|_{H^1(K_R)} \leq B_1(\varepsilon)\,\|u_i\|_{H^1(\partial K_R)} + B_2(\varepsilon)\left\|\frac{\partial u_i}{\partial \boldsymbol{n}_R}\right\|_{L^2(\partial K_R)} \tag{5.21}$$

for every $\mathcal{O}_{\boldsymbol{\rho}}$, with $\mathcal{O}_{\boldsymbol{\rho}}$ as in (5.9) and $\boldsymbol{\rho}$ any sequence of $(\boldsymbol{b},\varepsilon)^*$-admissible polyradii. The constants B_1 and B_2 are independent of $J\in\mathbb{N}$, $\boldsymbol{y}\in\mathcal{P}_J$ and $\boldsymbol{\rho}$.

In particular, the bound (5.21) holds for the mapping Φ given in (3.2).

To prove that part (i) of the $(\boldsymbol{b},p,\varepsilon)^*$-holomorphy assumption holds, we first show the existence of a holomorphic extension for the parameter-dependent radius (2.5) and its φ-derivative; from this, analyticity of the map $\Phi(\boldsymbol{y})$ and then of the solution to the PDE on the nominal configuration follow. The proof is rather general and actually it applies, with minor modifications, to any elliptic PDE as long as the parameter-dependent configuration can be mapped to a reference configuration through a mapping satisfying Assumption 5.7 and depending smoothly (in a sense to be specified later, see Remark 5.12) on the stochastic quantity $r = r(\boldsymbol{y})$.

Lemma 5.10. *For every $\boldsymbol{z}\in\mathcal{O}_{\boldsymbol{\rho}}$, with $\mathcal{O}_{\boldsymbol{\rho}}$ as in (5.9) and $\boldsymbol{\rho}$ any $(\boldsymbol{b},\varepsilon)^*$-admissible sequence, the maps $\boldsymbol{z}\mapsto r(\boldsymbol{z})\in C^k_{per}([0,2\pi))$ and $\boldsymbol{z}\mapsto\dfrac{\partial r}{\partial\varphi}(\boldsymbol{z})\in C^{k-1}_{per}([0,2\pi))$, $k\geq 1$, with $r = r(\boldsymbol{z})$ given by (2.5), are holomorphic.*

Proof. Thanks to Hartogs' theorem on separate analyticity (see e.g. [26, Section 2.4]), it is sufficient to show that $r(\boldsymbol{z})$ and $\dfrac{\partial r}{\partial\varphi}(\boldsymbol{z})$ are holomorphic with respect to each of the variables z_l, for every $l\geq 1$. Being both maps affine with respect to each of the z_l, $l\geq 1$, they are also holomorphic in $\mathcal{O}_{\rho_l}, l\geq 1$. □

Let $\mathrm{Diff}^k_{+,\hat{\mathrm{pw}}}(K_R, K_R)$ be the space of diffeomorphisms which are of order C^k in each of the two subdomains $\overline{\hat{D}_1 \cap K_R}$ and $\overline{\hat{D}_2}$, and with determinant with positive real part. Since algebraic sum, multiplication and division by holomorphic functions which are not zero is still holomorphic, it follows immediately from Lemma 5.10 that:

Lemma 5.11. *The mappings $\boldsymbol{z} \mapsto \Phi(\boldsymbol{z}, \cdot) \in \mathit{Diff}^k_{+,\hat{pw}}(K_R, K_R)$ and $\boldsymbol{z} \mapsto D\Phi^{-1}(\boldsymbol{z}, \cdot)$, with Φ defined in (3.2), are holomorphic in $\mathcal{O}_{\boldsymbol{\rho}}$, for every $k \geq 1$ such that $r(\boldsymbol{z}) \in C^k_{per}([0, 2\pi))$, and with $\mathcal{O}_{\boldsymbol{\rho}}$ as defined in (5.9) for any $(\boldsymbol{b}, \varepsilon)^*$-admissible sequence $\boldsymbol{\rho}$.*

Together with Lemma 5.8, this implies that the mapping defined in (3.2) satisfies Assumption 5.7.

Proof. It is easy to check that, thanks to Assumption 2.3, the denominators in (3.2) and in the entries of $D\Phi(\boldsymbol{z})$ and $D\Phi^{-1}(\boldsymbol{z})$ are never zero, for every $\boldsymbol{z} \in \mathcal{O}_{\boldsymbol{\rho}}$; thus $\boldsymbol{z} \mapsto \Phi(\boldsymbol{z})$, $\boldsymbol{z} \mapsto D\Phi(\boldsymbol{z})$ and $\boldsymbol{z} \mapsto D\Phi^{-1}(\boldsymbol{z})$ are holomorphic. □

Remark 5.12. *It is clear that our framework and in particular Lemma 5.11 fit not only the specific map Φ given in (3.2), but any map involving composition of r with holomorphic maps, as well as linear combinations, multiplications and divisions (when never zero), as long as Assumption 5.7 is satisfied.*

For the same reasons as for the previous lemma, we also have:

Lemma 5.13. *Let Assumption 5.7 be fulfilled. Then the coefficients $\hat{\alpha}(\boldsymbol{y})$, $\hat{k}^2(\boldsymbol{y})$ as defined in (4.3) are holomorphic when considered as maps from $\boldsymbol{z} \in \mathcal{O}_{\boldsymbol{\rho}}$ to $C^{k-1}_{\hat{pw}}(\overline{K_R})$.*

This lemma implies immediately:

Lemma 5.14. *Let Assumptions 4.4 and 5.7 hold, the former with $\tau < T$ and T as in Lemma 4.5. Then, if $\hat{u}$ is a solution to (4.2), the solution map $\boldsymbol{z} \mapsto \hat{u}(\boldsymbol{z})$, admits a holomorphic extension to any open set $\mathcal{O}_{\boldsymbol{\rho}} \subset \mathbb{C}^{\mathbb{N}}$ as defined in (5.9) with $\boldsymbol{\rho}$ a $(\boldsymbol{b}, \varepsilon)^*$-admissible sequence.*

For each variable z_l, $l \geq 1$, the complex derivative $(\partial_{z_l}\hat{u})(\boldsymbol{z}) \in \hat{V}$ is the weak solution to the variational problem:

$$
\begin{aligned}
&\textit{Find } (\partial_{z_l}\hat{u})(\boldsymbol{z}) \in \hat{V} : \\
&\int_{K_R} \left(\hat{\alpha}(\boldsymbol{z}, \hat{\boldsymbol{x}}) \hat{\nabla} \partial_{z_l}\hat{u}(\boldsymbol{z}, \hat{\boldsymbol{x}}) \cdot \hat{\nabla}\hat{v}(\hat{\boldsymbol{x}}) - \hat{k}^2(\boldsymbol{z}, \hat{\boldsymbol{x}}) \partial_{z_l}\hat{u}(\boldsymbol{z}, \hat{\boldsymbol{x}}) \hat{v}(\hat{\boldsymbol{x}}) \right) d\hat{\boldsymbol{x}} \\
&- \int_{\partial K_R} DtN(\partial_{z_l}\hat{u}(\boldsymbol{z}, \hat{\boldsymbol{x}}))\hat{v}(\hat{\boldsymbol{x}})\, dS = L_0(\boldsymbol{z}, \hat{v}) \quad \textit{for all } \hat{v} \in \hat{V} \textit{ and all } \boldsymbol{z} \in \mathcal{O}_{\boldsymbol{\rho}}. \qquad (5.22)
\end{aligned}
$$

The right-hand side L_0 is given by

$$
L_0(\boldsymbol{z}, \hat{v}) = \int_{K_R} -\frac{\partial \hat{\alpha}}{\partial z_l}(\boldsymbol{z}, \hat{\boldsymbol{x}}) \hat{\nabla}\hat{u}(\boldsymbol{z}, \hat{\boldsymbol{x}}) \cdot \hat{\nabla}\hat{v}(\hat{\boldsymbol{x}})\, d\hat{\boldsymbol{x}} + \frac{\partial \hat{k}^2}{\partial z_l}(\boldsymbol{z}, \hat{\boldsymbol{x}}) \hat{u}(\boldsymbol{z}, \hat{\boldsymbol{x}}) \hat{v}(\hat{\boldsymbol{x}})\, d\hat{\boldsymbol{x}}.
$$

In particular, this result holds if Assumption 4.4 if fulfilled (with $\tau < T$) and the domain mapping is the one defined in (3.2).

Proof. Lemma 5.13 shows that the bilinear form in (4.2), with $\boldsymbol{y} \in \mathcal{P}_J, J \in \mathbb{N}$, replaced by $\boldsymbol{z} \in \mathcal{O}_{\boldsymbol{\rho}}$, is holomorphic in $\mathcal{O}_{\boldsymbol{\rho}}$. The right-hand side in (4.2) does not depend on the stochastic parameter, so in this particular case we do not have to show its analyticity. Then, the result follows from Theorem 4.1 in [11]. □

We summarize the results obtained so far in the following proposition:

Proposition 5.15. *Let the parameter-dependent radius $r(\boldsymbol{y})$ characterizing a star-shaped stochastic interface be given by the expansion* (2.5) *and let Assumptions 2.2, 2.3, and 2.4.A or 2.4.B hold. If the map $\Phi(\boldsymbol{y}) : K_R \to K_R$ satisfies Assumption 5.7 and in particular if the mapping is given by* (3.2)*, then the solution $\hat{u}$ to* (4.2) *is holomorphic in every $\mathcal{O}_{\boldsymbol{\rho}}$ as defined in* (5.9)*, with $\boldsymbol{\rho}$ a $(\boldsymbol{b}, \varepsilon)^*$-admissible sequence of polyradii and $0 < \varepsilon < \frac{r^-}{2}$.*

It remains to prove that the convergence results of Theorems 5.3 and 5.4 are still valid for $(\boldsymbol{b}, \varepsilon)^*$-admissible sequences:

Proposition 5.16. *Let the positive sequence $\boldsymbol{b}$ in the $(\boldsymbol{b}, p, \varepsilon)$-holomorphy assumption fulfill Assumption 2.4.A.*

Then Theorem 2.2 in [11] and consequently Theorems 5.3 and 5.4 still hold if the $(\boldsymbol{b}, p, \varepsilon)$-holomorphy assumption is replaced by the $(\boldsymbol{b}, p, \varepsilon)^*$-assumption.

Proof. We have to show that the $(\boldsymbol{b}, p, \varepsilon)^*$-holomorphy assumption still guarantees the ℓ^p-summability of the sequence $(\|g_\nu\|_V)_{\nu\in\mathcal{F}}$, where g_ν, $\nu \in \mathcal{F}$, are the coefficients in the sparse Legendre expansion of the quantity of interest g (with L^∞-normalized univariate Legendre polynomials).

The result in the case that the $(\boldsymbol{b}, p, \varepsilon)$-holomorphy assumption is fulfilled is stated in Theorem 2.2 in [11]. The argument we present here boils down to a slight modification of the proof of that theorem. The estimate (2.16) in [11] reads

$$\|g_\nu\|_V \le \mathrm{B} \prod_{l\ge 1:\nu_l\neq 0} (2\nu_l + 1)\phi(\rho_l)\rho_l^{-\nu_l}, \quad \nu \in \mathcal{F}, \tag{5.23}$$

where $\phi(t) := \frac{\pi t}{2(t-1)}$ for $t > 1$, with in the case $\nu = \mathbf{0} = (0, 0, \ldots)$ the convention that the empty product equals 1.

This estimate is still valid in our case, because the only requirement for it is that a uniform upper bound $\sup_{\boldsymbol{z}\in\mathcal{E}_{\boldsymbol{\rho}}}\|g(\boldsymbol{z})\|_V \le \mathrm{B}$ holds, and in our case this is ensured by Proposition 5.9.

As for Theorem 2.2 in [11], for each coefficient g_ν, $\nu \in \mathcal{F}$, we design a particular sequence of polyradii $\boldsymbol{\rho}$ that depends on ν.

Let $M > 0$ be arbitrary but fixed, and $\bar{L} \in \mathbb{N}$, $\bar{L} > 1$, such that $\sum_{l>\bar{L}} lb_l \le \frac{\varepsilon}{4M}$ (and this choice of $\bar{L}$ is the only difference to the proof of Theorem 2.2 in [11]); $\bar{L}$ exists because, thanks to Assumption 2.4.A, the sequence $\boldsymbol{b}$ is polynomially decaying and belongs to $\ell^p(\mathbb{N})$ with $0 < p < \frac{1}{2}$ (for details see Corollary A.2 in the appendix and Proposition 2.5, respectively). Also, let $F := \{l \in \mathbb{N} : l > \bar{L}\}$ and $\nu_F := (\nu_{\bar{L}+1}, \nu_{\bar{L}+2}, \ldots)$, for any $\nu \in \mathcal{F}$. We define the sequence $\boldsymbol{\rho} = \boldsymbol{\rho}(\nu)$ as

$$\rho_l := 1 + \frac{\varepsilon}{4\|\boldsymbol{b}\|_{\ell^1(\mathbb{N})}} \text{ for } l \le \bar{L} \text{ and } \rho_l := 1 + \frac{\varepsilon}{4\|\boldsymbol{b}\|_{\ell^1(\mathbb{N})}} + M + \frac{\varepsilon}{2b_l}\frac{\nu_l}{1+|\nu_F|} \text{ for } l > \bar{L}, \tag{5.24}$$

where $|\nu_F| := \sum_{l>\bar{L}} \nu_l$. This sequence is the same as in the proof of Theorem 2.2 in [11], with just the different choice for $\bar{L}$ which still guarantees, however, that $\sum_{l>\bar{L}} b_l \le \frac{\varepsilon}{4M}$, as required in that proof. Thus, $\boldsymbol{\rho}$ as in (5.24) is still $(\boldsymbol{b}, \varepsilon)$-admissible. To show that the sequence is also $(\boldsymbol{b}, \varepsilon)^*$-admissible, it remains to check that it satisfies (5.13). We have:

$$\begin{aligned}\sum_{l\ge 1}(\rho_l - 1)lb_l &= \sum_{l\le\bar{L}}(\rho_l - 1)lb_l + \sum_{l>\bar{L}}(\rho_l - 1)lb_l \le \\ &\le \frac{\varepsilon}{4\|\boldsymbol{b}\|_{\ell^1(\mathbb{N})}}\sum_{l\le\bar{L}} lb_l + \frac{\varepsilon}{4\|\boldsymbol{b}\|_{\ell^1(\mathbb{N})}}\sum_{l>\bar{L}} lb_l + M\sum_{l>\bar{L}} lb_l + \frac{\varepsilon}{2}\sum_{l>\bar{L}}\frac{1}{b_l}\frac{\nu_l}{1+|\nu_F|}lb_l. \end{aligned}\tag{5.25}$$

Thanks to the assumptions on the sequence $\boldsymbol{b}$, Assumption 2.4.A guarantees that there exists a constant $C_{\boldsymbol{b}} > 0$, independent of ε, such that

$$\frac{\varepsilon}{4\|\boldsymbol{b}\|_{\ell^1(\mathbb{N})}} \sum_{l \le \bar{L}} l b_l + \frac{\varepsilon}{4\|\boldsymbol{b}\|_{\ell^1(\mathbb{N})}} \sum_{l > \bar{L}} l b_l \le C_{\boldsymbol{b}} \frac{\varepsilon}{2\|\boldsymbol{b}\|_{\ell^1(\mathbb{N})}}$$

(see Corollary A.2 in the appendix for details). Also, for the way we have chosen $\bar{L}$, it holds that $M \sum_{l>\bar{L}} l b_l \le \frac{\varepsilon}{4}$. For the last addend in (5.25), we get:

$$\sum_{l>\bar{L}} \frac{l\nu_l}{1+|\nu_F|} = \frac{1}{1+|\nu_F|} \sum_{l>\bar{L}} l\nu_l \le \frac{1}{1+|\nu_F|} m|\nu_F| < m,$$

with $m = \inf\{n \in \mathbb{N} : \nu_l = 0 \text{ for every } l > n\}$; we have that m is finite because $\nu \in \mathcal{F}$.

Collecting all the estimates for the addends in (5.25), we finally obtain:

$$\sum_{l\ge 1} (\rho_l - 1) l b_l \le C_{\boldsymbol{b}} \frac{\varepsilon}{2\|\boldsymbol{b}\|_{\ell^1(\mathbb{N})}} + \frac{\varepsilon}{4} + m\frac{\varepsilon}{2} = \left(C_{\boldsymbol{b}} \frac{1}{2\|\boldsymbol{b}\|_{\ell^1(\mathbb{N})}} + \frac{1}{4} + m\frac{1}{2} \right) \varepsilon. \tag{5.26}$$

Since $C_{\boldsymbol{b}}$ and m are independent of ε, we have that $C(\varepsilon) := \left(C_{\boldsymbol{b}} \frac{1}{2\|\boldsymbol{b}\|_{\ell^1(\mathbb{N})}} + \frac{1}{4} + m\frac{1}{2} \right) \varepsilon$ tends to 0 as ε tends to 0, which means that (5.13) is fulfilled.

The $(\boldsymbol{b}, \varepsilon)^*$-admissibility of the sequence ensures the bound (5.21). Thus, using the bound (5.23) with $\mathrm{B} = B(\varepsilon)$ the right-hand side in (5.21) and $\boldsymbol{\rho} = \boldsymbol{\rho}(\nu)$, we obtain the estimate

$$\|g_\nu\|_V \le B(\varepsilon) \prod_{l \ge 1 : \nu_l \neq 0} (2\nu_l + 1) \phi(\rho_l) \rho_l^{-\nu_l}, \quad \nu \in \mathcal{F} \setminus \{\mathbf{0}\}.$$

The rest of the proof is now a mere repetition of the proof of Theorem 2.2 in [11] (which is not affected by our different choice of $\bar{L}$). □

The last proposition together with Propositions 5.9 and 5.15 give finally

Theorem 5.17. *Let Assumptions 2.2, 2.3, 2.4.A or 2.4.B, and 4.4 be satisfied. Then the $(\boldsymbol{b}, p, \varepsilon)^*$-holomorphy assumption is fulfilled for the domain mapping (3.2) and the convergence rates given by Theorems 5.3 and 5.4 are achieved.*

For a generic domain mapping, the $(\boldsymbol{b}, p, \varepsilon)^*$-holomorphy assumption is satisfied and the convergence rates of Theorems 5.3 and 5.4 are achieved if the map fulfills Assumption 5.7.

6 Spatial regularity and convergence of the finite element solution

This section is devoted to first establishing the relationship between the order of summability p of the coefficient series $\mathcal{C} = (c_j)_{j\ge 1}$, $\mathcal{S} = (s_j)_{j\ge 1}$ in (2.5) and the regularity of the solution to (4.2) for a single parameter realization (subsection 6.1). This information is then used to get the order of convergence of the finite element solution and couple it to the convergence results for sparse interpolation and quadrature in the parameter space, so that in the end we get convergence estimates for the fully discretized solution. The latter estimates are first obtained in the simpler case that the same finite element discretization is used for all realizations (subsection 6.2.1); then, a more refined estimate is obtained for the case that the spatial discretization is different for each interpolation / quadrature point (subsection 6.2.2), although these results are restricted to nested sequences of points in the parameter space. Finally (subsection 6.3), the above convergence results are extended for linear output functionals as quantities of interest.

6.1 Spatial regularity of the parametric solution

We are going to prove that, under summability assumptions on the coefficient sequences $\mathcal{C} = (c_j)_{j\geq 1}$, $\mathcal{S} = (s_j)_{j\geq 1}$, the radius $r = r(\boldsymbol{y}, \varphi)$ given by (2.5) belongs to some regularity class; this will imply smoothness of the coefficients in the mapped equation (4.2) and thus smoothness of the solution.

It is important to highlight that, in view of the convergence estimates, we need norm bounds which are independent of the truncation dimension $J \in \mathbb{N}$ in the radius expansion.

The theorem implying smoothness of the solution to a PDE from the smoothness of the coefficients requires the latter to have essentially bounded derivatives. It turns out that the proper spaces in which to state regularity are the Sobolev spaces $W^{k,\infty}$ of functions with essentially bounded weak derivatives up to the k-th order. However, since we do not want to distinguish between weak and strong measurability of the coefficient maps $\omega \mapsto \hat{\alpha}(\omega)$, $\omega \mapsto \hat{k}(\omega)$, and, thus, of the solution map $\omega \mapsto \hat{u}(\omega)$, we prefer to work in separable Banach spaces. For this reason, we are going to state the regularity results in the spaces of piecewise-C^k functions.

6.1.1 From the regularity of the physical domain to the regularity of the PDE coefficients

Stating the regularity of the subdomains $D_1(\boldsymbol{y}) \cap K_R$ and $D_2(\boldsymbol{y})$ boils down to stating the regularity of the radius $r = r(\boldsymbol{y}, \varphi)$, expressed by the following lemma:

Lemma 6.1. *If the coefficient sequences $\mathcal{C}$, $\mathcal{S}$ satisfy Assumption 2.4.A (i.e. $\mathcal{C}, \mathcal{S} \in \ell^p(\mathbb{N})$ for $0 < p < \frac{1}{2}$), then the radius $r(\boldsymbol{y})$ given by (2.5) satisfies*

$$r(\boldsymbol{y}) \in C^k_{per}([0, 2\pi)), \quad \|r(\boldsymbol{y})\|_{C^k_{per}([0,2\pi))} \leq C(\mathcal{C}, \mathcal{S}), \quad \text{for all } J \in \mathbb{N} \text{ and all } \boldsymbol{y} \in \mathcal{P}_J, \tag{6.1}$$

under the assumption that the nominal radius r_0 belongs to $C^k_{per}([0, 2\pi))$ too. The constant C depends on the regularity parameter k and on the sequences $\mathcal{C} = (c_j)_{j\geq 1}$ and $\mathcal{S} = (s_j)_{j\geq 1}$, but not on the truncation dimension $J \in \mathbb{N}$ and on the realization $\boldsymbol{y} \in \mathcal{P}_J$. The regularity parameter k is given by:

$$k = \begin{cases} \left\lfloor \frac{1}{p} - 1 \right\rfloor & \text{if } \frac{1}{p} - 1 \text{ is not an integer} \\ \frac{1}{p} - 2 & \text{otherwise.} \end{cases} \tag{6.2}$$

In particular, if $0 < p < \frac{1}{4}$, then Assumption 2.4.A implies Assumption 2.4.B.

Proof. The proof consists of elementary computations and we refer to subsection A.7 in the appendix for it. □

We now investigate how the boundary smoothness entails smoothness of the map $\Phi(\boldsymbol{y})$. In particular, we show here that Assumption 3.1 is fulfilled in the case of the specific domain mapping 3.2, with an order of smoothness k depending on the smoothness of the stochastic radius. The same procedure can be adapted for other domain mappings.

Lemma 6.2. *Let Assumptions 2.3 and 2.4.A be satisfied, and let the nominal radius r_0 belong to $C^k_{per}([0, 2\pi))$, with k as in (6.2). Then the mapping Φ given by (3.2), with a mollifier fulfilling Assumption 3.2, satisfies Assumption 3.1, with k the smoothness parameter of the radius r.*

Proof. The statement is quite clear from (3.2), once one observes that $\Phi(\boldsymbol{y})$ consists just of scalings by $r(\boldsymbol{y})$ and r_0 smoothed by a function χ with the same smoothness as the nominal radius. The technical proof can be found in the Appendix, subsection A.8. □

From this we immediately have the following result, which holds in particular for the map (3.2).

Corollary 6.3. *Let Assumption 2.4.A hold and let the map $\Phi : \mathcal{P}_J \times K_R \longrightarrow \mathcal{P}_J \times K_R$ satisfy Assumption 3.1.*

Then, for every $r(\boldsymbol{y})$ given by (2.5) and every $\boldsymbol{y} \in \mathcal{P}_J$, the coefficients $\hat{\alpha}$ and $\hat{k}^2$ in (4.2) satisfy

$$\|\hat{\alpha}(\boldsymbol{y})\|_{C^{k-1}_{\hat{pw}}(\overline{K_R})} \leq C_1(\mathcal{C}, \mathcal{S}), \quad \|\hat{k}^2(\boldsymbol{y})\|_{C^{k-1}_{\hat{pw}}(\overline{K_R})} \leq C_2(\mathcal{C}, \mathcal{S}),$$

with $\|\cdot\|_{C^{k-1}_{\hat{pw}}(\overline{K_R})} := \|\cdot\|_{C^{k-1}(\overline{\hat{D}_1 \cap K_R}) \cap C^{k-1}(\overline{\hat{D}_2})}$, under the additional hypothesis (not needed if Assumption 2.4.B holds) that the nominal radius r_0 belongs to $C^k_{per}([0, 2\pi))$. The constants C_1 and C_2 depend on the regularity parameter k and on the coefficient sequences $\mathcal{C} = (c_j)_{j\geq 1}$, $\mathcal{S} = (s_j)_{j\geq 1}$, but they are independent of the truncation dimension $J \in \mathbb{N}$ and of and of $\boldsymbol{y} \in \mathcal{P}_J$; the regularity parameter k is the same as in Lemma 6.1.

6.1.2 Regularity of the solution

We are going to state this result in three steps: local interior regularity, local regularity at the interface $\hat{\Gamma}$ and at the boundary ∂K_R, and global regularity.

The local interior regularity is a consequence of Theorem 8.10 in [20]:

Theorem 6.4. *Let Assumptions 2.3 and 2.4.A hold and let the nominal radius r_0 belong to $C^k_{per}([0, 2\pi))$, with k as in Lemma 6.1. If $k \geq 2$, then, for any subdomain D' such that $\overline{D'} \subset K_R \cap \hat{D}_1$ or $\overline{D'} \subset \hat{D}_2$, the solution $\hat{u}(\boldsymbol{y})$ to (4.2) belongs to $H^k(D')$ and satisfies*

$$\|\hat{u}(\boldsymbol{y})\|_{H^k(D')} \leq C \|\hat{u}(\boldsymbol{y})\|_{H^1(K_R)}, \tag{6.3}$$

for $C = C(a_-, \mathcal{K}, d', k, |\hat{D}_1 \cap K_R|, |\hat{D}_2|)$, where $|\hat{D}_1 \cap K_R|$ and $|\hat{D}_2|$ denote the sizes of the two subdomains, $d' = \min\left\{dist(D', \partial K_R), dist(D', \hat{\Gamma})\right\}$ and

$$\mathcal{K} = \max\left\{ \sup_{\boldsymbol{y}\in\mathcal{P}_J, J\in\mathbb{N}} \|\hat{\alpha}(\boldsymbol{y})\|_{C^{k-1}_{\hat{pw}}(\overline{K_R})}, \sup_{\boldsymbol{y}\in\mathcal{P}_J, J\in\mathbb{N}} \|\hat{k}^2(\boldsymbol{y})\|_{C^{k-2}_{\hat{pw}}(\overline{K_R})} \right\}.$$

The symbol a_- denotes the uniform coercivity constant as in Lemma 4.5 (a), depending on the lower and upper singular value bounds $\sigma_{min}, \sigma_{max}$ for $D\Phi^{-1}(\boldsymbol{y})$ as from Assumption 3.1. In (6.3) we denoted $C^{k-1}_{\hat{pw}}(\overline{K_R}) := C^{k-1}\left(\overline{K_R \cap \hat{D}_1}\right) \cap C^{k-1}\left(\overline{\hat{D}_2}\right)$ and similarly for $C^{k-2}_{\hat{pw}}(\overline{K_R})$.

Furthermore, if Assumption 4.4 holds, then we have a J- and $\boldsymbol{y}$-independent bound:

$$\|\hat{u}(\boldsymbol{y})\|_{H^k(D')} \leq \tilde{C}\left(\|u_i\|_{H^{\frac{1}{2}}(\partial K_R)} + \left\| \frac{\partial u_i}{\partial \boldsymbol{n}_R} \right\|_{H^{-\frac{1}{2}}(\partial K_R)} \right) \tag{6.4}$$

with $\tilde{C} = \tilde{C}(R, a_-, \mathcal{K}, d', k, |\hat{D}_1 \cap K_R|, |\hat{D}_2|)$.

Proof. One can verify that, in Theorem 8.10 in [20], if the lower bound on the coercivity constant and the upper bounds on the PDE coefficients and right-hand side are independent on $J \in \mathbb{N}$ and $\boldsymbol{y} \in \mathcal{P}_J$, then the upper bound on $\|\hat{u}(\boldsymbol{y})\|_{H^k(D')}$ is also uniform in $J \in \mathbb{N}$ and $\boldsymbol{y} \in \mathcal{P}_J$.

In the case of equation (4.2), the lower bound on the coercivity constant is given by Lemma 4.5 (a), the upper bounds on the coefficients are ensured by Corollary 6.3, and the right-hand side is independent of $J \in \mathbb{N}$ and $\boldsymbol{y} \in \mathcal{P}_J$.

If Assumption 4.4 holds, then we can use (5.21) to bound $\|\hat{u}(\boldsymbol{y})\|_{H^1(K_R)}$, obtaining (6.4). □

The local regularity at the interface $\hat{\Gamma}$ and at ∂K_R follows from Theorem 4.20 in [30]:

Theorem 6.5. *Let Assumptions 2.3 and 2.4.A hold and let the nominal radius r_0 belong to $C^k_{per}([0,2\pi))$, with k as in Lemma 6.1. Moreover, let the interfaces $\hat{\Gamma}$ and ∂K_R be $C^{k-1,1}$. If k as in Lemma 6.1 is such that $k \geq 2$ (which automatically holds if Assumption 2.4.B is satisfied), then:*

- *for any subdomain $D' \subsetneq K_R$ intersecting $\hat{\Gamma}$ (but not ∂K_R), the solution $\hat{u}(\boldsymbol{y})$ to (4.2) belongs to $H^k(D' \cap \hat{D}_1) \cap H^k(D' \cap \hat{D}_2)$ and satisfies*

$$\|\hat{u}(\boldsymbol{y})\|_{H^k(D'\cap\hat{D}_1)\cap H^k(D'\cap\hat{D}_2)} \leq C\|\hat{u}(\boldsymbol{y})\|_{H^1(K_R\cap\hat{D}_1)\cap H^1(\hat{D}_2)} \tag{6.5}$$

  with $C = C(a_-, \mathcal{K}, d', k, |K_R|)$, where $d' = dist(D', \partial K_R)$ and the other constants defined as in Theorem 6.4.

- *for any open set D' intersecting ∂K_R (but not $\hat{\Gamma}$), the solution $\hat{u}(\boldsymbol{y})$ to (4.2) satisfies*

$$\|\hat{u}(\boldsymbol{y})\|_{H^k(D'\cap K_R)\cap H^k(D'\setminus K_R)} \leq C\|\hat{u}(\boldsymbol{y})\|_{H^1(K_{R'})},$$

  with $K_{R'}$ a circle of radius $R' > R$ containing D' in its interior, $C = C(a_-, \mathcal{K}, d', k, |K_{R'}|)$ with $d' = dist(D', \partial K_{R'})$ and the other constants defined as in Theorem 6.4.

Furthermore, if Assumption 4.4 holds in K_R and $K_{R'}$, then in both cases we have bounds on the norms which are independent of the truncation dimension $J \in \mathbb{N}$ and of $\boldsymbol{y} \in \mathcal{P}_J$:

$$\|\hat{u}(\boldsymbol{y})\|_{H^k(D'\cap\hat{D}_1)} + \|\hat{u}(\boldsymbol{y})\|_{H^k(D'\cap\hat{D}_2)} \leq \tilde{C}_1 \left(\|u_i\|_{H^{\frac{1}{2}}(\partial K_R)} + \left\| \frac{\partial u_i}{\partial \boldsymbol{n}_R} \right\|_{H^{-\frac{1}{2}}(\partial K_R)} \right)$$

$$\|\hat{u}(\boldsymbol{y})\|_{H^k(D'\cap K_R)} + \|\hat{u}(\boldsymbol{y})\|_{H^k(D'\setminus K_R)} \leq \tilde{C}_2 \left(\|u_i\|_{H^{\frac{1}{2}}(\partial K_{R'})} + \left\| \frac{\partial u_i}{\partial \boldsymbol{n}_{R'}} \right\|_{H^{-\frac{1}{2}}(\partial K_{R'})} \right)$$

Here, we considered the domain truncated at $\partial K_{R'}$ and ∂K_R as an interface because Assumption 3.1 allows the mapping Φ and its inverse to be nonsmooth across ∂K_R (and thus also the coefficients $\hat{\alpha}$ and $\hat{k}^2$ may be non smooth).

Proof. The proof is very similar to the one for Theorem 6.4: following the proof of Theorem 4.20 in [30], one can observe that a J- and $\boldsymbol{y}$-uniform lower bound on the coercivity constant and J- and $\boldsymbol{y}$-uniform upper bounds on the PDE coefficients and right-hand side ensure an upper bound on $\|\hat{u}(\boldsymbol{y})\|_{H^k(D')}$ that also uniform in $J \in \mathbb{N}$ and $\boldsymbol{y} \in \mathcal{P}_J$. Furthermore, applying Theorem 4.20 in [30] to our case, we do not need to care about boundary terms across the boundaries because we have no jumps of the solution or of its conormal derivative across $\hat{\Gamma}$ and ∂K_R. □

Considering Theorems 6.4 and 6.5 together we get the following global result:

Theorem 6.6. *Let Assumptions 2.3 and 2.4.A hold and let the nominal radius r_0 belong to $C^k_{per}([0,2\pi))$, with k as in Lemma 6.1. Let the map Φ be given by (3.2). Moreover, let the interface $\hat{\Gamma}$ be $C^{k-1,1}$. If k as in Lemma 6.1 is such that $k \geq 2$ (which automatically holds if Assumption 2.4.B is satisfied), then $\hat{u}$ belongs to $H^k(K_R \cap \hat{D}_1) \cap H^k(\hat{D}_2)$ and*

$$\|\hat{u}(\boldsymbol{y})\|_{H^k(K_R\cap\hat{D}_1)} + \|\hat{u}(\boldsymbol{y})\|_{H^k(\hat{D}_2)} \leq C\|\hat{u}(\boldsymbol{y})\|_{H^1(K_R)},$$

with $C = C(a_-, \mathcal{K}, k, |K_R|)$ independent of $J \in \mathbb{N}$ and of $\boldsymbol{y} \in \mathcal{P}_J$. In particular, if Assump-

tion 4.4 holds, then we have a J- and $\boldsymbol{y}$-independent bound

$$\|\hat{u}(\boldsymbol{y})\|_{H^k(K_R\cap\hat{D}_1)} + \|\hat{u}(\boldsymbol{y})\|_{H^k(\hat{D}_2)} \leq \tilde{C}\left(\|u_i\|_{H^{\frac{1}{2}}(\partial K_R)} + \left\|\frac{\partial u_i}{\partial \boldsymbol{n}_R}\right\|_{H^{-\frac{1}{2}}(\partial K_R)}\right), \tag{6.6}$$

with $\tilde{C} = \tilde{C}(a_-, \mathcal{K}, k, |K_R|)$. Here, a_- and $\mathcal{K}$ are defined as in Corollary 6.4.

Remark 6.7. *As it is evident from* (6.2)*, we have that $k \to \infty$ as $p \to 0$.*

Remark 6.8. *Theorem 6.6 holds not only for the map* (3.2)*, but for any map satisfying Assumption 3.1.*

6.2 Convergence of the fully discrete solution

The results stated in Theorems 5.3 and 5.4 assume that the solution $\hat{u} = \hat{u}(\boldsymbol{y})$ to (4.2) at the interpolation/quadrature points can be computed exactly, which is not usually the case in applications. Here we study instead the convergence of the sparse interpolation/quadrature algorithm coupled to a finite element discretization to compute the realizations. We consider a simplicial mesh on K_R, and assume that at ∂K_R the exact DtN map is available. Since we use a conforming discretization, for each $\boldsymbol{y} \in \mathcal{P}_J$ existence and uniqueness and stability of the discrete solution are inherited from the continuous case.

Throughout this subsection, $k \in \mathbb{N}$ denotes the spatial regularity of the exact solution as from Theorem 6.6.

6.2.1 Convergence estimate for fixed finite element discretization

We first observe that:

Lemma 6.9. *Let Assumptions 4.4 and 5.7 hold, the former with $\tau < T$ and T as in Lemma 4.5. Then the discrete finite element solution $\hat{u}_h(\boldsymbol{y})$ to* (4.2) *admits an analytic extension $\hat{u}_h(\boldsymbol{z})$ to the complex domain, with the same domain of analyticity $\mathcal{O}_{\boldsymbol{\rho}}$ as the exact solution $\hat{u}(\boldsymbol{y})$ ($\mathcal{O}_{\boldsymbol{\rho}}$ as defined in Eq.*(5.9)*, with $\boldsymbol{\rho}$ a $(\boldsymbol{b}, \varepsilon)^*$-admissible sequence) .*

Proof. Since the Galerkin solution still satisfies the variational formulation (4.2) on the discrete, finite-dimensional space, $\hat{V}_h \subset \hat{V}$, the proof is the same as for Lemma 5.14). □

The convergence estimate for the fully discrete solution follows then simply applying the triangle inequality:

Theorem 6.10. *Let $I_\Lambda \hat{u}_h$ and $Q_\Lambda \hat{u}_h$ denote the solutions obtained respectively from sparse interpolation and quadrature of the discrete solution $\hat{u}_h$ to* (4.2)*. For the interpolation, we assume that the Lebesgue constant λ_l associated to the univariate sequence of interpolation points $\left(\zeta_i^l\right)_{i=0}^{n_l}$ satisfies $\lambda_l \leq (l+1)^\theta$ for some $\theta > 0$; for the quadrature, we assume that Assumption 5.1 holds. Moreover, let Assumptions 4.4 and 5.7 be fulfilled. Assume that the same finite element discretization is used for all parameter realizations $\boldsymbol{y}_\nu$, $\nu \in \Lambda$, with polynomial order q and N_{dof} degrees of freedom, and that a q-th order boundary approximation is used for the interface $\hat{\Gamma}$.*

Then there exists a downward closed set Λ of cardinality at most N such that

$$\|\hat{u} - I_\Lambda \hat{u}_h\|_{L^\infty(\mathcal{P}_J, \hat{V})} \leq C N_{dof}^{-\frac{\min(k-1,q)}{2}} + C_1 N^{-s} \quad s = \frac{1}{p} - 1, \tag{6.7}$$

$$\|\mathcal{I}(\hat{u}) - Q_\Lambda \hat{u}_h\|_{\hat{V}} \leq C N_{dof}^{-\frac{\min(k-1,q)}{2}} + C_2 N^{-s} \quad s = \frac{1}{p} - 1. \tag{6.8}$$

with $k \geq 1$ and $s, C, C_1, C_2 > 0$ independent of N, N_{dof}, of the truncation dimension $J \in \mathbb{N}$ and of $\boldsymbol{y} \in \mathcal{P}_J$.

Proof. For each $\boldsymbol{y} \in \mathcal{P}_J$, we can write

$$\|\hat{u}(\boldsymbol{y}) - I_\Lambda \hat{u}_h(\boldsymbol{y})\|_{\hat{V}} \leq \|\hat{u}(\boldsymbol{y}) - \hat{u}_h(\boldsymbol{y})\|_{\hat{V}} + \|\hat{u}_h(\boldsymbol{y}) - I_\Lambda \hat{u}_h(\boldsymbol{y})\|_{\hat{V}}. \tag{6.9}$$

We highlight that when doing this splitting we exploit the fact that the same finite element space is used for all collocation / quadrature points, so that we can define $\hat{u}_h(\boldsymbol{y})$ for all $\boldsymbol{y} \in \mathcal{P}_J$.

Thanks to the classical results on finite element convergence (see e.g. [28], where the interface problem is considered), the first term is bounded by:

$$\|\hat{u}(\boldsymbol{y}) - \hat{u}_h(\boldsymbol{y})\|_{\hat{V}} \leq \tilde{C} N_{dof}^{-\frac{\min(k-1,q)}{2}} \|\hat{u}(\boldsymbol{y})\|_{H^k((K_R \cap \hat{D}_1)) \cap H^k(\hat{D}_2)}$$

for a constant $\tilde{C} > 0$ depending only on the mesh; combining this estimate with (6.6) in Theorem 6.6 (holding thanks to Assumptions 4.4 and 5.7), we obtain:

$$\|\hat{u}(\boldsymbol{y}) - \hat{u}_h(\boldsymbol{y})\|_{L^\infty(\mathcal{P}_J, \hat{V})} \leq C N_{dof}^{-\frac{\min(k-1,q)}{2}},$$

with C independent of $J \in \mathbb{N}$ and of $\boldsymbol{y} \in \mathcal{P}_J$. The bound for the second term in (6.9) follows directly from Lemma 6.9 and Theorem 5.3.

For the quadrature case, we have that

$$\|\mathcal{I}(\hat{u}(\boldsymbol{y})) - Q_\Lambda \hat{u}_h(\boldsymbol{y})\|_{\hat{V}} \leq \|\mathcal{I}(\hat{u}(\boldsymbol{y}) - \hat{u}_h(\boldsymbol{y}))\|_{\hat{V}} + \|\mathcal{I}(\hat{u}_h(\boldsymbol{y})) - Q_\Lambda \hat{u}_h(\boldsymbol{y})\|_{\hat{V}};$$

once we observe that $\|\mathcal{I}\| = 1$, the result follows as in the interpolation case using Theorem 5.4 to bound the second term. □

6.2.2 Convergence estimate for parameter-adaptive discretization

The idea is to distinguish the finite element error contribution for each difference operator Δ_ν^I as defined in (5.2) and (5.5) for the interpolation case, or Δ_ν^Q as defined in (5.2) and (5.6) for the quadrature case. The approach is the same as the one followed in [37] for the Legendre coefficients.

In the following theorem, we are going to denote by $\boldsymbol{H}_l(\boldsymbol{y})$ the multivariate hierarchical polynomial associated to the node $\boldsymbol{y}_l$ in the case of nested sequences of interpolation points (see [9] for details). Also, $\{\boldsymbol{y}_l \in \Delta_\nu^I\}$ (resp. $\{\boldsymbol{y}_l \in \Delta_\nu^Q\}$) indicates the set of new interpolation (resp. quadrature) points introduced by the difference operator Δ_ν^I (resp. Δ_ν^Q), w_l denotes the quadrature weight associated to $\boldsymbol{y}_l$ and $\mathbb{L}_{\mathcal{R}_\nu}$ is the Lebesgue constant of the interpolation operator $I_{\mathcal{R}_\nu}$ on $\mathcal{R}_\nu := \{\mu \in \mathcal{F} : \mu < \nu\}$.

Theorem 6.11. *Let $I_\Lambda \hat{u}_{h,\Lambda}$ and $Q_\Lambda \hat{u}_{h,\Lambda}$ denote the solutions obtained respectively from sparse interpolation and quadrature of the discrete solution $\hat{u}_{h,\Lambda}$ to (4.2). For the interpolation, we ask that the Lebesgue constant λ_l associated to the univariate sequence of interpolation points $\left(\zeta_i^l\right)_{i=0}^{n_l}$ satisfies $\lambda_l \leq (l+1)^\theta$ for some $\theta > 0$; for the quadrature, we assume that Assumption 5.1 holds. Let Assumptions 4.4 and 5.7 be fulfilled. Let us denote by q_l and $N_{dof,l}$ the polynomial order and number of degrees of freedom used to compute the solution $\hat{u}_{h,\Lambda}(\boldsymbol{y}_l)$ at the interpolation / quadrature point $\boldsymbol{y}_l$. Furthermore, let us suppose that, for each realization $\boldsymbol{y}_l$, a q_l-th order boundary approximation is used for the interface $\hat{\Gamma}$.*

Then there exists a downward closed set Λ of cardinality at most N such that

$$\|\hat{u} - I_\Lambda \hat{u}_{h,\Lambda}\|_{L^\infty(\mathcal{P}_J, \hat{V})} \leq \sum_{\nu \in \Lambda} \|\Delta_\nu^I(\hat{u} - \hat{u}_{h,\Lambda})\|_{L^\infty(\mathcal{P}_J, \hat{V})} + C_1 N^{-s} \quad s = \frac{1}{p} - 1, \tag{6.10}$$

$$\|\mathcal{I}(\hat{u}) - Q_\Lambda \hat{u}_{h,\Lambda}\|_{\hat{V}} \leq \sum_{\nu \in \Lambda} \|\Delta_\nu^Q(\hat{u} - \hat{u}_{h,\Lambda})\|_{\hat{V}} + C_2 N^{-s} \quad s = \frac{1}{p} - 1, \tag{6.11}$$

with $s, C_1, C_2 > 0$ independent of N, N_{dof}, of $J \in \mathbb{N}$ and of $\boldsymbol{y} \in \mathcal{P}_J$.

If the sequences $(\zeta_i)_{i\geq 0}$ of interpolation / quadrature points are nested, then the addends in the first sum satisfy, for the interpolation and quadrature case respectively:

$$\|\Delta_\nu^I(\hat{u} - \hat{u}_{h,\Lambda})\|_{L^\infty(\mathcal{P}_J,\hat{V})} \leq (1 + \mathbb{L}_{\mathcal{R}_\nu})C(k) \cdot \sum_{\boldsymbol{y}_l \in \Delta_\nu^I} \|\boldsymbol{H}_l(\cdot)\|_{L^\infty(\mathcal{P}_J)} N_{dof,l}^{-\frac{\min(k-1,q_l)}{2}} \|\hat{u}(\boldsymbol{y}_l)\|_{H^k((K_R\cap\hat{D}_1))\cap H^k(\hat{D}_2)} \tag{6.12}$$

$$\|\Delta_\nu^Q(\hat{u} - \hat{u}_{h,\Lambda})\|_{\hat{V}} \leq C(k) \sum_{\boldsymbol{y}_l \in \Delta_\nu^Q} |w_l| N_{dof,l}^{-\frac{\min(k-1,q_l)}{2}} \|\hat{u}(\boldsymbol{y}_l)\|_{H^k((K_R\cap\hat{D}_1))\cap H^k(\hat{D}_2)}, \tag{6.13}$$

with C independent of N, N_{dof}, of $J \in \mathbb{N}$ and of $\boldsymbol{y} \in \mathcal{P}_J$. The Lebesgue constant is bounded by $\mathbb{L}_{\mathcal{R}_\nu} \leq (\sharp\mathcal{R}_\nu)^{\theta+1}$.

We have $\|\boldsymbol{H}_l(\cdot)\|_{L^\infty(\mathcal{P}_J)} \geq 1$ for every sequence of interpolation points and $\|\boldsymbol{H}_l(\cdot)\|_{L^\infty(\mathcal{P}_J)} = 1$ for every l in the case of Leja points on the real interval $[-1, 1]$ (see e.g. [10] for their definition).

Proof. We first consider the interpolation case. Simply applying the triangle inequality we obtain:

$$\begin{aligned}\|\hat{u} - I_\Lambda \hat{u}_{h,\Lambda}\|_{L^\infty(\mathcal{P}_J,\hat{V})} &\leq \|\hat{u} - I_\Lambda \hat{u}\|_{L^\infty(\mathcal{P}_J,\hat{V})} + \|I_\Lambda \hat{u} - I_\Lambda \hat{u}_{h,\Lambda}\|_{L^\infty(\mathcal{P}_J,\hat{V})} \\ &\leq \|\hat{u} - I_\Lambda \hat{u}\|_{L^\infty(\mathcal{P}_J,\hat{V})} + \sum_{\nu\in\Lambda} \|\Delta_\nu^I \hat{u} - \Delta_\nu^I \hat{u}_{h,\Lambda}\|_{L^\infty(\mathcal{P}_J,\hat{V})};\end{aligned}$$

thanks to Lemma 5.14, Theorem 5.3 holds and thus we get (6.10).

If the sequence of interpolation points is nested, then, according to [9, Formula (2.25)], one can write, for a generic element $g \in L^\infty(\mathcal{P}_J, \hat{V})$,

$$\Delta_\nu^I g(\boldsymbol{y}) = \sum_{\boldsymbol{y}_l \in \Delta_\nu^I} (g(\boldsymbol{y}_l) - I_{\mathcal{R}_\nu} g(\boldsymbol{y}_l))\, \boldsymbol{H}_l(\boldsymbol{y}),$$

(with $I_{\mathcal{R}_\nu}$ the interpolation operator on $\mathcal{R}_\nu$). Thus, we can write, for each $\nu \in \Lambda$:

$$\begin{aligned}&\|\Delta_\nu^I \hat{u} - \Delta_\nu^I \hat{u}_{h,\Lambda}\|_{L^\infty(\mathcal{P}_J,\hat{V})} \\ &\leq \sum_{\boldsymbol{y}_l \in \Delta_\nu^I} \|\hat{u}(\boldsymbol{y}_l) - \hat{u}_{h,\Lambda}(\boldsymbol{y}_l) - I_{\mathcal{R}_\nu}(\hat{u}(\boldsymbol{y}_l) - \hat{u}_{h,\Lambda}(\boldsymbol{y}_l))\|_{\hat{V}} \|\boldsymbol{H}_l(\cdot)\|_{L^\infty(\mathcal{P}_J)} \\ &\leq \sum_{\boldsymbol{y}_l \in \Delta_\nu^I} (1 + \mathbb{L}_{\mathcal{R}_\nu}) \|\hat{u}(\boldsymbol{y}_l) - \hat{u}_{h,\Lambda}(\boldsymbol{y}_l)\|_{\hat{V}} \|\boldsymbol{H}_l(\cdot)\|_{L^\infty(\mathcal{P}_J)} \\ &\leq (1 + \mathbb{L}_{\mathcal{R}_\nu}) C(k) \sum_{\boldsymbol{y}_l \in \Delta_\nu^I} N_{dof,l}^{-\frac{\min(k-1,q_l)}{2}} \|\hat{u}(\boldsymbol{y}_l)\|_{H^k((K_R\cap\hat{D}_1))\cap H^k(\hat{D}_2)} \|\boldsymbol{H}_l(\cdot)\|_{L^\infty(\mathcal{P}_J)}.\end{aligned}$$

Under the hypothesis on the Lebesgue constant for the univariate operator, we have that $\mathbb{L}_{\mathcal{R}_\nu} \leq (\sharp\mathcal{R}_\nu)^{\theta+1}$ and thus it grows with $\sharp\mathcal{R}_\nu$. Hence, we have obtained (6.12), with $\|\boldsymbol{H}_l(\cdot)\|_{L^\infty(\mathcal{P}_J)} \geq 1$ in general and $\|\boldsymbol{H}_l(\cdot)\|_{L^\infty(\mathcal{P}_J)} = 1$ for every l in the case of Leja points [9].

The result for the quadrature operator follows the same lines. The difference is, of course, in the definition of the difference operators for nested sequences; indeed, in this case, we have that, for a continuous $g \in L^1(\mathcal{P}_J, \hat{V})$, $\Delta_\nu^Q g = \sum_{\boldsymbol{y}_l \in \Delta_\nu^Q} w_l g(\boldsymbol{y}_l)$, and thus

$$\|\Delta_\nu^Q \hat{u} - \Delta_\nu^Q \hat{u}_{h,\Lambda}\|_{\hat{V}} \leq C(k) \sum_{\boldsymbol{y}_l \in \Delta_\nu^Q} |w_l| N_{dof,l}^{-\frac{\min(k-1,q_l)}{2}} \|\hat{u}(\boldsymbol{y}_l)\|_{H^k((K_R\cap\hat{D}_1))\cap H^k(\hat{D}_2)}.$$

□

The above theorem can be considered as a starting point for an adaptive strategy, where one tries to minimize the total number of degrees of freedom in such a way that the finite element error does not exceed the Smolyak algorithm error ($\sim N^{-s}$). The study of an adaptive strategy is postponed to a future work.

We remark that the smoothness $s = \frac{1}{p} - 1$ in the parameter space and the spatial smoothness k of the exact solution are not independent, owing to Theorem 6.6. This is formalized in the following important corollary, obtained by combining Theorem 6.6 with Theorem 6.10 or Theorem 6.11:

Corollary 6.12. *Let $\mathcal{I}_\Lambda \hat{u}_h$, $Q_\Lambda \hat{u}_h$ $\mathcal{I}_\Lambda \hat{u}_{h,\Lambda}$, $Q_\Lambda \hat{u}_{h,\Lambda}$ as in Theorem 6.10 and 6.11 respectively. Let Assumptions 2.3 and 4.4 be fulfilled, and Φ given by* (3.2)*.*

Then if the coefficient sequences $\mathcal{C} = (c_j)_{j\geq 1}$, $\mathcal{S} = (s_j)_{j\geq 1}$ satisfy Assumption 2.4.A and the nominal radius r_0 belongs to $C^k_{per}([0, 2\pi))$, with k as below, then the estimates (6.7)-(6.8) *and* (6.12)-(6.13) *hold with*

$$k = \begin{cases} \left\lfloor \frac{1}{p} - 1 \right\rfloor & \text{if } \frac{1}{p} - 1 \text{ is not an integer} \\ \frac{1}{p} - 2 & \text{otherwise.} \end{cases} \tag{6.14}$$

6.3 Convergence of linear output functionals

We extend here the results of the previous subsection to the case that we want to interpolate or compute moments of a linear output functional $F = F(u)$. Let $\hat{F} = \hat{F}(\boldsymbol{y}, \hat{u})$ denote the functional F after change of coordinates to the nominal space.

Throughout this subsection, $k \in \mathbb{N}$ denotes the spatial regularity of the exact solution as from Theorem 6.6.

If the functional depended only on the solution $\hat{u}$, then, thanks to linearity, the analyticity of $\hat{F}$ would follow immediately from the analyticity of the solution and of the map Φ, with the same polyradii for the polydiscs. However, in general this is not the case, and, to make sure that the $(\boldsymbol{b}, p, \epsilon)^*$-holomorphy assumption is satisfied, we state the following assumption:

Assumption 6.13. *The linear output functional $\hat{F} = \hat{F}(\boldsymbol{y}, \hat{u})$ admits an analytic extension to the complex plane, with the same domain of analyticity as the solution $\hat{u}$.*

In particular, this assumption is satisfied when

$$\hat{F}(\boldsymbol{y}, \hat{u}) = \int_{\hat{A}} \mathcal{L}_1(\hat{u}(\boldsymbol{y}))\, d\hat{\boldsymbol{x}}, \tag{6.15}$$

where $\hat{A} \subseteq K_R$ is a nonzero measure set and $\mathcal{L}_1$ is a first order linear differential operator of the form $\mathcal{L}_1(v) = \hat{a}_1(\boldsymbol{y}, \hat{\boldsymbol{x}}) \cdot \hat{\nabla} \hat{v} + \hat{b}_1(\boldsymbol{y}, \hat{\boldsymbol{x}}) \hat{v}$, with coefficients which are measurable with respect to $\hat{\boldsymbol{x}}$ and holomorphic in $\boldsymbol{y} \in \mathcal{P}_J$ in the same domain of analyticity as $\hat{u}$.

We also require that the linear output functional is stable in the following sense:

Assumption 6.14. *The linear output functional $\hat{F}$ belongs to $(H^m(K_R))'$ for an integer $m \leq 1$, i.e. there exist $C > 0$ such that*

$$\left| \hat{F}(\boldsymbol{y}, \hat{v}) \right| \leq C \|\hat{v}\|_{H^m(K_R)}$$

for all $\hat{v} \in H^m(K_R)$, with C independent of the truncation dimension $J \in \mathbb{N}$ and of $\boldsymbol{y} \in \mathcal{P}_J$ (but possibly on the radius R of K_R).

This assumption is fulfilled for $m = 0$ by functionals of the form (6.15).

We denote by $\hat{F}_h := \hat{F}(\boldsymbol{y}, \hat{u}_h)$ and $\hat{F}_{h,\Lambda} := \hat{F}(\boldsymbol{y}, \hat{u}_{h,\Lambda})$ the value of $\hat{F}$ when evaluated on the discrete solutions $\hat{u}_h$ and $\hat{u}_{h,\Lambda}$ respectively (nonadaptive and adaptive case).

For the case of uniform finite element order, if $\hat{F} = \hat{F}(\hat{u})$ satisfies Assumption 6.13, also its discrete version $\hat{F}_h$ does thanks to Lemma 6.9, and we have:

Theorem 6.15. *Let $\hat{F}$ be a linear output functional defined on the nominal configuration and satisfying Assumption 6.13. We denote by $I_\Lambda \hat{F}_h$ and $Q_\Lambda \hat{F}_h$ the solutions obtained respectively from sparse interpolation and sparse quadrature of $\hat{F}_h = \hat{F}(\boldsymbol{y}, \hat{u}_h(\boldsymbol{y}))$. Let the assumptions of Theorem 6.10 be satisfied.*

Then there exists a downward closed set Λ of cardinality at most N such that the following estimates hold:

$$\|\hat{F} - I_\Lambda \hat{F}_h\|_{L^\infty(\mathcal{P}_J, \hat{V})} \leq C N_{dof}^{-t} + C_1 N^{-s} \quad s = \frac{1}{p} - 1, \tag{6.16}$$

$$\|\mathcal{I}(\hat{F}) - Q_\Lambda \hat{F}_h\|_{\hat{V}} \leq C N_{dof}^{-t} + C_2 N^{-s} \quad s = \frac{1}{p} - 1. \tag{6.17}$$

with $s, C, C_1, C_2 > 0$ independent of N, N_{dof}, of $J \in \mathbb{N}$ and of $\boldsymbol{y} \in \mathcal{P}_J$.

If $\hat{F}$ fulfills Assumption 6.14, then $t = \frac{\min(k-1,q)+1}{2}$ for $m \leq 0$, $t = \frac{\min(k-1,q)}{2}$ for $m = 1$, $k \geq 1$.

For the parameter-adaptive case:

Theorem 6.16. *Let $\hat{F}$ be a linear output functional defined on the nominal configuration and satisfying Assumption 6.13. We denote by $I_\Lambda \hat{F}_{h,\Lambda}$ and $Q_\Lambda \hat{F}_{h,\Lambda}$ the solutions obtained respectively from sparse interpolation and sparse quadrature of $\hat{F}_{h,\Lambda} = \hat{F}(\boldsymbol{y}, \hat{u}_{h,\Lambda}(\boldsymbol{y}))$. Let the assumptions of Theorem 6.11 be satisfied.*

Then there exists a downward closed set Λ of cardinality at most N such that

$$\|\hat{F} - I_\Lambda \hat{F}_{h,\Lambda}\|_{L^\infty(\mathcal{P}_J, \hat{V})} \leq \sum_{\nu \in \Lambda} \|\Delta_\nu^I(\hat{F} - \hat{F}_{h,\Lambda})\|_{L^\infty(\mathcal{P}_J, \hat{V})} + C_1 N^{-s} \quad s = \frac{1}{p} - 1, \tag{6.18}$$

$$\|\mathcal{I}(\hat{F}) - Q_\Lambda \hat{F}_{h,\Lambda}\|_{\hat{V}} \leq \sum_{\nu \in \Lambda} \|\Delta_\nu^Q(\hat{F} - \hat{F}_{h,\Lambda})\|_{\hat{V}} + C_2 N^{-s} \quad s = \frac{1}{p} - 1, \tag{6.19}$$

with $s, C_1, C_2 > 0$ independent of N, N_{dof}, of $J \in \mathbb{N}$ and of $\boldsymbol{y} \in \mathcal{P}_J$.

If the sequences $(\zeta_i)_{i \geq 0}$ of interpolation / quadrature points are nested, then the addends in the first sum satisfy, for the interpolation and quadrature case respectively:

$$\begin{aligned} \|\Delta_\nu^I(F - \hat{F}_{h,\Lambda})\|_{L^\infty(\mathcal{P}_J, \hat{V})} &\leq (1 + \mathbb{L}_{\mathcal{R}_\nu}) C(k) \sum_{\boldsymbol{y}_l \in \Delta_\nu^I} \|\boldsymbol{H}_l(\cdot)\|_{L^\infty(\mathcal{P}_J)} N_{dof,l}^{-t} \|\hat{u}(\boldsymbol{y}_l)\|_{H^k((K_R \cap \hat{D}_1)) \cap H^k(\hat{D}_2)} \\ \|\Delta_\nu^Q(F - \hat{F}_{h,\Lambda})\|_{\hat{V}} &\leq C(k) \sum_{\boldsymbol{y}_l \in \Delta_\nu^Q} |w_l| N_{dof,l}^{-t} \|\hat{u}(\boldsymbol{y}_l)\|_{H^k((K_R \cap \hat{D}_1)) \cap H^k(\hat{D}_2)}, \end{aligned} \tag{6.20}$$

(6.21)

with $C > 0$ independent of N, N_{dof}, of $J \in \mathbb{N}$ and of $\boldsymbol{y} \in \mathcal{P}_J$, and the Lebesgue constant bounded as in Theorem 6.11.

If $\hat{F}$ fulfills Assumption 6.14, then $t = \frac{\min(k-1,q)+1}{2}$ for $m \leq 0$, $t = \frac{\min(k-1,q)}{2}$ for $m = 1$, $k \geq 1$.

The proofs for the two theorems are analogous to the proofs of Theorem 6.10 and 6.11, respectively. The gain of one order of convergence in (6.16) and (6.20) is a standard result of finite element analysis using a duality argument (see e.g. [5]).

7 Numerical experiments

The geometry is as shown in Figure 1.1 with a nominal, angle-independent radius of size $r_0 = 10\text{nm}$. We consider the transverse electric mode (TE), i.e. the solution u represents the component of the electric field which is perpendicular to the plane in which the equations are solved (plane of incidence); in this case we have $\mu = 1$ in (1.2). The incident wave u_i is coming from the left with an incidence angle 0 with respect to the horizontal axis, and frequency $f = 10^4\text{THz}$. The wave number modulus in free space is $k_0 = \frac{2\pi f}{c_0}$, with $c_0 = 3 \cdot 10^8\text{m/s}$ the light speed. The scatterer is a dielectric with relative permittivity $\varepsilon_2 = 2$ and the surrounding medium is air ($\varepsilon_1 = 1$), so that the wavenumbers are $\boldsymbol{k}_1 = (k_0, 0)$ and $\boldsymbol{k}_2 = (k_0\sqrt{\varepsilon_2}, 0)$ respectively.

To compute interpolants and means of the quantities of interest, we use the sparse grid algorithm described in subsection 5.2 (Algorithm 1) with $\vartheta = 1$.

In the numerical experiments, our focus is on the convergence of the Smolyak algorithm rather than on the finite element convergence. For this reason, instead of the domain mapping described in subsection 3.2, we use a mapping that is less regular with respect to $\hat{\boldsymbol{x}} \in K_R$, but easier to implement, namely:

$$\boldsymbol{x}(\boldsymbol{y}) = \Phi(\boldsymbol{y}, \hat{\boldsymbol{x}}) = \begin{cases} \boldsymbol{0} & \text{for } \hat{\boldsymbol{x}} = \boldsymbol{0} \\ \frac{\hat{\boldsymbol{x}}}{r_0(\varphi)} r(\boldsymbol{y}, \varphi) & \text{for } 0 < \|\hat{\boldsymbol{x}}\| < r_0(\varphi) \\ \frac{R - r(\boldsymbol{y},\varphi)}{R - r_0(\varphi)} \left(1 + \frac{R(r(\boldsymbol{y},\varphi) - r_0(\varphi))}{R - r(\boldsymbol{y},\varphi)} \frac{1}{\|\hat{\boldsymbol{x}}\|}\right) \hat{\boldsymbol{x}} & \text{for } r_0(\varphi) \le \|\hat{\boldsymbol{x}}\| < R \\ \hat{\boldsymbol{x}} & \text{for } \|\hat{\boldsymbol{x}}\| = R \end{cases} \tag{7.1}$$

It can be easily checked that with this map the $(\boldsymbol{b}, \boldsymbol{\rho}, \varepsilon)^*$-assumption is still fulfilled.

For each experiment, we compare two choices for the univariate sequence $(\zeta_k)_{k \ge 0}$ of interpolation/quadrature points:

- Clenshaw-Curtis (CC):

$$\begin{aligned} &\zeta_0^k = 0 \ \text{ if } n_k = 1 \\ &\zeta_i^k = -\cos\left(\frac{\pi i}{n_k - 1}\right),\ i = 0, \dots, n_k - 1, \ \text{ if } n_k > 1, \end{aligned}$$

  with $n_0 = 1$ and $n_k = 2^k + 1$, for $k \ge 1$;

- $\mathfrak{R}$-Leja sequence (RL): projection on $[-1, 1]$ of a Leja sequence for the complex unit disk initiated at 1:

$$\begin{aligned} &\zeta_0^k = 0, \zeta_1^k = 1, \zeta_2^k = -1, \ \text{ if } i = 0, 1, 2, \\ &\zeta_i^k = \mathfrak{R}(\hat{z}), \ \text{ with } \hat{z} = \text{argmax}_{|\zeta|=1} \prod_{l=1}^{i-1} |\zeta - \zeta_l^k|,\ i = 3, \dots, n_k, \ \text{ if } i \text{ odd}, \\ &\zeta_i^k = -\zeta_{i-1}^k,\ i = 3, \dots, n_k, \ \text{ if } i \text{ even}, \end{aligned}$$

  with $n_k = 2k + 1$, for $k \ge 0$, see [6].

The Clenshaw-Curtis points satisfy Assumption 5.1 with part (a) for the second part, while the $\mathfrak{R}$-Leja points satisfy Assumption 5.1 with part (b) in (ii).

The finite element solutions are computed using the C++ NGSolve library[2], providing high order elements for any shape; NGSolve has been linked to the MKL version of the PARDISO library to compute the solution of the resulting symmetric positive definite algebraic system.

[2] http://sourceforge.net/apps/mediawiki/ngsolve

To truncate the domain and approximate the DtN map, we consider a circular Perfectly Matched Layer (PML, see [3, 14]) around the boundary ∂K_R; for every $\boldsymbol{y} \in \mathcal{P}_J$, the mapping $\Phi(\boldsymbol{y})$ is prolongated as the identity in the PML. In [27] it is shown that, if the fictitious absorption coefficient in the PML is properly chosen, then the PML can be used in the finite element framework to truncate the domain for Helmholtz equation in a almost reflectionless manner for all frequencies. We use a PML that starts at radius $R = 100$nm and ends at radius $R' = 150$nm, with absorption coefficient (or dumping parameter) $\alpha = 0.5$ [14].

As quantities of interest, we consider the interpolation and quadrature of the real part of the solution to (4.2) and of the modulus of the far field pattern (defined below).

7.1 Test cases

7.1.1 Interpolation of the real part of the solution on the nominal configuration

We consider the expansion of the stochastic radius (2.1) for three variations of the sparsity parameter: $s_j = c_j = \frac{0.01 r_0}{j^{\frac{1}{p}}}, j \geq 1$, for $\frac{1}{p} = 2, 3, 4$. For each value of p, we compare the cases $2J = 16$, $2J = 32$ and $2J = 64$, with $2J = d$ the dimension of the parameter space. The maximal shape variations with respect to r_0 are of the order of 2.3% for $\frac{1}{p} = 2$, 1.7% for $\frac{1}{p} = 3$ and 1.5% for $\frac{1}{p} = 4$ (for all the three truncations of the radius expansion).

To compute the finite element solution given a parameter realization, we have used globally continuous, piecewise 4-th order polynomial ansatz functions on an unstructured, regular triangulation, leading to a total of 60705 degrees of freedom (including the PML); a 4-th order polynomial boundary approximation is considered, so that the error introduced by the discretization of the boundaries is of the same order as the error due to the finite element discretization. The Smolyak interpolation has been applied to the part of the solution that is not inside the PML, corresponding to an array carrying 37563 degrees of freedom.

As measure of the error we have considered $\sup_{\boldsymbol{y} \in \mathcal{P}_J} \| \mathrm{Re}\, \hat{u}_h(\boldsymbol{y}) - I_\Lambda(\mathrm{Re}\, \hat{u}_h)(\boldsymbol{y}) \|_{H^1(K_R)}$, where each realization $\mathrm{Re}\, \hat{u}_h(\boldsymbol{y})$ and the interpolated quantity $I_\Lambda(\mathrm{Re}\, \hat{u}_h)(\boldsymbol{y})$, $\boldsymbol{y} \in \mathcal{P}_J$, have been computed using the same finite element space as described above. To estimate the supremum norm, we have considered the maximum H^1-norm error among 2^{16} realizations of $\boldsymbol{y} \in \mathcal{P}_J$ corresponding to the quadrature points generated by the high order Quasi Monte-Carlo method described in [17] using $C = 0.1$ for the Walsh coefficient bound.

Figure 7.1 shows the forementioned interpolation error versus the cardinality of the index set Λ and versus the number of PDE solves. In Figure 7.2, instead, we compare, for each variation of the sparsity parameter, the performance of the algorithm for the three different dimensions of the parameter space considered. In both cases, we have computed the error every 10 iterations of the Smolyak algorithm, starting from the last one and going backward until the last iteration with number bigger or equal to 10.

7.1.2 Interpolation of the modulus of the far field pattern

Given a radiating solution $u_s = u - u_i$ to the Helmholtz equation, the far field pattern is a function defined on the unit sphere S^1 describing the asymptotic behavior of $u_s(\boldsymbol{x})$ for $|\boldsymbol{x}| \to \infty$.

The far field mapping $F : H^1_{\mathrm{loc}}(\mathbb{R}^2) \to C^\infty(S^1)$ associates to a scattered wave u_s its far field pattern; it is given by [31, Formulae (3) and (5)]

$$F(u_s)(\hat{\boldsymbol{\xi}}) = C_F \int_\Sigma \left\{ u_s(\boldsymbol{x}) \frac{\partial G(\hat{\boldsymbol{\xi}}, \boldsymbol{x})}{\partial \boldsymbol{n}(\boldsymbol{x})} - \frac{\partial u_s}{\partial \boldsymbol{n}}(\boldsymbol{x}) G(\hat{\boldsymbol{\xi}}, \boldsymbol{x}) \right\} \mathrm{d}S(\boldsymbol{x}), \quad \hat{\boldsymbol{\xi}} \in S^1, \tag{7.2}$$

where Σ is a simple closed path around the scatterer and $\boldsymbol{n}$ its outward unit normal vector field. $G = G(\hat{\boldsymbol{\xi}}, \boldsymbol{x})$ describes the behavior of the Green's function when the first argument

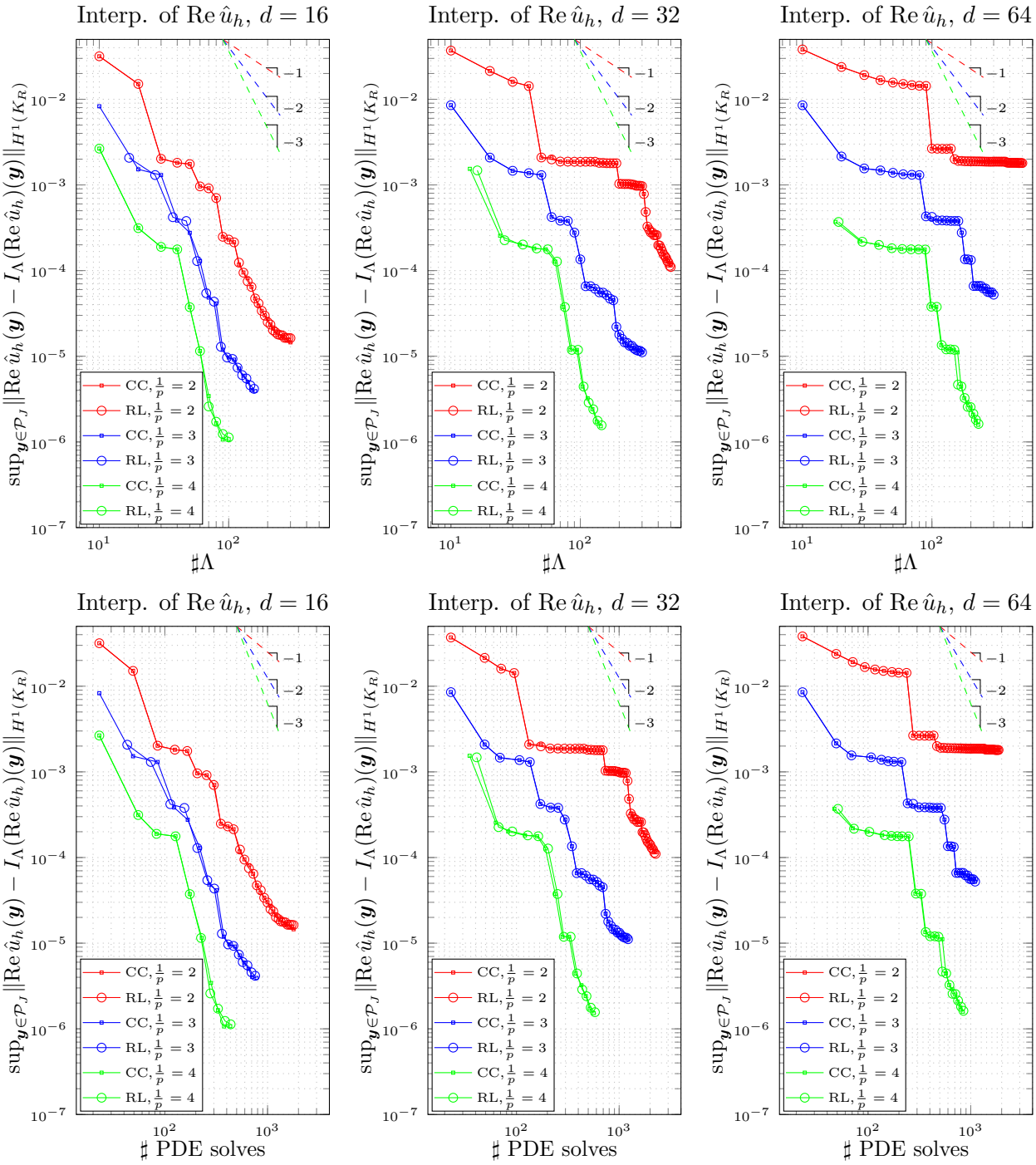

Figure 7.1: Comparison of the errors for the interpolated solution with respect to the cardinality of the index set Λ (top) and to the number of PDE solves (bottom), using Clenshaw-Curtis and $\mathfrak{R}$-Leja points for 16 (left), 32 (middle) and 64 (right) dimensions. Maximal shape variations with respect to r_0 of about 2.3% for $\frac{1}{p} = 2$, 1.7% for $\frac{1}{p} = 3$ and 1.5% for $\frac{1}{p} = 4$.

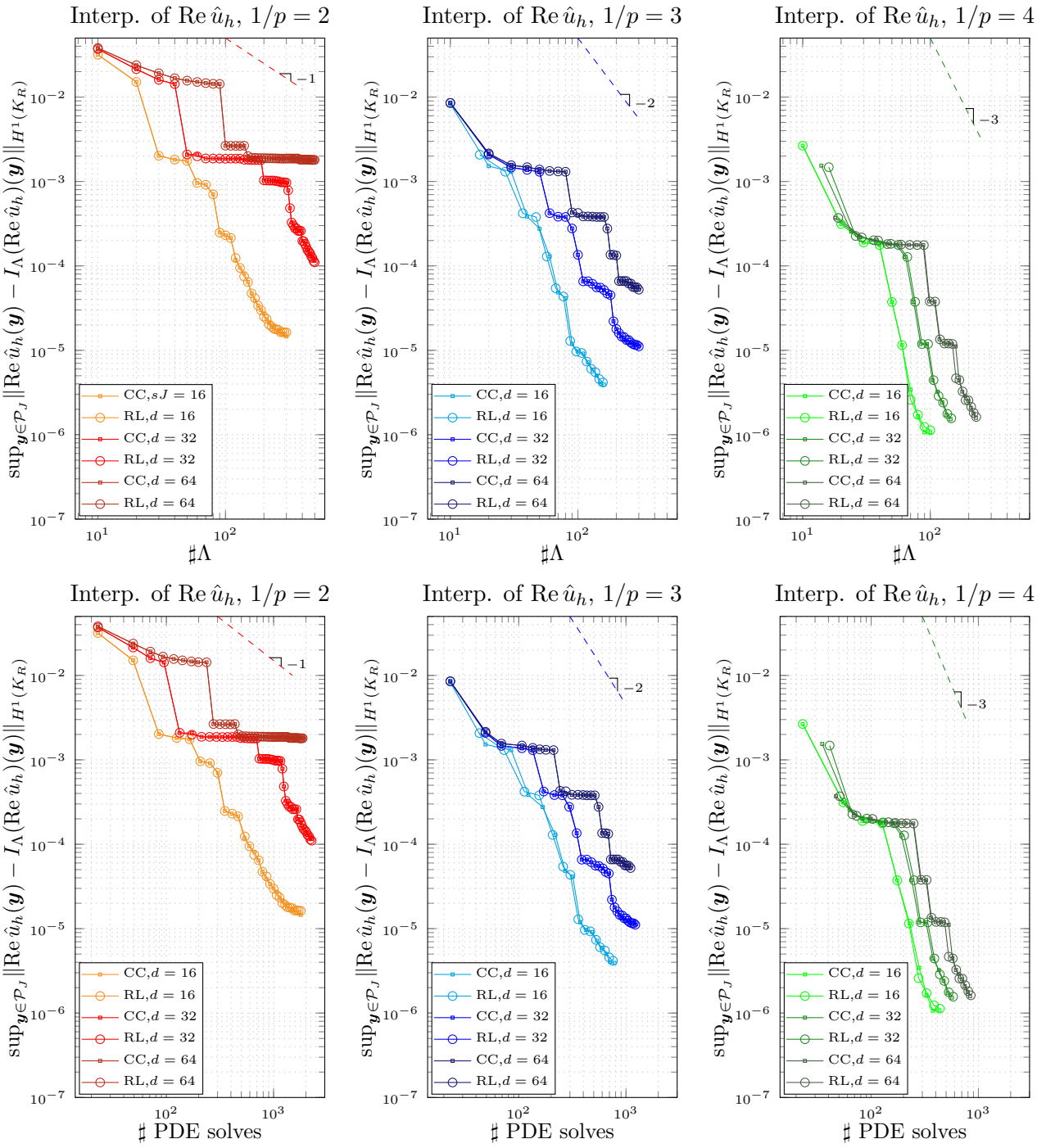

Figure 7.2: Comparison of the errors for the interpolated solution with respect to the cardinality of the index set Λ (top) and to the number of PDE solves (bottom), using Clenshaw-Curtis and $\mathfrak{R}$-Leja points for variations of the sparsity parameter $\frac{1}{p} = 2$ (left), 3 (middle) and 4 (right). Maximal shape variations with respect to r_0 of about 2.3% for $\frac{1}{p} = 2$, 1.7% for $\frac{1}{p} = 3$ and 1.5% for $\frac{1}{p} = 4$.

tends to infinity (we refer to [15, Section 2.2] for details); for a particle in free space, we have $G(\hat{\boldsymbol{\xi}}, \boldsymbol{x}) = \frac{1}{4\pi} e^{-ik_1 \hat{\boldsymbol{\xi}} \cdot \boldsymbol{x}}$ (with k_1 the wavenumber modulus in free space). C_F is a normalizing constant, that we consider to be $C_F = \sqrt{\frac{2\pi}{k_1}} e^{i\frac{\pi}{4}}$.

A simple application of Green's formula shows that the far field pattern is independent of the path Σ chosen to enclose the scatterer. Thus, we can consider two circles Σ_1 and Σ_2 around the particle, with Σ_1 contained in Σ_2, and the annulus A enclosed between them, and choose a cut-off function $\psi \in C^2(A)$ such that

$$\psi|_{\Sigma_2} = 1, \quad \psi|_{\Sigma_1} = 0, \quad \nabla\psi|_{\Sigma_1} = \nabla\psi|_{\Sigma_2} = \mathbf{0}. \tag{7.3}$$

Applying Green's formula, it's easy to see [25] that (7.2) is equivalent to the modified far field mapping

$$F^*(u_s)(\hat{\boldsymbol{\xi}}) = C_F \int_A \nabla\psi(\boldsymbol{x}) \cdot \Big(u_s(\boldsymbol{x}) \nabla G(\hat{\boldsymbol{\xi}}, \boldsymbol{x}) - \nabla u_s(\boldsymbol{x}) G(\hat{\boldsymbol{\xi}}, \boldsymbol{x}) \Big) \, \mathrm{d}\boldsymbol{x}, \quad \hat{\boldsymbol{\xi}} \in S^1. \tag{7.4}$$

The advantage of formula (7.4) with respect to (7.2) is that, for fixed $\hat{\boldsymbol{\xi}} \in S^1$, $u_s \mapsto F^*(u_s)(\hat{\boldsymbol{\xi}})$ is a linear functional that is continuous on the energy space $H^1(A)$.

If we now apply the far field computation to the case when the scatterer has a stochastic boundary, we can fix an annular integration region $\hat{A}$ and a cut-off function $\hat{\psi}$ on the *nominal* domain $\hat{D}_2$, and (7.4) reads:

$$\begin{aligned} \hat{F}^*(\hat{u}_s(\boldsymbol{y}))(\hat{\boldsymbol{\xi}}) = C_F &\int_{\hat{A}} D\Phi(\boldsymbol{y})^{-\top} \hat{\nabla}\hat{\psi}(\hat{\boldsymbol{x}}) \cdot \hat{u}_s(\hat{\boldsymbol{x}}) D\Phi(\boldsymbol{y})^{-\top} \hat{\nabla}\hat{G}(\hat{\boldsymbol{\xi}}, \hat{\boldsymbol{x}}) \, \mathrm{d}\hat{\boldsymbol{x}} \\ &- \int_{\hat{A}} D\Phi^{-\top}(\boldsymbol{y}) \hat{\nabla}\hat{\psi} \cdot D\Phi(\boldsymbol{y})^{-\top} \hat{\nabla}\hat{u}_s(\hat{\boldsymbol{x}}) \hat{G}(\hat{\boldsymbol{\xi}}, \hat{\boldsymbol{x}}) \, \mathrm{d}\hat{\boldsymbol{x}}, \quad \hat{\boldsymbol{\xi}} \in S^1, \end{aligned} \tag{7.5}$$

where $\Phi(\boldsymbol{y})$ is the mapping from the nominal configuration, as considered in the previous sections, $\hat{u}_s(\boldsymbol{y}, \hat{\boldsymbol{x}}) = \hat{u}(\boldsymbol{y}, \hat{\boldsymbol{x}}) - u_i(\Phi(\boldsymbol{y}, \hat{\boldsymbol{x}}))$ and $\hat{G}(\hat{\boldsymbol{\xi}}, \hat{\boldsymbol{x}}) = G(\hat{\boldsymbol{\xi}}, \Phi(\boldsymbol{y}, \hat{\boldsymbol{x}}))$. For each $\hat{\boldsymbol{\xi}} \in S^1$, the functional $\hat{F}^*(\hat{\boldsymbol{\xi}})$ satisfies Assumption 6.13 because Φ and $\hat{u}_s$ are analytic, and thus Theorems 6.15 and 6.16 hold. Moreover, if $\hat{\psi} \in C^2(\hat{A})$ and if Φ fulfills Assumption 3.1 with $k \geq 2$, integration by parts shows that, for fixed $\hat{\boldsymbol{\xi}} \in S^1$, the functional $\hat{F}^*(\hat{\boldsymbol{\xi}})$ fulfills Assumption 6.14 with $m = 0$; therefore, for each realization $\boldsymbol{y}$, we can expect the gain in one order for the finite element convergence as explained in the second part of Theorems 6.15 and 6.16.

In the simulations, for the interpolation of $|\hat{F}^*(\hat{u}_s(\boldsymbol{y}))(\hat{\boldsymbol{\xi}})|$, $\hat{\boldsymbol{\xi}} \in S^1$, we consider the first 11 coefficients in its real Fourier expansion with respect to the angle $\varphi \in [0, 2\pi)$.

Again, we compare three variations of the sparsity parameter: $s_j = c_j = \frac{0.1 r_0}{j^{\frac{1}{p}}}$, $j \geq 1$, for $\frac{1}{p} = 2, 3, 4$; they correpond to maximal shape variations of 22%, 17% and 15% with respect to r_0, respectively. The annulus $\hat{A}$ has been chosen with inner radius 0.02nm and outer radius 0.1nm. For each realization, we have considered a 3-rd order finite element space (with 3-rd order boundary approximation), carrying in total 403481 degrees of freedom, of which 37414 are located inside the annulus $\hat{A}$.

The results for the 16-dimensional case are shown in Figure 7.3. The error considered is $\sup_{\boldsymbol{y} \in \mathcal{P}_J} \|\hat{\mathbf{f}}_h(\hat{u}_h))(\boldsymbol{y}) - I_\Lambda(\hat{\mathbf{f}}_h(\hat{u}_h))(\boldsymbol{y})\|_{\ell^2(\mathbb{R}^{11})}$, where $\hat{\mathbf{f}}_h$ denotes the vector of the approximated 11 Fourier coefficients, and both $\hat{\mathbf{f}}_h(\hat{u}_h))(\boldsymbol{y})$ and $\hat{\mathbf{f}}_h(\hat{u}_h))(\boldsymbol{y})$ have been computed on the finite element space described above. The supremum norm has been approximated by the maximum of the ℓ^2-norm error among 2^{16} realizations coinciding with the quadrature points of the algorithm presented in [17], with again $C = 0.1$ as Walsh coefficient bound. The error has been computed every 10 iterations, with the same rule as in the interpolation of the solution.

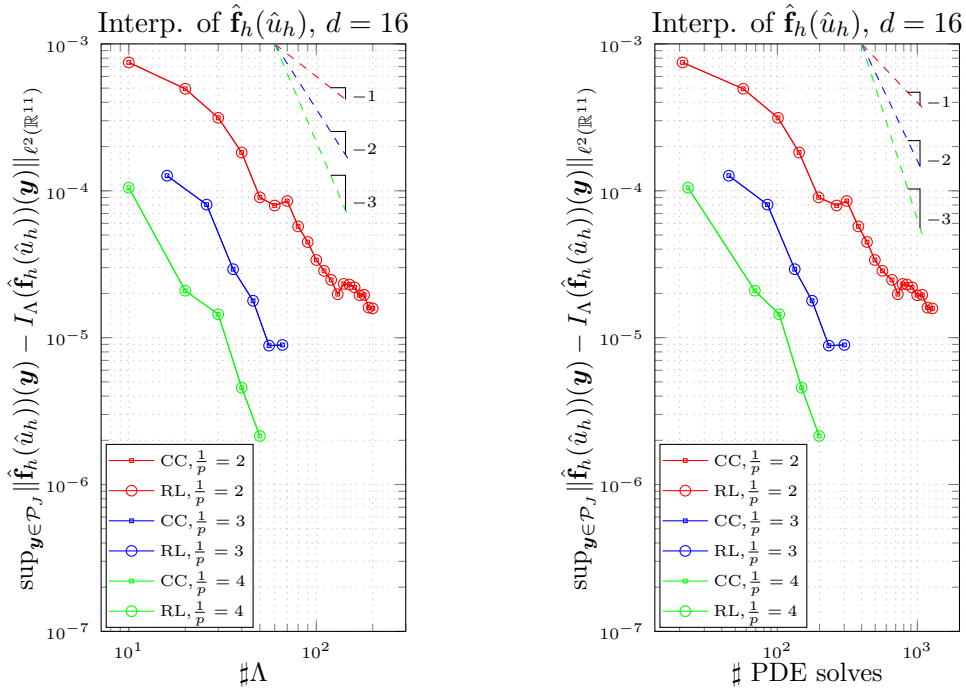

Figure 7.3: Comparison of the errors for the interpolated far field Fourier coefficients with respect to the cardinality of the index set Λ (left) and the number of PDE solves (right), using Clenshaw-Curtis and $\mathfrak{R}$-Leja points for 16 dimensions. Maximal shape variations with respect to r_0 of 22% for $\frac{1}{p} = 2$, 17% for $\frac{1}{p} = 3$ and 15% for $\frac{1}{p} = 4$.

The computational cost required for the far field interpolation is very high, because, for each interpolation point, additionally to the full solution, one has also to evaluate formula (7.5) for many values of the variable $\hat{\boldsymbol{\xi}}$ (the same number as the Fourier coefficients when using the real Fast Fourier Transform); hence, this application highlights the importance of developing a parameter-adaptive strategy to use different finite element resolutions for different interpolation points.

7.1.3 Quadrature of the real part of the solution on the nominal configuration

For these experiments we have considered the quadrature on the nominal space. The setting is the same as in the interpolation case, that is same scaling of the coefficients ($s_j = c_j = \frac{0.01 r_0}{j^{\frac{1}{p}}}$, $j \geq 1$, for $\frac{1}{p} = 2, 3, 4$) and same finite element space.

The error considered is $\|\mathcal{I}(\operatorname{Re} \hat{u}_h) - Q_\Lambda(\operatorname{Re} \hat{u}_h)\|_{H^1(K_R)}$, and it has been computed for every iteration. The reference solution used to estimate $\mathcal{I}(\operatorname{Re} \hat{u}_h)$ has been computed with the high order Quasi-Monte Carlo algorithm described in [17] using 2^{18} quadrature points and $C = 0.1$ as bound on the Walsh coefficient; each realization in the computation of the reference solution belongs to the same finite element space as the one used for the realizations of the Smolyak algorithm.

Figure 7.4 shows the quadrature error for different dimensions of the parameter space, versus the cardinality of the index set Λ and versus the number of PDE solves. Figure 7.5 shows instead, for each variation of the sparsity parameter, the comparison of the performance of the algorithm for dimension 16, 32 and 64 of the parameter space.

As an example, the estimated mean of the real part of the total field for $\frac{1}{p} = 3$, dimension 16 of the parameter space and Clenshaw-Curtis points is represented in the left plot of Figure 7.7; in this picture, the grey annulus represents the PML.

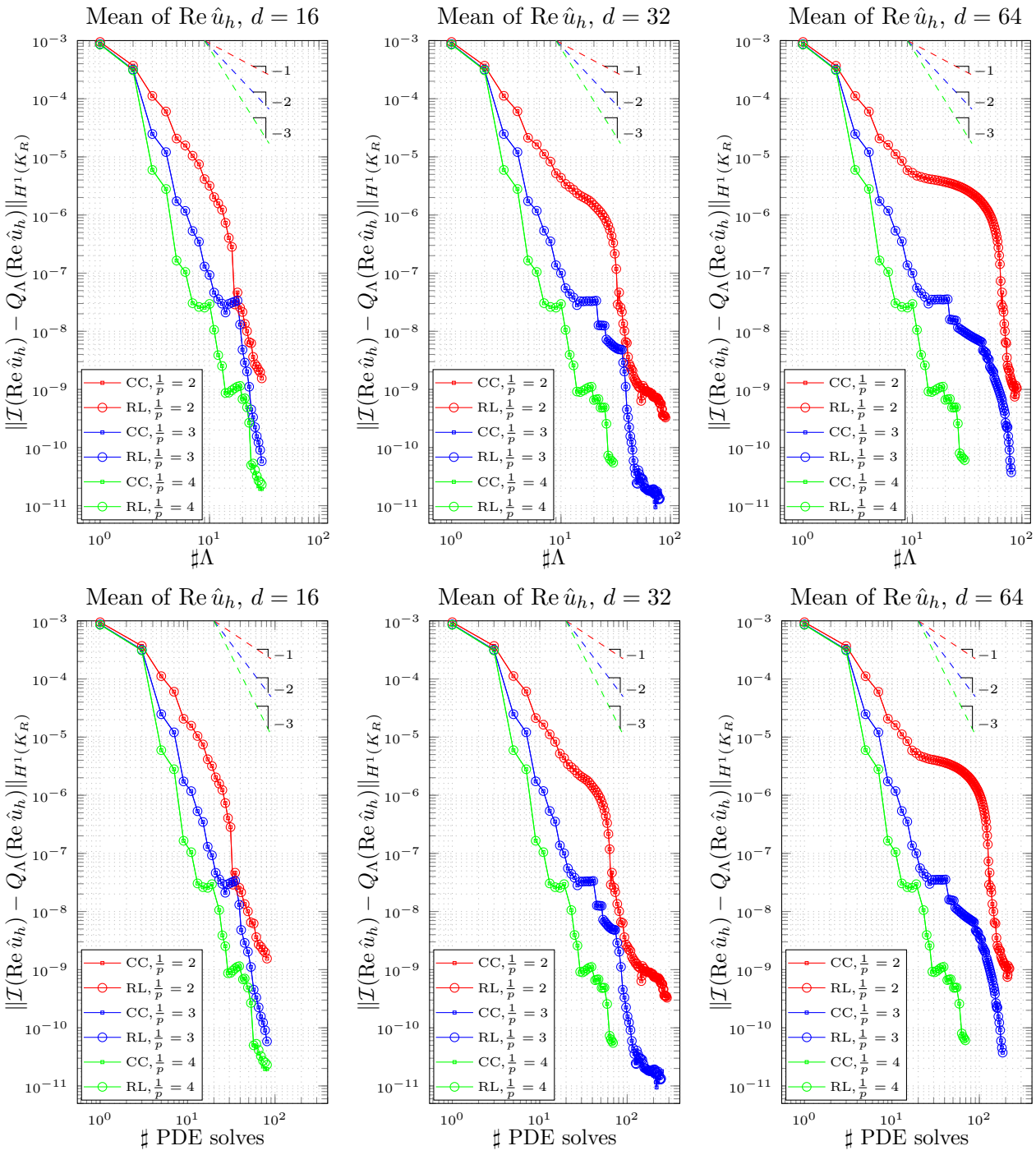

Figure 7.4: Comparison of the errors for the quadrature of the real part of the solution with respect to the cardinality of the index set Λ (top) and to the number of PDE solves (bottom), using Clenshaw-Curtis and $\mathfrak{R}$-Leja points for 16 (left), 32 (middle) and 64 (right) dimensions. Maximal shape variations with respect to r_0 of about 2.3% for $\frac{1}{p} = 2$, 1.7% for $\frac{1}{p} = 3$ and 1.5% for $\frac{1}{p} = 4$.

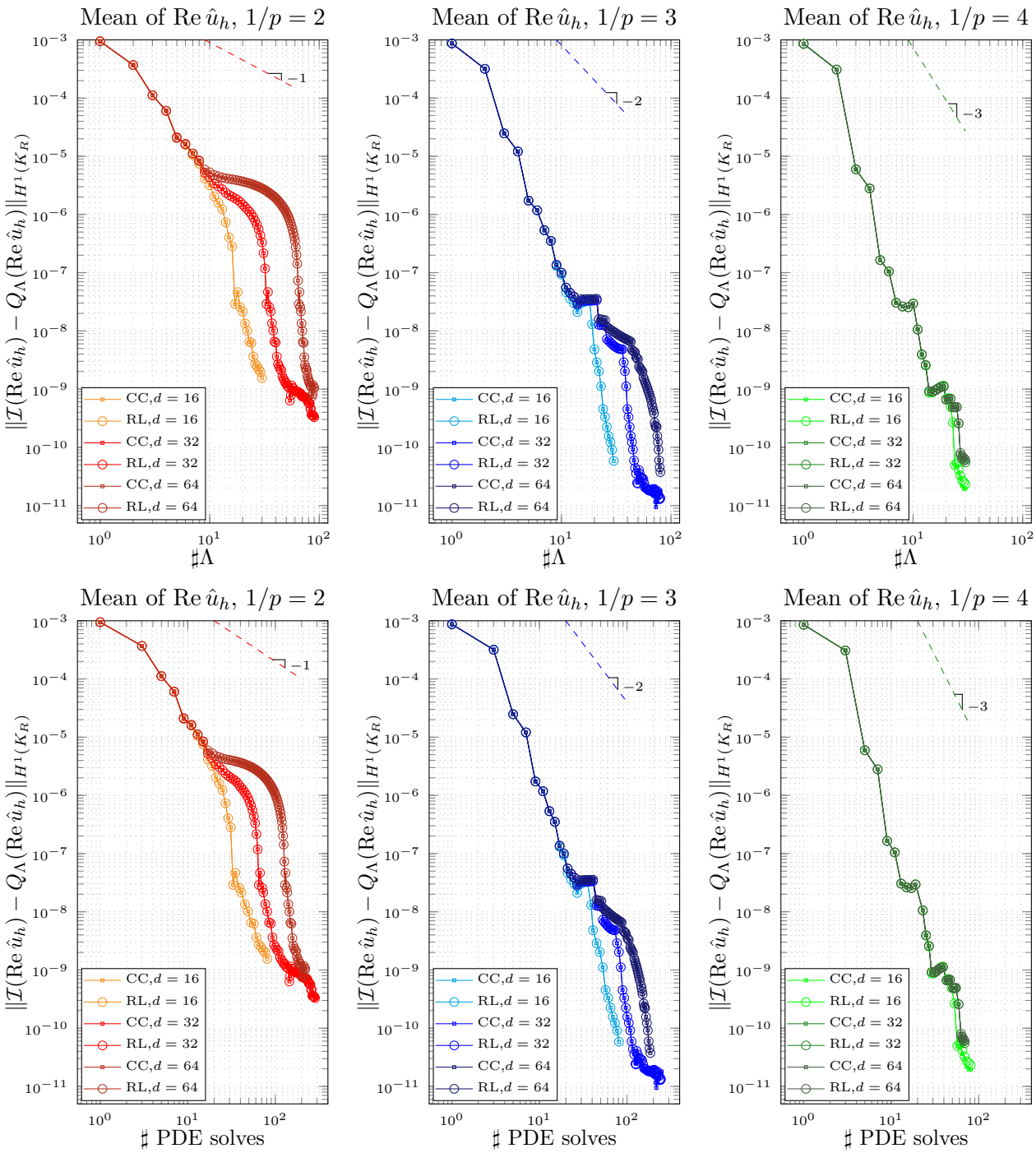

Figure 7.5: Comparison of the errors for the quadrature of the real part of the solution with respect to the cardinality of the index set Λ (top) and to the number of PDE solves (bottom), using Clenshaw-Curtis and $\mathfrak{R}$-Leja points for variations of the sparsity parameter $\frac{1}{p} = 2$ (left), 3 (middle) and 4 (right). Maximal shape variations with respect to r_0 of about 2.3% for $\frac{1}{p} = 2$, 1.7% for $\frac{1}{p} = 3$ and 1.5% for $\frac{1}{p} = 4$.

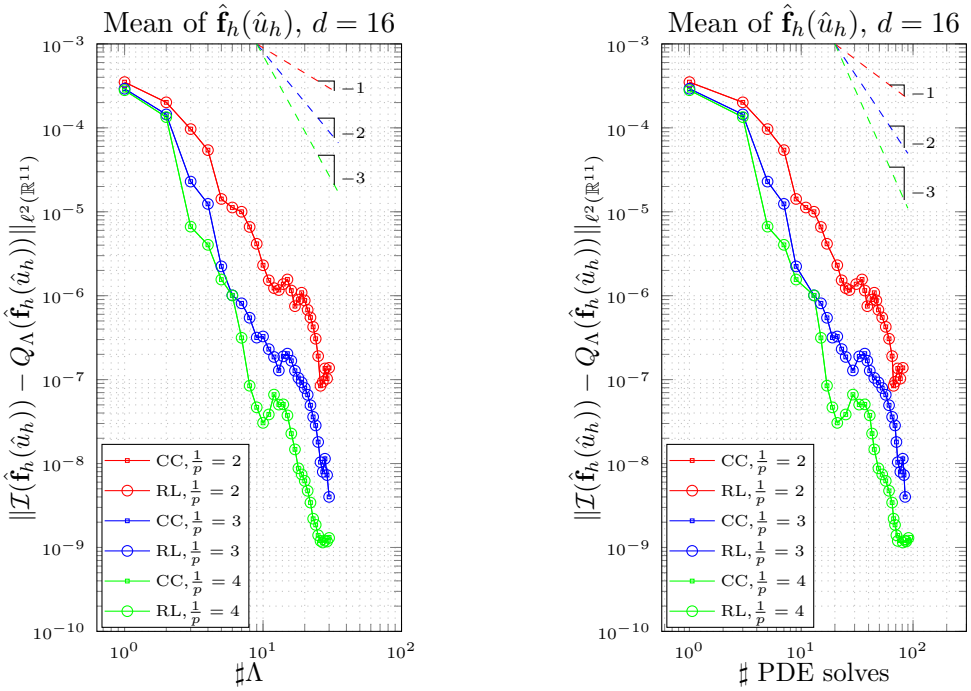

Figure 7.6: Comparison of the errors for the quadrature of the far field Fourier coefficients with respect to the cardinality of the index set Λ (left) and the number of PDE solves (right), using Clenshaw-Curtis and $\mathfrak{R}$-Leja points for 16 dimensions. Maximal shape variations with respect to r_0 of 22% for $\frac{1}{p} = 2$, 17% for $\frac{1}{p} = 3$ and 15% for $\frac{1}{p} = 4$.

7.1.4 Quadrature of the modulus of the far field pattern

The setting (coefficient scaling, finite element space) is the same as in the interpolation case. The results are depicted in Figure 7.6, where the error reported is $\|\mathcal{I}(\hat{\mathbf{f}}_h(\hat{u}_h)) - Q_\Lambda(\hat{\mathbf{f}}_h(\hat{u}_h))\|_{\ell^2(\mathbb{R}^{11})}$ (with again $\mathbf{f}$ the vector of real Fourier coefficients) and it has been computed for every iteration. The reference solution has been computed using the algorithm described in [17], using 2^{16} quadrature points and $C = 0.1$ for the Walsh coefficient bound.

The left plot in Figure 7.7 represents the modulus of the far field pattern computed from the estimated mean of the Fourier coefficients, for $\frac{1}{p} = 2, 3, 4$, using Clenshaw-Curtis points; in the plot, we have denoted by 'nominal' the far field pattern that is obtained when the scatterer has the nominal radius r_0. We can see that the mean values for different values of $\frac{1}{p}$ and for the nominal case are nearly coinciding, as one may expect from the fact that the far field functional is not sensitive to small variations in the shape of the scatterer.

7.2 Comments on the results of the numerical experiments

The results reported in the previous subsection hint that, for both interpolation and quadrature, the theoretical convergence rates of $s = \frac{1}{p} - 1$, for $p = 2, 3, 4$, are achieved, independently of the dimension of the parameter space.

Of course, the error is bigger when more dimensions are activated, cf. for instance Figures 7.2 and 7.5. This is expected, since, although the rates are dimension-independent, the constants on the right-hand sides of (5.10) and (5.11) are not. Indeed, they depend on the norms of the interpolation and quadrature operators, respectively, which are bounded from above by a power of the cardinality of the index set (see [9, Lemma 3.1] for interpolation and [35, Lemma 4.4] for quadrature).

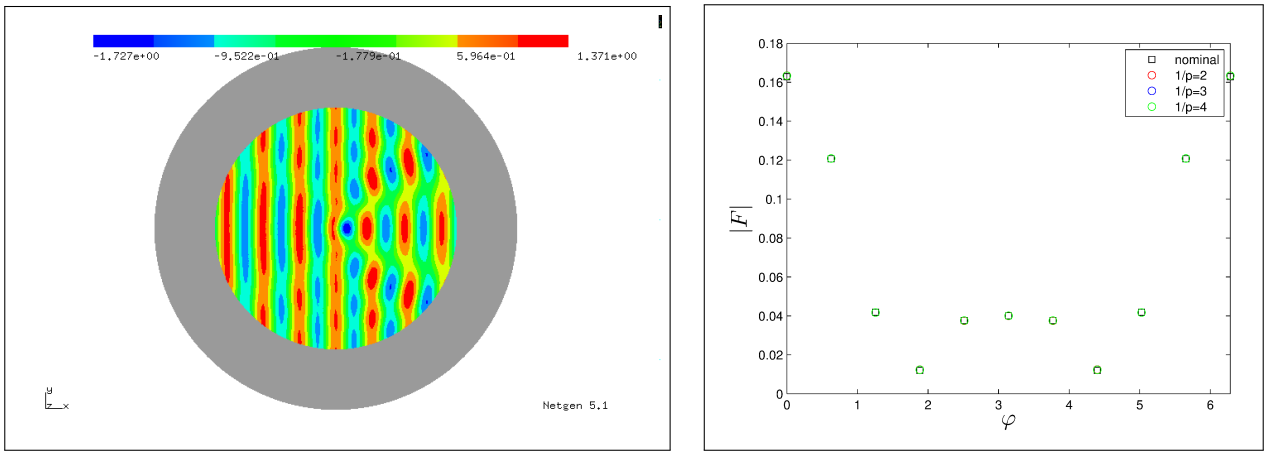

Figure 7.7: Particle in free space, 16 dimensions, Clenshaw-Curtis points: estimated mean of the real part of the solution when $\frac{1}{p} = 3$ (left) and of the far field modulus for $\frac{1}{p} = 2, 3, 4$ (right).

The plots also show that there is no significant difference in the performance of Clenshaw-Curtis and $\mathfrak{R}$-Leja points, also when considering the convergence with respect to the number of PDE solves. This is due to the fact that, although in the univariate case the number of Clenshaw-Curtis points increases exponentially with the order of the quadrature rule while the number of $\mathfrak{R}$-Leja points increases polynomially, when the index set contains indices associated to low order interpolation / quadrature operators, the number of PDE solves required by the two families of quadrature points do not differ significantly.

8 Non-analyticity of the mapped solution for interface problems

Thus far, we have always considered interpolation and quadrature in the parameter space applied to the solution $\hat{u}$ *on the nominal configuration*. However, in applications, one is mostly interested in having information on the solution u on *physical* space.

For interpolation, since the interpolated discrete solution $I_\Lambda \hat{u}_h = I_\Lambda \hat{u}_h(\boldsymbol{y}, \hat{\boldsymbol{x}})$ (or $I_\Lambda \hat{u}_{h,\Lambda} = I_\Lambda \hat{u}_{h,\Lambda}(\boldsymbol{y}, \hat{\boldsymbol{x}})$ for the parameter-adaptive case) still depends on $\boldsymbol{y} \in \mathcal{P}_J$, once we consider a particular realization $\boldsymbol{y} \in \mathcal{P}_J$ we also know the domain mapping $\Phi(\boldsymbol{y})$ and thus the solution on physical space.

For quadrature, the situation is different, because the result $Q_\Lambda \hat{u}_h$ does not depend on $\boldsymbol{y}$ anymore and thus the domain mapping is no more available. The first idea that would come to mind would be to consider a mesh in physical space, fixed for all realizations $\boldsymbol{y} \in \mathcal{P}_J$, and, for each realization $\boldsymbol{y}$ requested by the Smolyak algorithm, map the solution from the nominal coordinates to this grid using the mapping $\Phi(\boldsymbol{y})$; then, one could apply the Smolyak quadrature on the mapped solution. However, from Theorem (6.6), we can see that, for each $\boldsymbol{y} \in \mathcal{P}_J$, the solution $\hat{u}(\boldsymbol{y})$ is smooth in each subdomain but *not* across the interface $\hat{\Gamma}$; this destroys the analytic dependence of $u(\boldsymbol{y}, \boldsymbol{x}) = \hat{u}(\boldsymbol{y}, \Phi(\boldsymbol{y})\hat{\boldsymbol{x}})$ on $\boldsymbol{y}$ (or rather that of the extension of $\boldsymbol{y}$ to complex polydiscs), and we cannot expect convergence of the Smolyak algorithm.

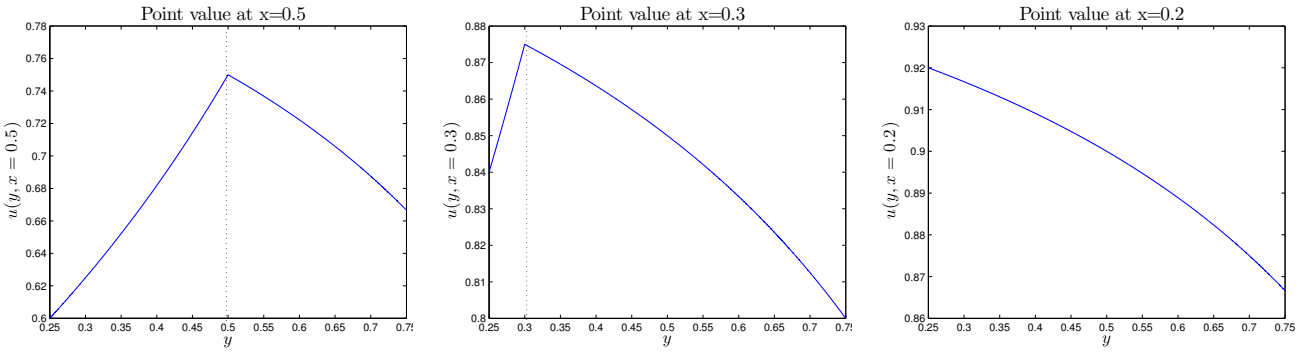

Figure 8.1: Solution to (8.1) for $\alpha_l = 3$, $\alpha_r = 1$ and $y = \frac{1}{2}$.

To better understand this loss of analyticity, we consider the one-dimensional problem:

$$\begin{cases} -\left(\alpha(y,x)u'(y,x)\right)' = 0 \quad x \in (0,1) \\ u(0) = 1 \quad u(1) = 0 \\ \text{for every } y \in \left[\frac{1}{4}, \frac{3}{4}\right], \end{cases} \tag{8.1}$$

where $'$ denotes the derivative with respect to x, and, introducing $\alpha_l, \alpha_r \in \mathbb{R}^+ \setminus \{0\}$, $\alpha_l \neq \alpha_r$:

$$\alpha(y,x) = \begin{cases} \alpha_l & \text{if } x \in (0,y) \\ \alpha_r & \text{if } x \in (y,1) \end{cases}$$

The location $y \in \left[\frac{1}{4}, \frac{3}{4}\right]$ of the interface is the image of a uniformly distributed random variable $Y \sim \mathcal{U}[\frac{1}{4}, \frac{3}{4}]$. The solution is given by

$$u(y,x) = \begin{cases} -\frac{\alpha_r}{\alpha_l(1-y)+\alpha_r y}x + 1 & \text{if } x \in (0,y) \\ \frac{\alpha_l}{\alpha_l(1-y)+\alpha_r y}(1-x) & \text{if } x \in (y,1), \end{cases}$$

and presents a kink at the interface y. Consequently, the evaluation of the solution at a fixed point x in the physical space cannot be analytic as function of y if this point is crossed by the interface. This is evident from Figure 8.1, which shows, for three different points in the domain, the value of the solution to (8.1) as a function y. In the left and center plots, since the points $x = 0.5$ and $x = 0.3$, respectively, are crossed by the interface, we can see that $u(y,x)$ is not analytic as a function of y and has a kink when $y = x$. The right plot correponds to the value of the solution at the point $x = 0.2$, never crossed by the interface ($y \in \left[\frac{1}{4}, \frac{3}{4}\right]$), and thus $u(y,x)$ is analytic in y.

Still, if we consider a mapping from a nominal configuration where the preimage of the interface y corresponds to the point $\frac{1}{2}$:

$$x(y) = \Phi(y,\hat{x}) = \begin{cases} 2y\hat{x} & \text{if } 0 \leq \hat{x} < \frac{1}{2} \\ 2(1-y)\hat{x} + (2y-1) & \text{if } \hat{x} \geq \frac{1}{2}, \end{cases}$$

then, since in the nominal configuration the location of the interface is *fixed*, we can directly see (as we expect from the discussion of subsection 5.3) that the pulledback solution $\hat{u}(y,\hat{x}) := u(y, \Phi(y)(\hat{x}))$ is holomorphic in a complex discs of center $\frac{1}{2}$ and radius $\frac{1}{4} + \varepsilon$, $\varepsilon > 0$:

$$\hat{u}(y,\hat{x}) = \begin{cases} -\frac{2\alpha_r y}{\alpha_l(1-y)+\alpha_r y}\hat{x} + 1 & \text{if } x \in \left(0, \frac{1}{2}\right) \\ \frac{2\alpha_l(1-y)}{\alpha_l(1-y)+\alpha_r y}(1-\hat{x}) & \text{if } x \in \left(\frac{1}{2}, 1\right). \end{cases} \tag{8.2}$$

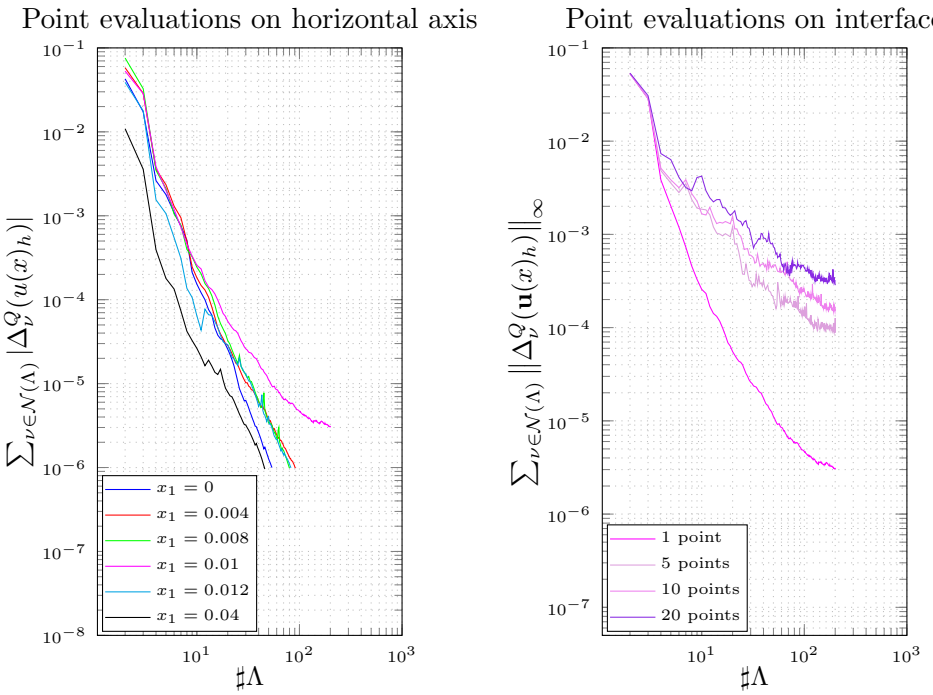

Figure 8.2: Convergence plots for the estimated quadrature error for the value of the real part of the solution when evaluated in a point in the physical space, $d = 16$. Left: point evaluations at different points along the horizontal axis in physical space; right: convergence results considering respectively only one, 5, 10 or 20 point evaluations at points that in *physical* space are on the circumference of radius r_0. Maximal shape variation of 34% with respect to r_0.

We can conclude that the $(\boldsymbol{b}, p, \varepsilon)$-holomorphy assumption (subsection 5.1) is in general not fulfilled by the solution on physical space in the case of stochastic interface problems with discontinuous coefficients. Thus, the convergence of the sparse quadrature (and interpolation) operator is not ensured by Theorem 5.4 (resp. Theorem 5.3). This statement has also been confirmed by the numerical results that we present here.

Consider, in the radius expansion, $s_j = c_j = \frac{0.2 r_0}{j^{\frac{1}{3}}}, j = 1, \ldots, 8$, correponding to a 16-dimensional parameter space, and to a shape variation of 34% with respect to r_0; all the other physical and discretization parameters are the same as in subsection 7.1.3. We have run the sparse quadrature algorithm with Clenshaw-Curtis abscissas for the evaluation of the real part of the solution in one point *in the physical space*, which thus corresponds to a different point in the nominal space for each realization.

The left plot in Figure 8.2 shows the convergence plots considering the point evaluation at different points along the horizontal axis. We report the value of the numerical *error estimator* $\sum_{\nu\in\mathcal{N}(\Lambda)} |\Delta_\nu^I(u(x)_h)|$, computed by the algorithm at each iteration. The first point is the center of the scatterer $\boldsymbol{x} = (0, 0)$, which is mapped back to itself by the domain mapping 3.2. Since this point is never crossed by the interface, this point evaluation is analytic and we observe convergence of the algorithm. For the same reason, the algorithm converges for the points $\boldsymbol{x} = (0.004, 0)$ and $\boldsymbol{x} = (0.04, 0)$, which are inside the scatterer and in the far field region, respectively. The points $\boldsymbol{x} = (0.008, 0)$ and $\boldsymbol{x} = (0.012, 0)$ might be crossed by the interface, but we still observe convergence. This can be explained by the fact that these two points are crossed by the interface only for some realizations, but for most of the quadrature points selected by the algorithm they remain either inside the scatterer (for $\boldsymbol{x} = (0.008, 0)$), either outside it (for $\boldsymbol{x} = (0.012, 0)$); thus, the algorithm still manages to converge in these cases. If we consider instead the point $\boldsymbol{x} = (0.01, 0)$, which is on the circumference of radius r_0 and thus

it is always crossed by the interface, we can see that the convergence curve saturates. However, the curve saturates after an error of 10^{-5}, which may still be acceptable. When we want to consider the entire solution on physical space, though, we may need more point evaluations simultaneously. For this reason, we have run a second experiment.

The right plot in Figure 8.2 shows the convergence curves for the quadrature when considering as quantity of interest only one, 5, 10 or 20 point evaluations for equispaced points in the physical space that are on the circumference of radius r_0. Again, we plot the value of the numerical error estimator $\sum_{\nu\in\mathcal{N}(\Lambda)} \left\|\Delta_\nu^I(\mathbf{u}(x)_h)\right\|_\infty$ calculated by the algorithm at each iteration. Here, the quantity $\mathbf{u}$ represents an array with one, 5, 10 or 20 entries respectively, and $\|\|_\infty$ the maximum norm. As we may observe, the higher is the number of point evaluations that we consider simultaneously, the sooner the error curve saturates; this is expected, because, when considering more points at the same time, there are more regions in the parameter space where the smoothness is lost, and it gets harder for the algorithm to build a set of indices giving a good approximation to the mean for all the point evaluations.

Conclusions

We have presented a methodology for shape uncertainty quantification for the Helmholtz transmission problem, generalizable to any elliptic partial differential equation on a stochastic domain. We have proved and supported by numerical experiments that, under some regularity assumptions on the stochastic interface, it is possible to obtain high order, dimension independent convergence rates for the sparse interpolation and quadrature. We have also developed a regularity theory with respect to the spatial coordinates on the nominal domain, with norm bounds that are independent of the dimension truncation in the parameter space. An important observation that needs further investigation is the loss of smoothness with respect to the high-dimensional parameter when considering evaluations of the solution in the physical configuration, if the points considered can be crossed by the interface.

A Appendix

A.1 Assumption 2.4.A implies a polynomial decay of the coefficient sequences

We can reformulate the statement in the following way:

Lemma A.1. *Let $\boldsymbol{q} = (q_j)_{j\geq 1}$ be a real, monotonically decreasing sequence belonging to $\ell^1(\mathbb{N})$.*

Then there exists a real constant $C_{\boldsymbol{q}} > 0$ (depending on the sequence $\boldsymbol{q}$) and an integer $J \geq 1$ such that

$$|q_j| \leq C_{\boldsymbol{q}} \frac{1}{j} \quad \text{for every } j > J. \tag{A.1}$$

Proof. We prove this result by contradiction. If the statement were not true, then, for all $C > 0$ and all $J_n \in \mathbb{N}$, $n \in \mathbb{N}$, we could find an index $j_n > J_n$ such that $j_n|q_{j_n}| > C$. Let us choose $C = 1$.

We construct our sequence inductively. For $n = 1$, let $J_1 := 1$; then there exists $j_1 > J_1$ such that $j_1|q_{j_1}| > 1$. For $n = 2$, we can select $J_2 := 2j_1$, and by assumption we can find $j_2 > J_2$ such that $j_2|q_{j_2}| > 1$. In general, for any $n \in \mathbb{N}$, given j_{n-1} such that $j_{n-1}|q_{j_{n-1}}| > 1$, we define $J_n := 2j_{n-1}$, and we can find $j_n > J_n$ for which $j_n|q_{j_n}| > 1$. In this way, we have constructed a subsequence $(q_{j_n})_{n\geq 1}$ of $(q_j)_{j\geq 1}$.

Being the sequence $(q_j)_{j\geq 1}$ monotonically decreasing, it holds that

$$\sum_{j=1}^{\infty}|q_j| \geq \sum_{n=1}^{\infty}(j_n - j_{n-1})\frac{1}{j_n},$$

with the convention that $j_0 = 0$. Since we have $j_n > J_n = 2j_{n-1}$ for every $n \in \mathbb{N}$, then

$$\sum_{j=1}^{\infty}|q_j| \geq \sum_{n=1}^{\infty}\left(1 - \frac{j_{n-1}}{j_n}\right) > \sum_{n=1}^{\infty}\left(1 - \frac{1}{2}\right) = \sum_{n=1}^{\infty}\frac{1}{2} = +\infty,$$

which contradicts the hypothesis that the sequence belongs to $\ell^1(\mathbb{N})$. □

From this result, it follows trivially:

Corollary A.2. *Let $\boldsymbol{q} = (q_j)_{j\geq 1}$ be a real, monotonically decreasing sequence belonging to $\ell^p(\mathbb{N})$, $0 < p < \infty$.*

Then there exists a real constant $C_{\boldsymbol{q}} > 0$ (depending on the sequence $\boldsymbol{q}$) and an integer $J \geq 1$ such that

$$|q_j| \leq C_{\boldsymbol{q}}\frac{1}{j^{\frac{1}{p}}} \quad \text{for every } j > J. \tag{A.2}$$

A.2 Proof of Proposition 2.5 (Assumption 2.4.B implies Assumption 2.4.A)

If a function $f = f(\varphi)$ belongs to $C^k_{\text{per}}([0, 2\pi))$, then Corollary 3.3.10 in [21] implies that its Fourier coefficients $\hat{f}_j, j \geq 1$, are bounded by

$$|\hat{f}_j| \leq \lambda(k)\left\|\frac{d^k f}{d\varphi^k}\right\|_{L^1_{\text{per}}([0,2\pi))}\frac{1}{1+j^k}, \quad j \geq 1,$$

with $\lambda = \lambda(k)$ a constant depending only on k but not on j and f. The Fourier coefficients of the radius are given by $|c_j Y_{2j-1}(\omega)| \leq |c_j|$ (resp. $|s_j Y_{2j}(\omega)| \leq |s_j|$), $j \geq 1$, with the equality when $Y_{2j-1}(\omega) = \pm 1$ (resp. $Y_{2j}(\omega) = \pm 1$). Then, for every $j \geq 1$,

$$|c_j| \leq \lambda(k)\sup_{\omega\in\Omega}\left\|\frac{d^k r}{d\varphi^k}(\omega)\right\|_{L^1_{\text{per}}([0,2\pi))}\frac{1}{1+j^k},$$

and similarly for $|s_j|$, $j \geq 1$. This proves (2.2) with $C(k) := \lambda(k)\sup_{\omega\in\Omega}\left\|\frac{d^k r}{d\varphi^k}(\omega)\right\|_{L^1_{\text{per}}([0,2\pi))}$, which is not infinite thanks to the uniform bound required by Assumption 2.4.B.

Since the constant $C(k)$ is independent of j, $j \geq 1$, the coefficients sequences $\mathcal{C} = (c_j)_{j\geq 1}$ and $\mathcal{S} = (s_j)_{j\geq 1}$ are in $\ell^p(\mathbb{N})$ for every p such that $kp > 1$, i.e. $p > \frac{1}{k}$.

A.3 Case of not identically distributed random variables

In Remark 2.7, we have mentioned that the hypothesis that all random variables are identically distributed can be relaxed with not too much effort. Indeed, if $\{Y_j\}_{j=1}^{2J}$, $J \in \mathbb{N}$, are still independent but not identically distributed as uniform random variables, the joint probabily distribution μ can still be factorized as $\mu := \bigotimes_{j=1}^{2J}\mu_j$; then, denoting by $g = g(\boldsymbol{y})$, $\boldsymbol{y} \in \mathcal{P}_J$, the quantity of interest, if each univariate probability distribution has still compact image, one can apply the forthcoming analysis and algorithms to $g(\boldsymbol{y})\mu(\boldsymbol{y})$ in place of $g(\boldsymbol{y})$, $\boldsymbol{y} \in \mathcal{P}_J$.

A.4 Proof of Theorem 4.3 (existence and uniqueness of the solution to the model problem)

Let $\boldsymbol{y} \in \mathcal{P}_J$, $J \in \mathbb{N}$ be fixed.

We denote

$$a^p_{\boldsymbol{y}}(u,v) := \int_{K_R} \alpha(\boldsymbol{y},\boldsymbol{x})\, \nabla u(\boldsymbol{y}) \cdot \nabla v \; d\boldsymbol{x} - \int_{\partial K_R} DtN(u(\boldsymbol{y}))v \; dS.$$

If we show that the bilinear form $a^p_{\boldsymbol{y}}(u,v)$ is coercive, then the associated operator $\mathcal{A}^p_{\boldsymbol{y}}$ defined as $(A^p_{\boldsymbol{y}}u, v) := a^p_{\boldsymbol{y}}(u,v)$ is Fredholm [30, Lemma 2.32].

The operator $\mathcal{B}_{\boldsymbol{y}} : H^1(K_R) \to H^{-1}(K_R)$ associated to $\int_{K_R} k^2(\boldsymbol{y},\boldsymbol{x})u(\boldsymbol{y})v \, d\boldsymbol{x}$ is given by $\mathcal{B}_{\boldsymbol{y}} = k^2(\boldsymbol{y},\boldsymbol{x})I$, with $I : H^1(K_R) \to H^{-1}(K_R)$ the identity operator. Since K_R is bounded, $I : H^1(K_R) \to H^{-1}(K_R)$ and thus $\mathcal{B}_{\boldsymbol{y}}$ are compact thanks to Rellich's embedding theorem [30, Theorem 3.27].

Therefore, if $a^p_{\boldsymbol{y}}(u,v)$ is coercive, then the operator $\mathcal{A}^p_{\boldsymbol{y}} + \mathcal{B}_{\boldsymbol{y}}$ is Fredholm [30, Theorem 2.33] and we can apply the Fredholm Alternative [30, Theorem 2.27] to get existence of the solution and uniqueness if the associated homogeneous problem

$$a_{\boldsymbol{y}}(u(\boldsymbol{y}), v) = 0 \quad \text{for all } v \in V \tag{A.3}$$

admits only the trivial solution.

For the coercivity of $a^p_{\boldsymbol{y}}(\cdot,\cdot)$ it holds that, for every $w \in H^1(K_R)$:

$$\begin{aligned}
\text{Re } a^p_{\boldsymbol{y}}(w,w) &\geq \min\{1,\mu\}\, |w|^2_{H^1(K_R)} - \text{Re}\langle DtN w, w\rangle_{L^2(\partial K_R)} \\
&\geq \min\{1,\mu\}\, |w|^2_{H^1(K_R)} + \|w\|^2_{L^2(\partial K_R)} \\
&\geq \min\{1,\mu\}\, \frac{C(R)}{C(R)+1}\, \|w\|^2_{H^1(K_R)}.
\end{aligned}$$

The first inequality is obtained exploiting the sign conditions of the DtN map [33, Theorem 2.6.4], the second one is a Poincaré-Friedrichs-type inequality

$$|w|^2_{H^1(K_R)} + \|w\|^2_{L^2(\partial K_R)} \geq C(R)\, \|w\|^2_{L^2(K_R)} \quad \text{for every } w \in H^1(K_R), \tag{A.4}$$

where the constant $C > 0$ depends on the radius R of K_R. This latter inequality can be proven in the same way as the classical Poincaré-Friedrichs inequality. Thus, the Fredholm Alternative holds and we have existence of the solution.

For uniqueness, let us consider the homogeneous problem (A.3). It is sufficient to show that

$$a_{\boldsymbol{y}}(u,u) = 0 \iff u \equiv 0.$$

If $a_{\boldsymbol{y}}(u,u) = 0$, it means in particular that

$$\text{Im}\, a_{\boldsymbol{y}}(u,u) = \text{Im} \int_{\partial K_R} DtN(u(\boldsymbol{y}))u \; dS = 0.$$

For the sign properties of the DtN map [33, Theorems 2.6.1 and 2.6.4]

$$\text{Im}\langle DtN u, u\rangle_{L^2(\partial K_R)} = 0 \iff u \equiv 0 \text{ on } \partial K_R,$$

while the linearity of the DtN map implies that also $\dfrac{\partial u}{\partial \boldsymbol{n}_R} = 0$ on ∂K_R and thus $u \equiv 0$ for $|\boldsymbol{x}| \geq R$.

Consider now a ball B_r with center on ∂K_R and radius $r < \operatorname{dist}(\partial K_R, D_2)$. In B_r the solution u satisfies the homogeneous equation $\Delta u - k^2(\boldsymbol{y}, \boldsymbol{x})u = 0$ and thus $u|_{B_r} \in H^2(B_r)$; also, from the previous considerations we know that there exists a ball $B_{r'} \subset B_r \setminus K_R$, with $r' < r$, such that $u|_{B_{r'}} \equiv 0$. Then, the unique continuation principle [15, Theorem 8.6] implies that $u = 0$ in the whole B_r. Iterating this argument and using the compactness of K_R, we obtain that $u \equiv 0$ in K_R.

Then, the solution to (4.2) exists and is unique thanks to the bijectivity of the maps $\Phi(\boldsymbol{y})$, $\boldsymbol{y} \in \mathcal{P}_J$ (and Definition 4.2).

A.5 Proof of Lemma 4.5 ($\boldsymbol{y}$-uniform stability bound)

Coercivity of the bilinear form with coercivity constant independent of $J \in \mathbb{N}$ and $\boldsymbol{y} \in \mathcal{P}_J$:

Thanks to Assumption 3.1, we have that there exist $\sigma_{\min}, \sigma_{\max} > 0$ such that, for every $J \in \mathbb{N}$ and every $\boldsymbol{y} \in \mathcal{P}_J$:

$$\sigma_{\min}^2 \|\boldsymbol{\xi}\|_{\mathbb{C}^2}^2 \leq \|D\Phi^{-\top}(\boldsymbol{y}, \hat{\boldsymbol{x}})\boldsymbol{\xi}\|_{\mathbb{C}^2}^2 \tag{A.5}$$

$$\frac{1}{\sigma_{\max}^2} \leq \det D\Phi(\boldsymbol{y}, \hat{\boldsymbol{x}}) \leq \frac{1}{\sigma_{\min}^2} \tag{A.6}$$

for every $\boldsymbol{\xi} \in \mathbb{C}^2$, $\hat{\boldsymbol{x}} \in K_R$. Then, for every $J \in \mathbb{N}$, $\boldsymbol{y} \in \mathcal{P}_J$ and every $\hat{w} \in H^1(K_R)$, we have:

$$\begin{aligned}
\operatorname{Re} \hat{a}_y(\hat{w}, \hat{w}) &\geq \min\{1, \mu\} \, |D\Phi^{-\top}(\boldsymbol{y})\hat{\nabla}\hat{w}(\det D\Phi(\boldsymbol{y}))^{\frac{1}{2}}|_{H^1(K_R)}^2 \\
&\quad - \max\left\{k_1^2, k_2^2\right\} \left\|\hat{w}(\det D\Phi(\boldsymbol{y}))^{\frac{1}{2}}\right\|_{L^2(K_R)}^2 - \operatorname{Re}\langle DtN(\hat{w}), \hat{w}\rangle_{L^2(\partial K_R)} \\
&\geq \min\{1, \mu\} \frac{\sigma_{\min}^2}{\sigma_{\max}^2} |\hat{w}|_{H^1(K_R)}^2 - \max\left\{k_1^2, k_2^2\right\} \frac{1}{\sigma_{\min}^2} \|\hat{w}\|_{L^2(K_R)}^2 + \|\hat{w}\|_{L^2(\partial K_R)}^2 \\
&\geq \left(\min\{1, \mu\} \frac{\sigma_{\min}^2}{\sigma_{\max}^2} - \frac{\tau}{\sigma_{\min}^2}\right) |\hat{w}|_{H^1(K_R)}^2 + \left(1 - \frac{\tau}{\sigma_{\min}^2}\right) \|\hat{w}\|_{L^2(\partial K_R)}^2 .
\end{aligned}$$

In the second inequality we have used equations (A.5)-(A.6) and the sign conditions of the DtN map [33, Theorem 2.6.4].

Now, if we choose τ in Assumption 4.4 such that $\tau < T := \sigma_{\min}^2 \min\left\{\frac{\sigma_{\min}^2}{\sigma_{\max}^2} \min\{1, \mu\}, 1\right\}$, we have that

$$C_1 := \min\{1, \mu\} \frac{\sigma_{\min}^2}{\sigma_{\max}^2} - \frac{\tau}{\sigma_{\min}^2} > 0, \qquad C_2 := 1 - \frac{\tau}{\sigma_{\min}^2} > 0.$$

Using a Poincaré-Friedrichs-type inequality on K_R as in (A.4), we finally obtain

$$\operatorname{Re} \hat{a}_y(\hat{w}, \hat{w}) \geq \min\{C_1, C_2\} \frac{C(R)}{C(R)+1} \|\hat{w}\|_{H^1(K_R)}^2 ,$$

for every $J \in \mathbb{N}$, every $\boldsymbol{y} \in \mathcal{P}_J$ and every $\hat{w} \in H^1(K_R)$; this means that the bilinear form $\hat{a}_y(\cdot, \cdot)$ is coercive with coercivity constant $\gamma = \min\{C_1, C_2\} \frac{C(R)}{C(R)+1}$ independent of $J \in \mathbb{N}$ and of $\boldsymbol{y} \in \mathcal{P}_J$.

J- and $\boldsymbol{y}$-uniform stability bound:

The right-hand side in (4.2) is continous with respect to the H^1-norm:

$$\begin{aligned}
\left|\int_{\partial K_R} \left(-DtN(u_i) + \frac{\partial u_i}{\partial \boldsymbol{n}_R}\right) v \, dS\right| &\leq \left(\|DtN(u_i)\|_{H^{-\frac{1}{2}}(\partial K_R)} + \left\|\frac{\partial u_i}{\partial \boldsymbol{n}_R}\right\|_{H^{-\frac{1}{2}}(\partial K_R)}\right) \|v\|_{L^2(\partial K_R)} \\
&\leq \left(\|DtN(u_i)\|_{H^{-\frac{1}{2}}(\partial K_R)} + \left\|\frac{\partial u_i}{\partial \boldsymbol{n}_R}\right\|_{H^{-\frac{1}{2}}(\partial K_R)}\right) \|v\|_{H^1(K_R)} \\
&\leq \left(\tilde{C}(R) \|u_i\|_{H^{\frac{1}{2}}(\partial K_R)} + \left\|\frac{\partial u_i}{\partial \boldsymbol{n}_R}\right\|_{H^{-\frac{1}{2}}(\partial K_R)}\right) \|v\|_{H^1(K_R)} ,
\end{aligned}$$

where we used the continuity of the DtN operator [33, Theorem 2.6.4]. We highlight that the constant $\tilde{C}$ depends only on the radius R.

Together with the coercivity of the bilinear form, this allows to apply Lax-Milgram's lemma and obtain (4.6) with $B_1 := \frac{\tilde{C}}{\gamma}$ and $B_2 := \frac{1}{\gamma}$.

A.6 Proof of Lemma 5.8 (Φ in (3.2) fulfills Assumption 5.7 (ii))

From (2.5), we have that:

$$r(\boldsymbol{z},\varphi) = r(\boldsymbol{y},\varphi) + \sum_{j=1}^{J} c_j(z_{2j-1} - y_{2j-1})\cos(j\varphi) + s_j(z_{2j} - y_{2j})\sin(j\varphi).$$

Since $\boldsymbol{z} \in \mathcal{O}_{\boldsymbol{\rho}}$, for every $J \in \mathbb{N}$ there exists $\boldsymbol{y} \in \mathcal{P}_J$ such that $|z_l - y_l| < \rho_l - 1$ for every $1 \le l \le J$; moreover, being $\boldsymbol{\rho}$ $(\boldsymbol{b},\varepsilon)^*$-admissible, it is in particular $(\boldsymbol{b},\varepsilon)$-admissible, which, together with (5.16), implies that

$$|r(\boldsymbol{z},\varphi)| \le r^+ + \varepsilon \quad \text{for every } \varphi \in [0,2\pi);$$

analogously, taking into account that $0 < \varepsilon < \frac{r^-}{2}$, we get

$$|r(\boldsymbol{z},\varphi)| \ge \operatorname{Re} r(\boldsymbol{z},\varphi) \ge r^- - \varepsilon \ge \frac{r^-}{2} \quad \text{for every } \varphi \in [0,2\pi). \tag{A.7}$$

Finally, using (5.17) and (5.13), for every $J \in \mathbb{N}$ and $\boldsymbol{y} \in \mathcal{P}_J$ such that $|z_l - y_l| < \rho_l - 1$ for every $1 \le l \le J$:

$$\begin{aligned}
\Big|\frac{\partial r}{\partial \varphi}(\boldsymbol{z},\varphi)\Big| &= \Big|\frac{\partial r}{\partial \varphi}(\boldsymbol{y},\varphi) + \sum_{j=1}^{J} c_j j(z_{2j-1} - y_{2j-1})\cos(j\varphi) + s_j j(z_{2j} - y_{2j})\sin(j\varphi)\Big| \\
&\le \Big\|\frac{\partial r}{\partial \varphi}(\boldsymbol{y})\Big\|_{C^0_{\mathrm{per}}([0,2\pi))} + C(\varepsilon) \\
&\le \Big\|\frac{\partial r_0}{\partial \varphi}\Big\|_{C^0_{\mathrm{per}}([0,2\pi))} + C_r + C(\varepsilon) \quad \text{for every } \varphi \in [0,2\pi).
\end{aligned}$$

We remark that all the bounds are independent of the truncation dimension $J \in \mathbb{N}$.

Proceeding as in the proof to show that $\Phi = \Phi(\boldsymbol{y})$ given by (3.2), $\boldsymbol{y} \in \mathcal{P}_J$, fulfills Assumption 3.1 (see subsection A.8 in this appendix), it is easy to see that the bounds proved in this lemma guarantee that this map fulfills Assumption 5.7 for $\boldsymbol{z} \in \mathcal{O}_{\boldsymbol{\rho}}$.

A.7 Proof of Lemma 6.1 (regularity of the radius)

From (2.5), computing the k-th derivative and considering that $\max_{\varphi\in[0,2\pi)} |\sin(j\pi\varphi)| = \max_{\varphi\in[0,2\pi)} |\cos(j\pi\varphi)| = 1$, $j \ge 1$, we obtain an upper bound for the $C^k_{per}([0,2\pi))$-seminorm of the radius:

$$\begin{aligned}
|r(\boldsymbol{y})|_{C^k_{per}([0,2\pi))} = \max_{\varphi\in[0,2\pi)} \Big|\frac{d^k r(\boldsymbol{y},\varphi)}{d\varphi^k}\Big| &\le |r_0|_{C^k_{per}([0,2\pi))} + \sum_{j=1}^{J} j^k \left(|y_{2j}c_j| + |y_{2j+1}s_j|\right) \le \\
&\le |r_0|_{C^k_{per}([0,2\pi))} + \sum_{j=1}^{\infty} j^k \left(|c_j| + |s_j|\right),
\end{aligned} \tag{A.8}$$

for every $\boldsymbol{y} \in \mathcal{P}_J$. If $(c_j)_{j\ge1} \in \ell^p(\mathbb{N})$ and it has a monotone majorant, then, thanks to Corollary A.2, there exists an integer $J \ge 1$ such that

$$|c_j| \lesssim \frac{1}{j^{\frac{1}{p}}} \quad \text{and thus} \quad j^k|c_l| \lesssim \frac{1}{j^{\frac{1}{p}-k}} \quad \text{for all } j > J$$

(where $\lesssim$ denotes inequality up to a constant that may depend on the sequence); the same holds for the coefficients $(s_j)_{j\geq 1}$. Then, the sum in (A.8) converges for every k such that

$$\frac{1}{p} - k > 1,$$

that is if we choose k as in (6.2). We remark that the bound that we obtain for (A.8) is independent of the truncation dimension $J \in \mathbb{N}$ and of $\boldsymbol{y} \in \mathcal{P}_J$.

A.8 Proof of Lemma 6.2 (regularity of the domain mapping for the particle in free space)

Fulfillment of Assumption 3.1(i)

We have to prove that $\Phi(\boldsymbol{y})$ is a C^k-orientation preserving diffeomorphism in each subdomain, with k the smoothness of the stochastic radius r and a J- and $\boldsymbol{y}$-independent norm bound.

In the regions where $\chi = 0$, then the mapping Φ given by (3.2) corresponds to the identity, and thus it is bijective. Where not zero, χ is monotone in each subdomain, and thus Φ is bijective everywhere in K_R.

We present here the computations for the smoothness of Φ in $\hat{D}_2$, the argument for the smoothness in $K_R \cap \hat{D}_1$ being analogous. More precisely, we consider the mapping in the region $\hat{D}_{2,\chi} := \left\{\hat{\boldsymbol{x}} \in \hat{D}_2 : \frac{r_0^-}{4} \leq \|\boldsymbol{x}\| \leq r_0(\varphi)\right\}$. Indeed, Assumption 3.1(i) is trivially satisfied for $\|\hat{\boldsymbol{x}}\| \leq \frac{r_0^-}{4}$, and the smoothness assumption on χ guarantees that the mapping is smooth across the circle of radius $\frac{r_0^-}{4}$. For the continuity of the inverse and its derivatives across the circle of radius $\frac{r_0^-}{4}$, let us consider an annulus together with its boundary, enclosing the circle of radius $\frac{r_0^-}{4}$ in its interior. Since the map Φ and, as we will show, its derivatives, are continous in the annulus with boundary, which is a compact subset of $\mathbb{R}^2$, then also Φ^{-1} and its derivatives are.

For the continuity of Φ and its inverse, using Assumption 2.3, we have the J- and $\boldsymbol{y}$-independent bounds:

$$\begin{aligned}
\|\Phi(\boldsymbol{y})\|_{C^0(\hat{D}_{2,\chi})} &\leq \max_{\hat{\boldsymbol{x}}\in\hat{D}_{2,\chi}} \|\hat{\boldsymbol{x}}\| + \max_{\hat{\boldsymbol{x}}\in\hat{D}_{2,\chi}} \|\chi(\hat{\boldsymbol{x}})\| \max_{\hat{\boldsymbol{x}}\in\hat{D}_{2,\chi}} |r(\boldsymbol{y},\hat{\varphi}) - r_0(\hat{\varphi})| = r_0^+ + \frac{r_0^-}{2}, \\
\|\Phi^{-1}(\boldsymbol{y})\|_{C^0(D_{2,\chi}(\boldsymbol{y}))} &= \max_{\boldsymbol{x}\in D_{2,\chi}(\boldsymbol{y})} \|\Phi^{-1}(\boldsymbol{y},\boldsymbol{x})\| = \max_{\hat{\boldsymbol{x}}\in\hat{D}_{2,\chi}} \|\Phi^{-1}\left(\boldsymbol{y},\Phi(\boldsymbol{y},\hat{\boldsymbol{x}})\right)\| = \max_{\hat{\boldsymbol{x}}\in\hat{D}_{2,\chi}} \|\hat{\boldsymbol{x}}\| = r_0^+,
\end{aligned}$$

where we have denoted $D_{2,\chi}(\boldsymbol{y}) := \Phi(\boldsymbol{y})(\hat{D}_{2,\chi})$ and $r_0^+ := \sup_{\varphi\in[0,2\pi)} r_0(\varphi)$.

For ease of computations of the derivatives, since the mapping from cartesian to polar coordinates is a C^∞-diffeomorphism away from the origin, we work with the mapping Φ in polar coordinates. Namely, we consider:

$$\tilde{\Phi}(\boldsymbol{y})(\hat{\rho},\hat{\varphi}) = \begin{pmatrix}\rho\\ \varphi\end{pmatrix} = \begin{pmatrix}\hat{\rho} + \tilde{\chi}(\hat{\rho},\hat{\varphi})(r(\boldsymbol{y},\hat{\varphi}) - r_0(\hat{\varphi}))\\ \hat{\varphi}\end{pmatrix} \quad \text{for } \frac{r_0^-}{4} \leq \hat{\rho} \leq r_0(\hat{\varphi}) \text{ and } \hat{\varphi} \in [0,2\pi), \tag{A.9}$$

where, denoting by Φ_p the mapping from cartesian to polar coordinates, $(\hat{\rho},\hat{\varphi}) = \Phi_p(\hat{\boldsymbol{x}})$, $(\rho,\varphi) = \Phi_p(\boldsymbol{x})$ and $\tilde{\chi} := \chi \circ \Phi_p^{-1}$.

The Jacobian matrices of $\tilde{\Phi}$ and $\tilde{\Phi}^{-1}$ are given by:

$$D\tilde{\Phi}(\boldsymbol{y}) = \begin{pmatrix} 1 + \dfrac{\partial\tilde{\chi}}{\partial\hat{\rho}}(r(\boldsymbol{y},\hat{\varphi}) - r_0(\hat{\varphi})) & \dfrac{\partial\tilde{\chi}}{\partial\hat{\varphi}}(r(\boldsymbol{y},\hat{\varphi}) - r_0(\hat{\varphi})) + \tilde{\chi}\dfrac{\partial}{\partial\hat{\varphi}}(r(\boldsymbol{y},\hat{\varphi}) - r_0(\hat{\varphi})) \\ 0 & 1 \end{pmatrix}$$

$$D\tilde{\Phi}^{-1}(\boldsymbol{y}) = (D\tilde{\Phi})^{-1} \circ \tilde{\Phi}^{-1}(\boldsymbol{y}) = \frac{1}{\det D\tilde{\Phi}(\boldsymbol{y})} \begin{pmatrix} 1 & -\dfrac{\partial\tilde{\chi}}{\partial\hat{\varphi}}(r(\boldsymbol{y},\hat{\varphi}) - r_0(\hat{\varphi})) - \tilde{\chi}\dfrac{\partial}{\partial\hat{\varphi}}(r(\boldsymbol{y},\hat{\varphi}) - r_0(\hat{\varphi})) \\ 0 & 1 + \dfrac{\partial\tilde{\chi}}{\partial\hat{\rho}}(r(\boldsymbol{y},\hat{\varphi}) - r_0(\hat{\varphi})). \end{pmatrix}$$

Using Assumption 3.2 on χ and Assumption 2.3 on the coefficients on the radius expansion, we can bound each entry of $D\tilde{\Phi}(\boldsymbol{y})$:

$$\begin{aligned} \left|1 + \frac{\partial\tilde{\chi}}{\partial\hat{\rho}}(r(\boldsymbol{y},\hat{\varphi}) - r_0(\hat{\varphi}))\right| &\leq 1 + \left|\frac{\partial\tilde{\chi}}{\partial\hat{\rho}}\right| \frac{r_0^-}{2} \leq 1 + \sqrt{2}\|\chi\|_{C^1(\hat{D}_{2,\chi})}\frac{r_0^-}{2} \leq 2 \\ \left|\frac{\partial\tilde{\chi}}{\partial\hat{\varphi}}(r(\boldsymbol{y},\hat{\varphi}) - r_0(\hat{\varphi})) + \tilde{\chi}\frac{\partial}{\partial\hat{\varphi}}(r(\boldsymbol{y},\hat{\varphi}) - r_0(\hat{\varphi}))\right| &\leq \left|\frac{\partial\tilde{\chi}}{\partial\hat{\varphi}}\right| |r(\boldsymbol{y},\hat{\varphi}) - r_0(\hat{\varphi})| + |\chi| \sum_{j=1}^{\infty} j\,(|c_j| + |s_j|) \\ &\leq \|\chi\|_{C^1(\hat{D}_{2,\chi})} \left(\sqrt{2}r_0^+\frac{r_0^-}{2} + C_r\right), \end{aligned}$$

with $C_r = \sum_{j=1}^{\infty} j\,(|c_j| + |s_j|) < \infty$.

The above estimates show that we have a J- and $\boldsymbol{y}$-independent bound on the C^1-norm of Φ.

It is clear from the expression of $D\tilde{\Phi}^{-1}$ that, if we provide also a J- and $\boldsymbol{y}$-independent (positive) lower bound on $\det D\tilde{\Phi}(\boldsymbol{y})$, then we also have a J- and $\boldsymbol{y}$-independent upper bound on the C^1-norm of Φ^{-1}. It holds:

$$\det D\tilde{\Phi}(\boldsymbol{y}) \geq 1 - |r(\boldsymbol{y},\hat{\varphi}) - r_0(\hat{\varphi})| \left|\frac{\partial\tilde{\chi}}{\partial\hat{\rho}}\right| \geq 1 - \frac{r_0^-}{2}\sqrt{2}\|\chi\|_{C^1(\hat{D}_{2,\chi})} \geq 1 - \frac{r_0^-}{2}\sqrt{2}C_\chi > 0,$$

where we have used the bound on $\|\chi\|_{C^1(\hat{D}_{2,\chi})}$ provided by Assumption 3.2.

For the higher order derivatives of Φ, it is clear from (3.2) that this map is as many times differentiable as $\chi(\cdot)$, $r(\boldsymbol{y},\cdot)$ and $r_0(\cdot)$ are. The mollifier χ and the nominal radius r_0 are assumed to be smooth and they do not depend on $\boldsymbol{y} \in \mathcal{P}_J$. Thus, the J- and $\boldsymbol{y}$-uniform bound on the $C^0(\hat{D}_{2,\chi})$-norm of the derivatives is ensured by the J- and $\boldsymbol{y}$-uniform bound on $\|r(\boldsymbol{y},\cdot)\|_{C^k_{per}([0,2\pi))}$, with k the highest differentiability order of the radius.

Concerning the higher order derivatives of Φ^{-1}, they are obtained from chain rule on the entries of $D\Phi^{-1} = (D\Phi)^{-1} \circ \Phi^{-1}$. More precisely, a m-th order derivative is given by the sum and product of powers of entries of $(D\Phi(\boldsymbol{y}))^{-1}$ times the product of derivatives of $\Phi(\boldsymbol{y})$ up to the m-th order. Since we have already stated the J- and $\boldsymbol{y}$- uniform upper bound on the derivatives of $\Phi(\boldsymbol{y})$ and on the entries of $(D\Phi(\boldsymbol{y}))^{-1}$, then we can conclude that Φ is a C^k-diffeomorphism, with k the smoothness of the radius $r(\boldsymbol{y},\hat{\varphi})$ and J- and $\boldsymbol{y}$-independent norm bounds.

Fulfillment of Assumption 3.1(ii)

It is clear from (3.2) that this assumption is satisfied.

Fulfillment of Assumption 3.1(iii)

Also in this case, we restrict our computations to the domain $\hat{D}_{2,\chi}$, being the case trivial for $\|\hat{\boldsymbol{x}}\| \leq \frac{r_0^-}{4}$ and analogous for $\|\hat{\boldsymbol{x}}\| \geq r_0(\hat{\varphi})$.

Again, it is convenient to work in polar coordinates. We use the notation $\tilde{\sigma}_1$ and $\tilde{\sigma}_2$ for minimum and maximum singular values of $D\tilde{\Phi}$, respectively.

It holds that $\tilde{\sigma}_2(\boldsymbol{y}) = \|D\tilde{\Phi}(\boldsymbol{y})\|_2 \leq \|D\tilde{\Phi}(\boldsymbol{y})\|_F$, where $\|\cdot\|_F$ denotes the Frobenius norm. Since from the previous computations we have a J- and $\boldsymbol{y}$-uniform upper bound on the $C^0(\hat{D}_{2,\chi})$-norm of each entry of $D\tilde{\Phi}$, then there exists a J- and $\boldsymbol{y}$-uniform upper bound on the $C^0(\hat{D}_{2,\chi})$-norm of $\tilde{\sigma}_1$ and $\tilde{\sigma}_2$, too.

Furthermore,

$$\tilde{\sigma}_1(\boldsymbol{y}) = \frac{\det(D\tilde{\Phi}^\top(\boldsymbol{y})D\tilde{\Phi}(\boldsymbol{y}))}{\tilde{\sigma}_2(\boldsymbol{y})} = \frac{\left(\det D\tilde{\Phi}(\boldsymbol{y})\right)^2}{\tilde{\sigma}_2(\boldsymbol{y})}.$$

Coupling the J- and $\boldsymbol{y}$-uniform upper bound on $\tilde{\sigma}_2$ with the J- and $\boldsymbol{y}$-uniform lower positive bound on $\det D\tilde{\Phi}(\boldsymbol{y})$ from the previous paragraph, we obtain a J- and $\boldsymbol{y}$-uniform lower bound on the $C^0(\hat{D}_{2,\chi})$-norm of $\tilde{\sigma}_1$.

Finally, since the mapping from cartesian to polar coordinates is a C^∞-diffeomorphism away from the origin, we can state that there exist J- and $\boldsymbol{y}$-uniform, upper and lower, positive bounds on the $C^0(\hat{D}_{2,\chi})$-norm of the singular values of $D\Phi$ and $D\Phi^{-1}$.

References

[1] I. Babuška, F. Nobile, and R. Tempone, *A stochastic collocation method for elliptic partial differential equations with random input data*, SIAM review, 52 (2010), pp. 317–355.

[2] J. Bäck, F. Nobile, L. Tamellini, and R. Tempone, *Stochastic spectral Galerkin and collocation methods for PDEs with random coefficients: a numerical comparison*, in Spectral and High Order Methods for Partial Differential Equations, Springer, 2011, pp. 43–62.

[3] J.-P. Berenger, *A perfectly matched layer for the absorption of electromagnetic waves*, Journal of Computational Physics, 114 (1994), pp. 185–200.

[4] M. Bieri, R. Andreev, and C. Schwab, *Sparse tensor discretization of elliptic SPDEs*, SIAM Journal on Scientific Computing, 31 (2009), pp. 4281–4304.

[5] S. C. Brenner and R. Scott, *The mathematical theory of finite element methods*, vol. 15, Springer Science & Business Media, 2008.

[6] J.-P. Calvi and P. Manh, *Lagrange interpolation at real projections of Leja sequences for the unit disk*, Proceedings of the American Mathematical Society, 140 (2012), pp. 4271–4284.

[7] C. Canuto and T. Kozubek, *A fictitious domain approach to the numerical solution of PDEs in stochastic domains*, Numerische mathematik, 107 (2007), pp. 257–293.

[8] J. E. Castrillon-Candas, F. Nobile, and R. F. Tempone, *Analytic regularity and collocation approximation for PDEs with random domain deformations*, arXiv preprint arXiv:1312.7845, (2013).

[9] A. Chkifa, A. Cohen, and C. Schwab, *High-dimensional adaptive sparse polynomial interpolation and applications to parametric PDEs*, Foundations of Computational Mathematics, 14 (2014), pp. 601–633.

[10] M. A. Chkifa, *On the Lebesgue constant of Leja sequences for the complex unit disk and of their real projection*, Journal of Approximation Theory, 166 (2013), pp. 176–200.

[11] A. Cohen, A. Chkifa, C. Schwab, et al., *Breaking the curse of dimensionality in sparse polynomial approximation of parametric PDEs*, (2013).

[12] A. Cohen, R. DeVore, and C. Schwab, *Convergence rates of best N-term Galerkin approximations for a class of elliptic sPDEs*, Foundations of Computational Mathematics, 10 (2010), pp. 615–646.

[13] ——, *Analytic regularity and polynomial approximation of parametric and stochastic elliptic PDEs*, Analysis and Applications, 9 (2011), pp. 11–47.

[14] F. Collino and P. Monk, *The perfectly matched layer in curvilinear coordinates*, SIAM Journal on Scientific Computing, 19 (1998), pp. 2061–2090.

[15] D. Colton and R. Kress, *Inverse acoustic and electromagnetic scattering theory*, vol. 93, Springer Science & Business Media, 2012.

[16] M. Eigel, C. J. Gittelson, C. Schwab, and E. Zander, *Adaptive stochastic Galerkin FEM*, Computer Methods in Applied Mechanics and Engineering, 270 (2014), pp. 247–269.

[17] R. N. Gantner and C. Schwab, *Computational Higher Order Quasi-Monte Carlo Integration*, Proc. MCQMC14, in review, (2014).

[18] T. Gerstner and M. Griebel, *Dimension–adaptive tensor–product quadrature*, Computing, 71 (2003), pp. 65–87.

[19] R. G. Ghanem and P. D. Spanos, *Stochastic finite elements: a spectral approach*, Courier Corporation, 2003.

[20] D. Gilbarg and N. S. Trudinger, *Elliptic partial differential equations of second order*, vol. 224, Springer Science & Business Media, 2001.

[21] L. Grafakos, *Classical and modern Fourier analysis*, AMC, 10 (2004).

[22] H. Harbrecht and J. Li, *First order second moment analysis for stochastic interface problems based on low-rank approximation*, ESAIM: Mathematical Modelling and Numerical Analysis, 47 (2013), pp. 1533–1552.

[23] H. Harbrecht, M. Peters, and M. Siebenmorgen, *Numerical solution of elliptic diffusion problems on random domains*, Preprint 2014-08, Mathematisches Institut, Universität Basel, (2014).

[24] H. Harbrecht, R. Schneider, and C. Schwab, *Sparse second moment analysis for elliptic problems in stochastic domains*, Numerische Mathematik, 109 (2008), pp. 385–414.

[25] R. Hiptmair and S. Sargheini, *Scatterers on the substrate: Far field formulas*, Report 2015-02, Seminar for Applied Mathematics, ETH Zürich, Switzerland.

[26] S. G. Krantz, *Function theory of several complex variables*, Wiley New York, 1982.

[27] M. Lassas and E. Somersalo, *On the existence and convergence of the solution of PML equations*, Computing, 60 (1998), pp. 229–241.

[28] J. Li, J. M. Melenk, B. Wohlmuth, and J. Zou, *Optimal a priori estimates for higher order finite elements for elliptic interface problems*, Applied numerical mathematics, 60 (2010), pp. 19–37.

[29] R. Li, T. Tang, and P. Zhang, *Moving Mesh Methods in Multiple Dimensions Based on Harmonic Maps*, Journal of Computational Physics, 170 (2001), pp. 562–588.

[30] W. C. H. McLean, *Strongly elliptic systems and boundary integral equations*, Cambridge university press, 2000.

[31] P. Monk and E. Süli, *The adaptive computation of far-field patterns by a posteriori error estimation of linear functionals*, SIAM Journal on Numerical Analysis, 36 (1998), pp. 251–274.

[32] M. Motamed, F. Nobile, and R. Tempone, *A stochastic collocation method for the second order wave equation with a discontinuous random speed*, Numerische Mathematik, 123 (2013), pp. 493–536.

[33] J.-C. Nédélec, *Acoustic and electromagnetic equations: integral representations for harmonic problems*, vol. 144, Springer Science & Business Media, 2001.

[34] A. Paganini, L. Scarabosio, R. Hiptmair, and I. Tsukerman, *Trefftz Approximations: A New Framework for Nonreflecting Boundary Conditions*, IEEE Transactions on Magnetics, PP (2015), pp. 1–1.

[35] C. Schillings and C. Schwab, *Sparse, adaptive Smolyak quadratures for Bayesian inverse problems*, Inverse Problems, 29 (2013), p. 065011.

[36] C. Schillings and C. Schwab, *Sparsity in Bayesian inversion of parametric operator equations*, Inverse Problems, 30 (2014), p. 065007.

[37] C. Schwab and C. J. Gittelson, *Sparse tensor discretizations of high-dimensional parametric and stochastic PDEs*, Acta Numerica, 20 (2011), pp. 291–467.

[38] D. M. Tartakovsky and D. Xiu, *Stochastic analysis of transport in tubes with rough walls*, Journal of Computational Physics, 217 (2006), pp. 248–259.

[39] N. Wiener, *The homogeneous chaos*, American Journal of Mathematics, (1938), pp. 897–936.

[40] D. Xiu and J. S. Hesthaven, *High-order collocation methods for differential equations with random inputs*, SIAM Journal on Scientific Computing, 27 (2005), pp. 1118–1139.

[41] D. Xiu and D. M. Tartakovsky, *Numerical methods for differential equations in random domains*, SIAM Journal on Scientific Computing, 28 (2006), pp. 1167–1185.

Recent Research Reports

Nr.	Authors/Title

2015-21 P. Chen and Ch. Schwab
Sparse-Grid, Reduced-Basis Bayesian Inversion: Nonaffine-Parametric Nonlinear Equations

2015-22 F. Kuo and R. Scheichl and Ch. Schwab and I. Sloan and E. Ullmann
Multilevel Quasi-Monte Carlo Methods for Lognormal Diffusion Problems

2015-23 C. Jerez-Hanckes and Ch. Schwab
Electromagnetic Wave Scattering by Random Surfaces: Uncertainty Quantification via Sparse Tensor Boundary Elements

2015-24 V. Kazeev and Ch. Schwab
Quantized tensor-structured finite elements for second-order elliptic PDEs in two dimensions

2015-25 S. Etter
Parallel ALS Algorithm for the Hierarchical Tucker Representation

2015-26 C. Hafner and R. Hiptmair and P. Souzangar
Data Sparse Numerical Models for SNOM Tips

2015-27 F. Leonardi and S. Mishra and Ch. Schwab
Numerical approximation of statistical solutions of incompressible flow

2015-28 P. Chen and Ch. Schwab
Model Order Reduction Methods in Computational Uncertainty Quantification

2015-29 G. S. Alberti and S. Dahlke and F. De Mari and E. De Vito and S. Vigogna
Continuous and discrete frames generated by the evolution flow of the Schrödinger equation

2015-30 P. Grohs and G. Kutyniok and J. Ma and P. Petersen
Anisotropic Multiscale Systems on Bounded Domains